Graphene Based High Performance Magnetic Resonance Imaging Contrast Agent

A Dissertation Presented

by

Shruti Kanakia

to

The Graduate School

in Partial Fulfillment of the

Requirements

for the Degree of

Doctor of Philosophy

in

Biomedical Engineering

Stony Brook University

December 2014

Stony Brook University

The Graduate School

Shruti Kanakia

We, the dissertation committee for the above candidate for the

Doctor of Philosophy degree, hereby recommend

acceptance of this dissertation.

Dr. Balaji Sitharaman – Dissertation Advisor
Associate Professor, Department of Biomedical Engineering, Stony Brook University

Dr. Mary D. Frame- Chairperson of Defense
Associate Professor, Department of Biomedical Engineering, Stony Brook University

Dr. Kenneth Shroyer
Professor and Chair, Department of Pathology, Stony Brook University

Dr. William Moore
Associate Professor, Department of Radiology, Stony Brook University

Dr. Terry Button
Associate Professor, Department of Radiology and Department of Biomedical Engineering, Stony Brook University

This dissertation is accepted by the Graduate School

Charles Taber
Dean of the Graduate School

Abstract of the Dissertation

Graphene Based High Performance Magnetic Resonance Imaging Contrast Agent

by

Shruti Kanakia

Doctor of Philosophy

in

Biomedical Engineering

Stony Brook University

2014

Magnetic resonance imaging (MRI) contrast agents (CA) are increasingly being used to enhance the contrast between normal and diseased tissues, and to help detect various anatomical and functional abnormalities in MRI scans. Today, 40-50% of the MRI procedures worldwide are performed with CAs, majority of them being gadolinium chelate based agents (GBCA). Theory suggests that the relaxivity (a quantitative measure of CA efficacy) of current clinical CAs is sub-optimal, and predicts the possibility of developing new contrast agents with relaxivities up to one to two orders of magnitude greater (depending on the magnetic field), that can allow the same clinical MRI performance at substantially lower dosages (micro or nanomolar dose), enabling advanced MRI applications such as cellular/molecular imaging and blood pool imaging. Also, the recent discovery and association with nephrogenic systemic fibrosis in patients with renal insufficiency has fostered concern and Food and Drug Administration restrictions on the clinical use of GBCA. Therefore, there is a need for a next-generation T_1 MRI CA that show lower toxicity profile, and possess greater relaxivity than current clinical CAs.

Herein, towards the goal of developing a safe and more efficacious T_1 MRI CA, I demonstrate a novel nanoparticle MRI CA comprising of manganese (Mn^{2+}) intercalated graphene nanoplatelets functionalized with dextran (hereafter called, Mangradex) with focus on the study of formulation development and *in vivo* safety and efficacy. The results suggest that Mangradex formulation is hydrophilic, water dispersible (up to 100 mg/ml), and forms stable colloidal dispersions in deionized water, that are iso-osmol and is-viscous to blood. The relaxometry and MRI phantom study suggest that graphene sheets in Mangradex amplify its r_1 relaxivity by up to ~ 20X greater than current clinical CAs. Acute toxicity and respiratory/cardiovascular safety pharmacology study performed for 1 day and 30 days in Wistar rats following single intravenous dose of Mangradex between 1-500 mg/kg, suggested that the maximum tolerated dose was (MTD) 50 mg/kg $\leq$ MTD $\leq$ 125 mg/kg, and Mangradex nanoparticles eliminate mainly through feces within 24 hours. Sub-acute toxicological assessment performed on rats intravenously injected with Mangradex formulations at 1, 50 or 100 mg/kg dosages 3 times per week for three weeks indicated that doses $\leq$ 50 mg/kg could serve as potential therapeutic doses. Whole body 7 Tesla MRI

performed on mice following intravenous injections of Mangradex at 25 mg/kg (455 nanomoles Mn^{2+}/kg; ~2 orders of magnitude lower than the paramagnetic ion concentration in a typical clinical dose) showed persistent (up to at least 2 hours) contrast enhancement in the vascular branches. Taken together, these results lay the foundations for its further development as a vascular and cellular/ molecular imaging probe.

Dedication

To my husband and parents for their love and support…

Table of Contents

LIST OF ABBREVIATIONS

MRI - Magnetic Resonance Imaging

CA - Contrast Agent

RF - Radio frequency

GCBCA - Gadolinium chelate-based contrast agent

NSF -Nephrogenic systemic fibrosis

RES - Reticuloendothelial system

SPIO -Superparamagnetic iron oxide

USPIO – Ultrasmall superparamagnetic iron oxide

MEMRI- Manganese enhanced MRI

SWNT - Single wall carbon nanotube

FIH - First in human

TEM - Transmission electron microscopy

AFM - Atomic force microscopy

TGA - Thermogravimetric analysis

ICP -Inductive coupled plasma mass spectrometry

DDI- Distilled deionized

FDA- Food and Drug Administration

ICH – International conference on harmonization

EMA – European medical agency

GLP - Good laboratory practices

IND - Investigational new drug applications

UV-Vis- Ultraviolet visible light

NIR –Near infrared

GO - Ggraphene oxide

PEG - Polyethylene glycol

GNP - Graphene nanoplatelets

CNT- Carbon nanotube

MWCNT- Multiwalled carbon nanotube

siRNA - Small interfering RNA

NMRD – Nuclear magnetic relaxation dispersion

IV- Intravenous

P_{ow} - Octanol-water partition coefficient

MWCO - Molecular weight cutoff

HSA - Human serum albumin

ELISA - Enzyme-linked immunosorbent assay

LOD – Limit of detection

BCA - Bicinchoninic acid

MTD - Maximum tolerated dose

MPD - Maximum permissible doses

H&E - Hematoxylin and Eosin

CLIA - Clinical Laboratory Improvement Amendments

RDW - Red cell distribution width

GLU -Glucose

BUN - Blood urea nitrogen

CRE – Creatinine

ALP - Alkaline phosphatase

TP - Total protein

ALB - Albumin

ALT - Alanine transaminase

AST - Aspartate transaminase

TG - Blood triglycerides

CHO - Cholesterol

TP - Total protein

TE- Echo time

TR- Repetition time

FA – Flip angle

MRA - Magnetic Resonance Angiography

GFR – Glomerulus filtration rate

NMR – Nuclear magnetic resonance

Amendments

RBC - Red blood cells

WBC - White blood cells

MCV - Mean corpuscular volume

MPV - Mean platelet volume

MCHC - Mean corpuscular hemoglobin concentration

ROI – Region of interest

SNR - Signal to noise ratio

CNR – Contrast to noise ratio

MIP – Maximum intensity projection

SNx - Subtotally nephroctomized

LIST OF FIGURES

corpuscular volume (MCV) and mean platelet volume (MPV). **c**) Mean corpuscular hemoglobin concentration (MCHC) and total hemoglobin concentration. **d**) Hematocrit and red cells distribution width (RDW). **e**) Markers for kidney function - blood urea nitrogen (BUN) level and creatinine level. **f**) Markers for liver function - alkaline phosphatase (ALP), alanine transaminase (ALT) and aspartate transaminase (AST).

Figure 14. Biodistribution and elimination of Mangradex in major organs. **a**) Biodistribution in organs at 1 day. **b**) Biodistribution in organs at 30 days. **c**) Blood retention of Mangradex. **d)** Elimination of Mangradex via feces. **e)** Elimination of Mangradex via urine.

Figure 15. Representative high (400X) magnification photomicrographs illustrating pulmonary and hepatic histology from chronic study animals at 1 mg/kg, 50 mg/kg, 100 mg/kg Mangradex and sham. Lung A) at 1 mg/kg, B) at 50 mg/kg and C) at 100 mg/kg- with pigment (arrows) within alveolar macrophages suggestive of the presence of graphene nanoparticles, D) sham - without diagnostic abnormality. Liver - E) at 1 mg/kg - showing minimal steatosis, but without diagnostic abnormality, F) at 50 mg/kg- showing pigmented macrophage in Kupffer cells suggestive of graphene particles. No sign of inflammation, G) at 100 mg/kg - more pigmented than at lower dose, H) sham - without diagnostic abnormality.

Figure 16. Plot of relaxation rate ($1/T_1$) vs. Mn^{2+} ions concentration fit to a linear regression line.

Figure 17. T_1 weighted MRI phantom images of Mangradex, DDI water and dextran solution obtained using a 1.5 T clinical scanner. Row 1 (left to right): DDI water and dextran solution in water at 4.68 mg/ml, Mangradex at concentrations 0.015, 0.39 mg/ml. Row 2 (left to right): Mangradex at 0.78, 1.9, 3.9 and 7.8 mg/ml. For each Mangradex concentration, the concentration of Mn^{2+} ions in μM is also shown.

Figure 18. Three-dimensional (3D) imaging of the whole mouse body in less than 12-minutes using a 7-T mouse MRI scanner equipped with a homemade RF coil enabling serial imaging with 200-µm isotropic spatial resolution. The example of image dataset shown compares different organ and body regions prior and following single injection of Mangradex at 25 mg/kg. **A)** coronal view covering the upper body including the head, neck, heart and lungs; **B)** axial slice re-orientation obtained from the same lung and heart area described in **A)**; **C)** the section covering the lung and liver region; **D)** a coronal view from the lower abdominal region that includes the kidneys and the spleen.

Figure 19. 3D visual rendering of the whole mouse body throughout the time course of this study via maximum-intensity-projections to facilitate the qualitative comparison of the bio-distribution and pharmacokinetics between CA injected in two groups. The effects of the contrast are illustrated as follow: **A)** Pre- & post- injection of Ablavar® (455 nmoles/kg of Gd^{3+}) as well as **B)** pre- & post Mangradex injection at 25 mg/kg (equivalent to 455 nmoles/kg of Mn^{2+}).

Figure 20. In vivo MRI (a-f) Representative T_1 weighted MR images of pelvic region (coronal view) that show the subtotally nephroctomized (SNx) rat kidney (red arrow) before (a) and 25 minutes after (b) injection of Ablavar (control); before (c) and 25 (d), 50 (e) and 85 (f) minutes after injection of Mangradex. (g,h) Representative MR angiograms (head of the rat is on the right side) of pelvic region that show the renal artery (red arrows) before (g) and 25 minutes after (h) injection of Mangradex.

Figure 21. Graph showing in vivo T_1 relaxation time in region of interest before and 25, 50 and 85 minutes after injection of Mangradex at 25 mg/kg (455 nmoles/kg of manganese) and Ablavar(455 nmoles/kg of gadolinium).

LIST OF TABLES

ACKNOWLEDGMENTS

Every beginning has an end, and when all the good and hard work ends on a positive and satisfying note then there is nothing like it. It gives me immense pleasure to finally write down all my work in the form of a doctoral dissertation. My PhD endeavor was possible with the help of a number of wonderful and inspiring people who contributed in shaping my educational experience, career path, and my life. I would like to take this opportunity to acknowledge them all.

First, I would like to thank Dr. Balaji Sitharaman, my thesis advisor, who believed in my abilities, continuously supported in all my endeavors, and motivated me to take up the challenges in areas out of my comfort zone. His interdisciplinary knowledge, wisdom, and collaborative skills provided me the opportunity to work on different dimensions of this research projects. I deeply appreciate his suggestions, guidance, and patience throughout this work.

I am grateful to my dissertation committee members and collaborators, Dr. Kenneth Shroyer for his guidance on histology, Dr. William Moore for being my clinical mentor, Dr. Terry Button for MRI studies and Dr. Molly Frame for her guidance and generously sharing advice that facilitated my research to achieve new heights. I am also thankful to Dr. Youssef Wadghiri and Dr. Praveen Kulkarni for their help with the MRI studies and data analysis. Insightful criticism and comments of all these experts have always sharpened my skills and expanded my knowledge in the area of MRI contrast agents.

I would like to thank my lab mates, Dr. Jimmy Toussaint, Dr. Sayan Mullick Chowdhury, and Stephen Lee for working in a team with interest and enthusiasm, without their help, I could not have done any of this. I cannot forget the great support on my research project from the undergraduate students, in particular, Tanuf Tembulkar, Priyanka Parmar, Slah Khan, and Sunil Chikmagalur. I am also thankful to the DLAR staff, Nicole Steinhauff, Jean Rooney, and Dr. Thomas Zimmerman, for their help and advice during animal studies. I would also like to thank all my lab mates…Gaurav Lalwani, Shawn Xie, Behzad Farshid, Sunny Patel, Jason Rashkow, Yahfi Talkudar and Cassandra Suhrland for being supportive and sharing their advice and constructive critiques when needed.

Most importantly, I owe the deepest gratitude to my parents, Mr. and Mrs. Ishvarlal and Kunjalata Kanakia for loving me unselfishly and for supporting me in all the endeavors of my life. I would also like to express my gratitude to my sisters, Sneha Dudhela and Dharitri Kansara for their love, support, and constant faith in me during the ups and downs of my life. I am also grateful to my in-laws Mr. and Mrs. Sharad and Smita Wadajkar for being supportive. Finally, a huge thanks to my husband, Dr. Aniket Wadajkar, who inspired me to initiate this graduate work and always encouraged me to realize my true potential. Without his love, support, and motivation, this dissertation would never have been written.

LIST OF PUBLICATIONS

1) **Kanakia S**, Toussaint J, Hoang DM, Mullick Chowdhury S, Lee S, Shroyer K, Moore W, Wadghiri YZ, Sitharaman B. Sub-acute Toxicity and Efficacy of A Graphene-Based Magnetic Resonance Imaging Contrast Agent in Small Animals. (Submitted) **2014**.

2) Toussaint J, **Kanakia S**, Lee S, Mullick Chowdhury S, Sitharaman B. Pre-clinical Studies of clinically-approved Magnetic Resonance imaging Contrast Agents. (In preparation) **2014**

3) **Kanakia S***, Toussaint J*, Kulkarni P, Lee S, Mullick Chowdhury S, Khan S, Shroyer K, Moore W, Sitharaman B. Graphene Based High Performance Magnetic Resonance Imaging Contrast Agent for Diagnosis and Monitoring of Renal Abnormalities. (In preparation) **2014**. (* contributed equally).

4) **Kanakia S**, Toussaint J, Mullick Chowdhury S, Tembulkar T, Lee S, Jiang Y, Lin R, Shroyer K, Moore W, Sitharaman B. Dose Ranging, Expanded Acute Toxicity and Safety Pharmacology Studies for Intravenously Administered Functionalized Graphene Nanoparticle Formulations. *Biomaterials*, **2014**; 35(25): 7022-7031.

5) Talukdar Y, Rashkow JT, Lalwani G, **Kanakia S**, Sitharaman B. The Effects of Graphene Nanostructures on Mesenchymal Stem Cells. *Biomaterials* **2014**; 35 (18): 4863-4877.

6) **Kanakia S**, Toussaint J, Mullick Chowdhury S, Lalwani G, Tembulkar T, Button T, Shroyer K, Moore W, Sitharaman B. Physicochemical Characterization of a Novel Graphene Based Magnetic Resonance imaging contrast agent. *International Journal of Nanomedicine*. 8, 2821, **2013**.

7) Mullick Chowdhury S, **Kanakia S**, Toussaint J. Frame M, Dewar A, Shroyer K, Moore W, Sitharaman B. *In vitro* and *in vivo* assessment of hematological toxicity of dextran functionalized graphene. *Scientific Reports*. **2013,** 3, 2584.

8) Lalwani G, Kwaczala A, **Kanakia S**, Patel S, Judex S, Sitharaman B. Fabrication and Characterization of Three-dimensional Macroscopic All-carbon Scaffolds. *Carbon*. **2013**; 53: 90-100.

9) Paratala BS, Jacobson BD, **Kanakia S**, Francis LD, Sitharaman B. Physicochemical Characterization, and Relaxometry Studies of Micro-graphite oxide, Graphene Nanoplatelets, and Nanoribbons. *PLoS ONE*. **2012**; 7(6): e38185.

CHAPTER 1

LITERATURE REVIEW AND INTRODUCTION

Magnetic Resonance Imaging

MRI is one of the powerful imaging modalities to visualize anatomical structures in biomedical research and clinical medicine.[1] MRI can non-invasively render information on anatomy of organs (e.g. detection of lesion or tumor) and physiological parameters (e.g. assessing cardiac function) for improved diagnosis of many pathologies and diseases without the use of ionizing radiation.[2]

The MRI signal is generated by the relaxation of *in vivo* water molecule protons. The contrast generated in the MR images mainly depends on 1) *in vivo* proton spin density, 2) longitudinal (T_1) and transverse (T_2) relaxation times of local tissue environment, and 3) applied magnetic field strength. The images in MRI are generated by measuring radiofrequency (RF) signal arising from magnetic moment of water protons *in vivo*. Water proton is used as a probe molecule in MRI since it abundantly (~70%) of the body weight) available in *in vivo*. Hydrogen nucleus is a single proton, and as proton is positively charged it spins and generated magnetic field, which is called 'magnetic moment'.

T_1 and T_2 Relaxation Time

When the patient is placed in MRI, the hydrogen nuclei in the patient's body aligns to the applied magnetic field and becomes temporarily magnetized. The hydrogen atom inside the body contains spin and precesses at a frequency called 'Larmor frequency' around z axis as shown in Figure 1a. The Larmor frequency (ω_0) depends on the strength of applied magnetic field and is given by equation:

$$\omega_0 = \gamma B_0$$

Where, γ = gyrometric ratio, B_0 = applied magnetic field

In the absence of magnetic field net magnetic moment is zero as the direction of these vectors is random are always cancel each other. When the external magnetic field (B_0) is applied, slightly greater number of hydrogen nuclei align parallel to the direction of field generating net magnetic field parallel to the z-axis. When external RF pulse with Larmor frequency is applied in transverse (XY) direction, the direction of the net magnetization flips to the XY plane as shown in Figure 1b. As a result, the net magnetization slowly decreases in Z-direction and increases in XY plane. When the RF pulse is removed, the net magnetization recovers in its original Z-direction. This process is called relaxation and has two components. 1) The recovery of magnetization (M_z) in longitudinal (Z) plane, called spin lattice relaxation time T_1.

$$M_z = M_o\,(1 - e^{-t/T_1})$$

2) The decay of magnetization in transverse (XY) plane, called spin-spin relaxation time T_2.

$$M_{XY} = M_{XYo}\, e^{-t/T2}$$

T_1 is the time required for longitudinal magnetization to recover to 63% of the equilibrium value (Figure. 1c), whereas T_2 is the time required for transverse magnetization to drop to 37% of its initial magnitude (Figure 1d).

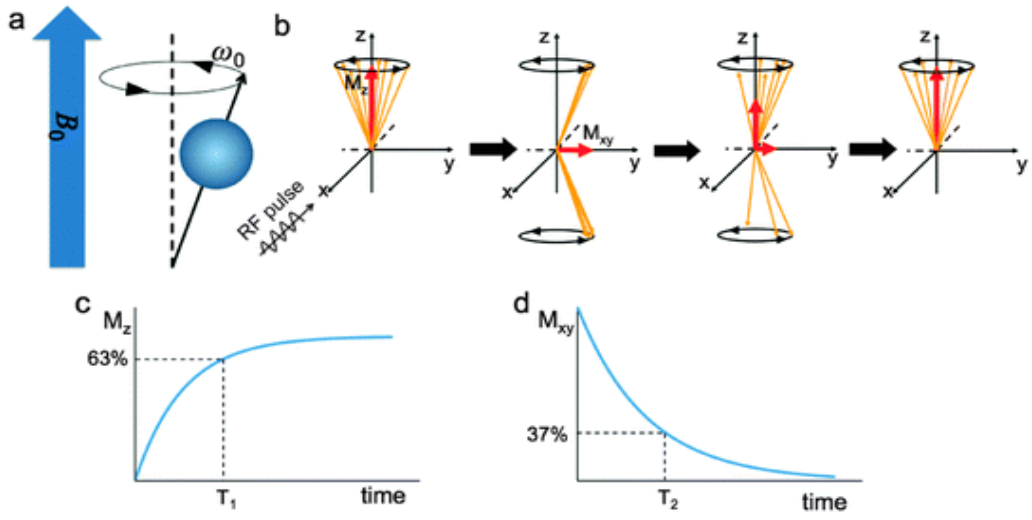

Figure 1. *Principles of MRI.*[3] *(a) In magnetic field, the hydrogen nuclear spins align with (parallel) or against (antiparallel) the external magnetic field. (b) Irradiation of resonant RF*

results in decrease in longitudinal magnetization (M_z) and generation of transverse magnetization (M_{xy}). Subsequently, the nuclear spins return to their initial state, referred to as relaxation. (c and d) T_1 is the time required for longitudinal magnetization to recover to 63% of its equilibrium (c), and T_2 is the time required for transverse magnetization to drop to 37% of its initial magnitude (d).

When the patient is placed in MRI, the hydrogen nuclei in the patient's body aligns to the applied magnetic field and becomes temporarily magnetized. When RF pulse at Larmor frequency is applied, the *in vivo* water protons respond by a signal with multiple frequencies referring to their positions along the magnetic field gradient. Using Fourier transform, this signal is broken down into individual frequency component. The magnitude of the signal at each frequency is proportional to the water proton density at that location, thus allowing an image to be constructed.

Contrast Agents

Differences in the environment of *in vivo* water molecules generates inherent contrast in MRI images. In many pathological conditions, the intrinsic contrast generated by the tissues does not provide sufficient changes in relaxation times (T_1 and T_2) to enable specific disease diagnosis. In such cases, CAs are commonly used to increase the diagnostic confidence.[1,4] The MRI CA can interact with surrounding water molecule and increase the relaxation rate of water protons. MRI CAs can significantly increase the signal differences between tissues, tissues and blood vessels or tissues and bones by shortening the characteristic T_1 and T_2 relaxation times.[1]

Since the 1980s, a variety of clinical MRI CAs were developed that are complexes of paramagnetic metal ions such as gadolinium (Gd^{3+}) and manganese (Mn^{2+}) as T_1 agents, or super-paramagnetic ion such as iron (Fe^{2+}) as T_2 agents. These ions, because of their unpaired electron structure, act as effective relaxation-enhancement agent and decrease T_1 and T_2 relaxation times of nearby protons.[1]

Gadolinium is naturally toxic to the body, and hence necessitates strongly coordinating ligands to keep Gd^{3+} completely bound *in vivo*. The Gd^{3+} chelate-based T_1 MRI CAs currently dominate the market (>95% market share) and worldwide, approximately 43% of the 65 million clinical MRI procedures worldwide use MRI CAs.[5]

Relaxivity

The quantitative measure of MRI CA efficacy is known as relaxivity. It is defined as the change in the relaxation rate of the water protons per molar concentration of the paramagnetic ion, and is expressed in units of mM^{-1} sec^{-1}. It is denoted as r_1 (for T_1-baseed CAs) or r_2 (for T_2-baseed CAs) and calculated by using the equation given below. **Figure 2** shows the representative graph of relaxivity, where the value of the slope of the line gives relaxivity value.

$$r_{1,2} = (1/T_{1,2})/[\text{Concentration of ions in mM}]$$

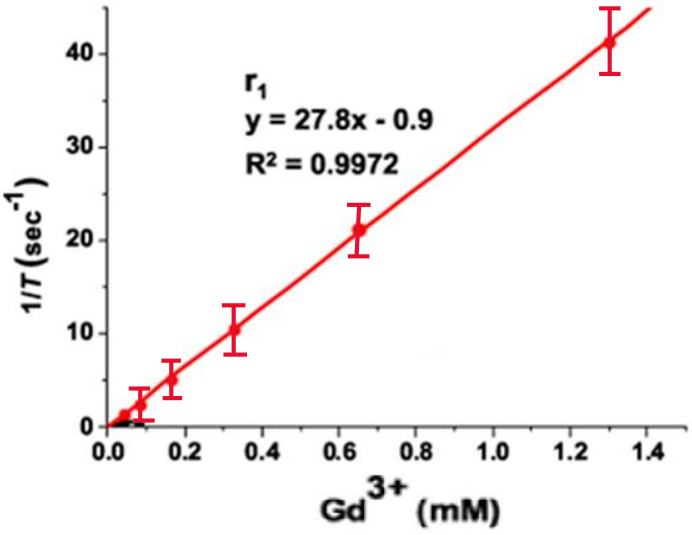

Figure 2. *A representative graph of relaxivity. The slope of the line gives relaxivity value.*

The table below lists FDA approved CAs and their relaxivity values.

Trade names	Generic names	Abbreviated names	Relaxivity(r_1, unless specified) ($mM^{-1}S^{-1}$) at 1.5 T[6]
Magnevist	Gadopentetate Dimeglumine	Gd-DTPA	3.3
Prohance	Gadoteridol	Gd-HP-DO3A	2.9
Omniscan	Gadodiamide	Gd-DTPA-BMA	3.3
Optimark	Gadoversetamide	Gd-DTPA-BMEA	3.8
Multihance	Gadobenate,	Gd-BOPTA	4.0
Ablavar (formerly a.k.a. Vasovist, AngioMark)	Gadofosveset trisodium	Diphenylcyclohexyl Phosphodiester Gd-DTPA	5.2
Eovist, Primovist, EOB Primovist	Gadoxetate disodium	Gd-EOB-DTPA	4.7
Gadavist	Gadobutrol	Gd-DO3A-butrol	3.3
Feridex	ferumoxide	AMI-25	r_2 = 4.7
Teslascan	Mangafodipir trisodium	Mn-DPDP	1.6

Table 2: FDA Approved MRI CA and their relaxivity at 1.5 T.

CAs increase both T_1 and T_2 relaxation rates. The ratio of r_2/r_1 gives an idea whether a given CA is suitable as T_1 or T_2 agent. If this ratio is about 1~2, the CA is suitable as T_1 agent. Super-paramagnetic materials mainly affect transverse T_2 relaxation and thus, higher r_2/r_1 ratio of 10 or more.[7]

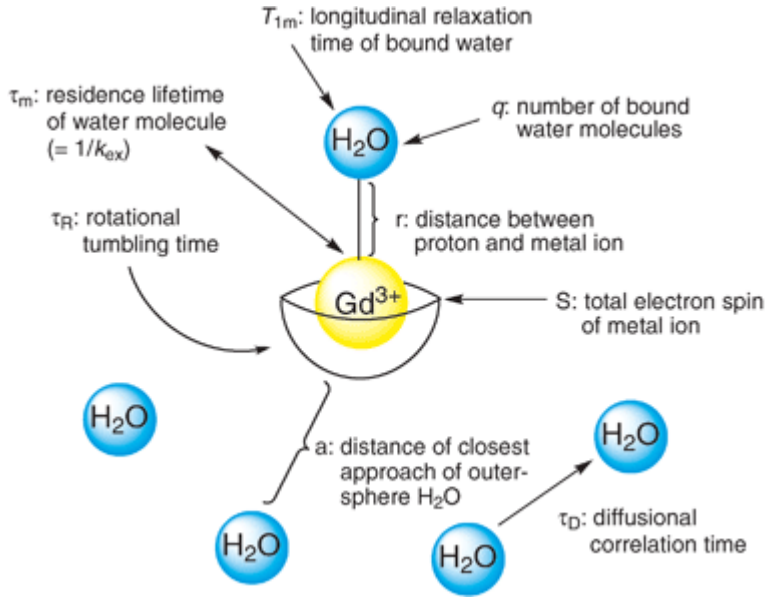

***Figure 3**. Variables contributing to contrast agent relaxivity*[8]

Relaxivity of a CA is affected by multiple parameters. A large body of experimental and theoretical research done in the last three decades now offers good understanding of the relaxation mechanism, and underlying structural, chemical and molecular dynamic properties that influence the relaxivity. **Figure 3** demonstrates major parameters contributing to relaxivity of paramagnetic-ion chelate complexes, which include 1) inner sphere relaxivity, and 2) outer sphere relaxivity. Inner sphere relaxivity is mainly governed by i) the number of inner-sphere water molecules (q), ii) the rotational tumbling time (τ_R), and iii) the residence lifetime of inner-sphere water molecules (τ_m). The Solomon-Bloembergen-Morgan equations are used to describe the relationship between variables contributing to inner-sphere relaxivity.[9-11] In general, higher q values, longer tumbling times (τ_R) and short τ_m yields high relaxivity values. The outer-sphere relaxation is described by the Freed theory and is mainly dependent on 1) distance of closest approach of outer-sphere water molecules (a) and 2) diffusional correlation time of outer-sphere water molecules

(τ_D). The inner sphere relaxivity parameters mainly govern the relaxivity and most often are taken into consideration in the design of CAs.[12]

Limitation in Relaxivity

MRI is widely used for imaging organs or tissues; however, its ability for advanced application such as cellular and molecular imaging is still lacking because of inadequate sensitivity. To understand the mechanism of disease at molecular level, it is important to be able to visually distinguish between different disease targets such as proteins, enzymes, hormones or small molecules at the very small concentration (nanomolar to picomolar) they are present in tissues.[13] In order to achieve this goal, CAs with relaxivity values at least 50-fold higher than the current clinical CAs are required. As shown in **Table 1,** the relaxivity values of clinical CAs are ~1.6-4.7 $mM^{-1}S^{-1}$, that can be improved by modulating the parameters described in previous section. Theoretically it is possible to achieve relaxivity up to ~ 10X to 100X greater (depending on the magnetic field strength) than current clinical CAs.[13,14] The high relaxivity of CAs can help achieve higher sensitivity in MRI necessary to visualize biomolecules. Hence, developing new CAs with high relaxivity still remains an active area of research.

Nephrogenic Systemic Fibrosis

GCBCAs are biologically inert in the patient with normal kidney function and are removed from the urinary excretion within few hours following injection (half- life ~90 minutes). As kidney is the exclusive route of excretion for Gd^{3+} chelate based contrast agents (GCBCAs), it can circulate significantly longer in patients with either sub-acute kidney disease, acute kidney injury or renal insufficiency (GFR < 30 mL/min/1.73m^2).

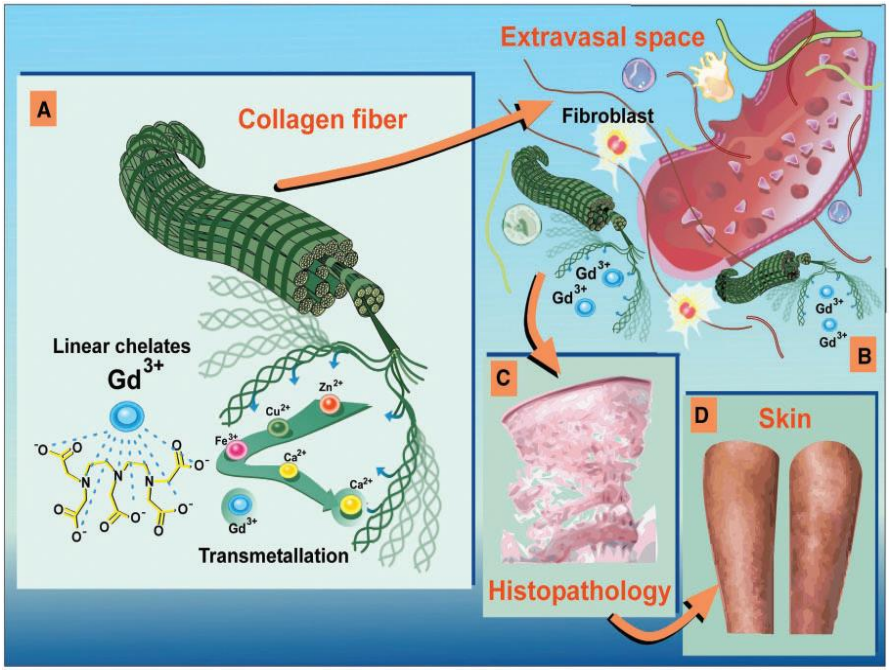

Figure 4.[15] *Gadolinium introduced into the human body by instable linear chelates has a prolonged half-life in the uraemic milieu due to reduced renal excretion, thus allowing free toxic gadolinium released from its chelate (A) after changing place with other ions (transmetallation reaction) to extravasate into the extravascular space where it may accelerate fibrillogenesis, as all the lanthanide ions (including gadolinium) have collagen fibrillogenetic properties (B). Histopathological photomicrographs show thickened dermis with spindle-shaped fibrocytes and mucin with plumped collagen bundles that infiltrate the septa of the subcutaneous fat deeply (C), eventually leading to the macroscopic appearance of the skin of patients (D).*

During this longer bio-retention, Gd^{3+}can de-chelate and transmetallate with the ions *in vivo* according to its affinity and quickly binds to ubiquitous phosphate, forming insoluble gadolinium phosphate and leading to prolonged exposure to biologically active gadolinium.[16] Also, multiple reports have revealed that the use of Gd^{3+} in GCBCAs in these patients lead to rare but potentially fatal disease Nephrogenic Systemic Fibrosis (NSF) in patients with kidney disease.[17-19] Gd^{3+} de-chelation is more common after exposure to linear ligands compared to macrocylic ones. Early clinical features of NSF include onset of limb edema accompanied by red or violate cutaneous papules and plaques overlying dermal and subcutaneous fat fibrosis and when fully developed, results in limb pain, contractures, and loss of mobility.[16] Furthermore, it can cause fibrotic damage

to internal viscera such as esophagus, heart, skeletal muscles, lungs and kidneys.[16,20,21] NSF is clinically it is manifested 2 to 10 weeks (medial 5 weeks) after GCBCA exposure and results in thickening of skin, joint contractures and decreased mobility of the organs that can lead to mortality.[16] The pathophysiology of NSF is not well understood and many theories exists to explain mechanism of NSF. A large number of study indicates that Gd^{3+} can either dissociate by transmetallation or stay intact in chelate complex stimulating skin macrophages or peripheral blood monocytes (PBMC). Activated macrophage or PBMC can stimulate fibroblast resulting in the fibrotic lesions and eventual skin thickening and joint contractures.[22]

Every year in the U.S., 0.6 million individuals are diagnosed with an acute kidney injury,[23] and over 20 million people are have sub-acute kidney disease,[24] with over 0.7 million of these cases classified as either stage IV or stage V.[24] MRI is routinely used in the clinical diagnosis of renal failure,[25] has the potential to provide both functional[26,27] and anatomical information about individual kidneys.[28] For patients with kidney transplant or renal failure, the use of MRI is becoming highly attractive over other methods such as CT and nuclear imaging as it does not require use of ionizing radiation or nephrotoxic iodinated contrast media and non-invasively renders anatomical details of soft and hard tissues for improved diagnosis of many pathologies and diseases.[29] Typically these patients either have to go for MRI without CA, or have to undergo dialysis increasing the burden on the health care costs. As a result, the FDA has restricted use of Gd^{3+}-based MRI CAs for renal imaging or for imaging of other pathologies/lesion in patients with renal failure.[30,31] Thus, there is a need for MRI CA that is safer and more efficacious than current clinical CAs. The FDA requires manufacturers to include mandatory black box warnings about the potential risks to patients with renal failure for all Gd^{3+}-based MRI CAs and also contraindication

information for Gd^{3+}-based MRI CAs (Magnevist, Omniscan, Optimark) reported to induce NSF.[32,33] The FDA warning also requires patients to undergo renal function laboratory tests prior to using GCBCAs and post imaging dialysis to remove CA in timely manner and to mitigate the risk of NSF. These findings have forced clinicians to outweigh the risk to benefit ratio of GCBCA in these patients or use them off label. Thus, there is a critical need for a next-generation T_1 MRI CA with a negligible nephrotoxicity profile compared to that provided by currently used Gd^{3+}-based CAs.

Manganese-based Contrast Agents

Due to the toxicity concerns on GCBCA, Manganese, the first element used as an MRI CA has again received attention and has been proposed as an alternative for GCBCA.[34,35] Manganese, a paramagnetic agent with five unpaired electrons and long electron relaxation time has great potential as an MRI CA. It was the first paramagnetic element suggested for enhancing imaging contrast in a phantom by Lauterbur in his landmark paper in 1973[36] and subsequently tested successfully on differentiating tissue contrast from various organs by the same group.[37] Yet, only one chelated form, manganese dipyridoxyl diphosphate (Mn-DPDP (brand name: Teslascan); Mangafodipir Trisodium) is FDA approved for clinical use.[38] Manganese, a natural cellular constituent resembling Ca^{2+}, often functions as a regulatory cofactor for receptors and enzymes including manganese superoxide dismutase which is an important defense against oxidative stress, and arginase involved in neurotransmission.[34,35] The daily dietary requirement of manganese is 1.8-2.3 mg per day (33-42 micromoles).[39] Manganese toxicity is rare, and has only been reported following long-term exposure at high concentrations (LD_{50} = 0.22mmol/kg of rat) resulting in Parkinson-like symptoms called Manganism.[34] Manganese based CAs, Teslascan®, clinically

utilized for liver, kidney, and cardiac imaging has been removed from the market recently.[34] Manganese enhanced MRI (MEMRI) that uses injection of $MnCl_2$ has been used for detailed visualization of brain structure, local brain or cardiac function, and tracing of neuronal tracts. However, the free $[Mn(H2O)_6]^{2+}$ associated with $MnCl_2$ is toxic at the concentration providing sufficient contrast, and hence its use is limited to rodents. $MnCl_2$ containing agent LumenHance®, that once was approved for gastrointestinal imaging has been removed from the market.[35] Therefore, manganese based high relaxivity CA that can allow MRI at significantly low concentration would constitute significant advancement.

Advantages of Nanoparticle-based Contrast Agents

Majority of the T_1-chelate based complexes excrete from the body within few minutes leaving very short life span in the body and making them unsuitable for several applications such as blood pool imaging, long term tracking or for some molecular imaging applications. On the other hand, by controlling size, shape, structure and other physicochemical attributes of nanoparticles, blood retention, tissue perfusion, excretion rate and excretion pathways can be controlled.[40] For example, superparamagnetic iron oxide (SPIOs) nanoparticles with diameter of >50 nm have been clinically used for the diagnosis of liver diseases because they are selectively taken up by the Kupffer cells.[40] While, USPIOs with diameter of < 20 nm, that can pass reticuloendothelial system (RES) and can be taken up in normal lymph nodes, have been used for lymph node imaging.[40,41] Furthermore, the large surface area of nanostructured materials can allow effective conjugation of a wide spectrum of compounds to be attached to it including paramagnetic or superparamagnetic ions, disease-specific biomarkers and targeting moieties to develop target specific contrast agents. In addition, multiple studies have demonstrated that paramagnetic or super paramagnetic ions when

encapsulated in nanoparticles exhibit greater thermal stability compared to their chelate counterpart.[42] Some carbon nanostructures have also been shown to affect the interaction of water with encapsulated paramagnetic ions increasing the relaxivity by 2 to 4 orders of magnitude higher than existing clinical CAs.[4,43,44] Hence, in the pursuit to avail all the unique features of nanostructures, research is growing in nanoparticle based CA to develop next generation high performance CAs.

Carbon Nanostructure Based Contrast Agents

Over the last decade, carbon nanostructures such as fullerene[45] (buckyball shaped structure), single and multiwalled[46] carbon nanotubes (cylindrical carbon nanostructure) and nanodiamonds[47] (diamond shaped), wherein paramagnetic Gd^{3+} ions covalently or non-covalently functionalized to the external carbon sheet or encapsulated within the carbon nanostructure have been reported as efficient MRI CAs with relaxivity values 2 fold to 2 orders higher than the clinically used GCBCAs.[43,4]

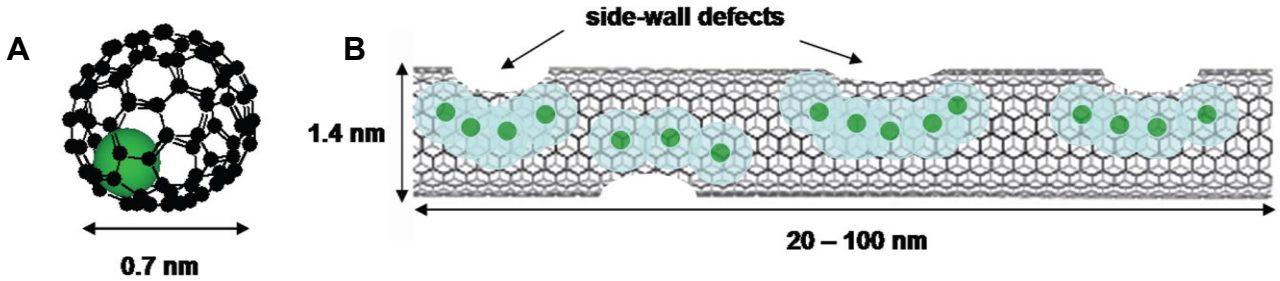

***Figure 5**: Depiction of a) gadofullerene (Gd@C60), b) a single US-tube loaded with hydrated Gd^{3+} ions.[4]*

Figure 5 shows the depiction of these structures. SWCNT (20-100 nm long) when treated with aqueous $GdCl_3$, Gd^{3+} enters the tubes via side wall defect or through the end tube opening. This

structure, called gadonanotubes have relaxivities 170 $mM^{-1}S^{-1}$ at 30- 60 MHz magnetic field, 40-90 times higher than current clinical CAs due to the outer sphere contribution from water.[44] Metallofulleres with Gd^{3+} encapsulated within the fullerene cage possess water proton relaxivities 80 $mM^{-1}S^{-1}$, 20 times higher than the current clinical CAs. Gadofullerenes such as Gd @C60(OH)*x* and Gd@C60[C(COOH)2 have exhibited relaxivity 20 to 100 $mM^{-1}S^{-1}$.[42] While confinement of the Gd^{3+} ions into nanoporous structures of silicon[48] or zeolites[49] increases the relaxivity by two or four times compared to Gd^{3+} chelate compounds, only when the Gd^{3+} ion are confined within single-walled carbon nanotubes[48,50] has there been an order of magnitude or more increase in relaxivity profiles significantly different that those reported for other Gd^{3+} ion-based complexes.[51] These studies have laid the foundation for providing a general strategy of amplifying relaxivity by encapsulating or covalently/non-covalently functionalizing paramagnetic ions within the carbon nanostructure. Even though these Gd^{3+}-carbon nanostructures based MRI CAs show higher relaxivity compared to clinical MRI CAs, none have translated into clinical use or reached first in human (FIH) trial.[5] The potential of Mn^{2+}-carbon nanostructure as an MRI CA is yet to be investigated.

Graphene

Graphene is a single sheet thick sp^2 -bonded allotrope of carbon with 2-dimensional properties. It possess unique electronic, optical, mechanical properties that has revolutionize many industries. Graphene can have many different shapes, such as platelet like graphene nanoplatelets, graphene nanoribbons or nano-onions. It can be synthesized from bottom up approach, like chemical vapor deposition or top-down approaches such as mechanically peeling single layer using scotch tape or chemical exfoliation of graphite. Hummer's method of oxidizing graphite in the presence of

potassium permanganate is one of the widely method to make graphene oxide and has been used in the large scale production of graphite oxide, graphene nanoplatelets, and graphene nanoribbons using starting materials such as graphite and MWCNTs.[52,53] Several studies have demonstrated that graphite oxide synthesized using Hummer's method leads to intercalation (insertion of species within the voids of graphene sheets) of trace amounts of paramagnetic impurities such as manganese ions in the graphene sheet that plays an important role in altering their electrical, chemical and magnetic properties.[54-56] The graphene sheets hold them in place by charge transfer complex.[54] Theoretical studies predict a variety of magnetic phenomena in graphene,[57] and to date, few of these effects have been explored experimentally.[58]

Relaxometric Properties of Graphene

As mentioned in previous section, Gd^{3+}-carbon nanostructures have shown two-fold to two-order increase in relaxivity (depending on the magnetic field) compared to Gd^{3+}-chelate complexes. Therefore, the next question was whether the high increase in relaxivity is unique to paramagnetic ions confined in single-walled carbon nanotubes, which are seamless cylinders formed from a graphene sheet, or fullerenes which are rolled up graphene sheet, or in general observed for paramagnetic ions confined in other graphene or graphitic structures. To systematically investigate whether the shape, structure or size of the carbon nanostructure has an effect on the observed increase in relaxivity, our lab has performed exhaustive study on the relaxometric properties of graphite and different shapes of graphene.[51] This includes 1) oxidized graphene nanoplatelets (GNP), 2 reduced graphene nanoplatelets - both disc shaped graphene nanoparticles synthesized from graphite, 3) graphene nanoribbons - graphene sheets synthesized by unzipping carbon

nanotubes and 4) oxidized micrographite. **Figure 6** demonstrates morphology of these graphene nanostructure.

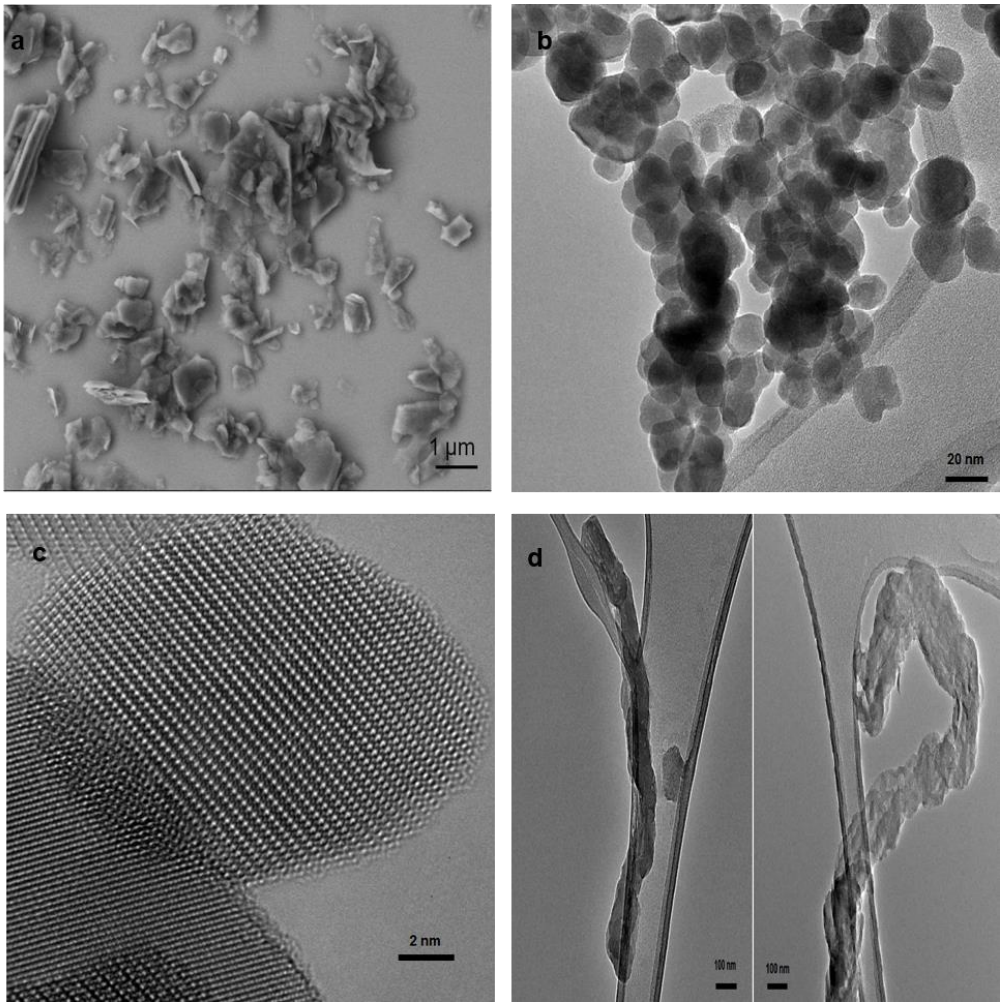

Figure 6. *Representative SEM image of (a) oxidized micro-graphite and TEM images of (b,c) reduced graphene nanoplatelets and (d) graphene nanoribbons*.[51]

Sample	r_1 **($mM^{-1}s^{-1}$)**	r_2 **($mM^{-1}s^{-1}$)**	r_2/r_1
Oxidized graphite	63 (61-78)	171 (169-184)	2.7
Oxidized Graphene nanoplatelets	52 (50-54)	114 (114-131)	2.2
Reduced graphene nanoplatelets	47 (34-49)	415 (389-430)	8.9
Graphene nanoribbons	62 (53-71)	303 (275-310)	4.9
Clinical Mn^{2+}Chelate Complexes [30]	1.8-2.0	2.0 - 2.2	-

Clinical Gd^{3+}Chelate Complexes[34]	3.4 -5.8	3.6 ± 7.0	-

Table 2. *Relaxivity of oxidized graphite, oxidized graphene nanoplatelets, reduced graphene nanoplatelets and graphene nanoribbons dispersed in 1%Pluronic F127 solutions compared with clinically used MRI contrast agents.*[51]

Table 2 shows the relaxivity values at 0.47T for oxidized micro-graphite, oxidized graphene nanoplatelets, reduced graphene nanoplatelets and graphene nanoribbons at 40°C. Also included for comparative purposes are range of relaxivity values of clinically approved Gd^{3+}-based and Mn^{2+} based chelate complexes.[6] The table clearly shows that all four compounds show significantly higher r_1 and r_2 relaxivities compared to paramagnetic chelate complexes. At 0.47 T, the r_1 and r_2 values for the graphite and graphene samples are ~8-10 times, and 19-60 times greater than paramagnetic chelate complexes. This study has shown that the trace amounts of Mn^{2+} ions get intercalated within the graphene sheets during the potassium permanganate based oxidation s process and these manganese intercalated graphitic and graphene nanostructure show disparate structural, chemical and magnetic properties, and high relaxivity (up to 2 order) compared to paramagnetic chelate compounds.[51] These results confirmed that it is not the shape or structure, but in general, confinement of paramagnetic ions in carbon nanostructure exhibit greater relaxivity[51] and also identifies nano-confinement of paramagnetic ions as a general strategy to develop paramagnetic metal-ion graphitic-carbon complexes as high relaxivity MRI CA.

The r_2/r_1 ratio is lower than iron-based T_2 contrast agents that have ratios of 10 or more. T_1 contrast agents have r_2/r_1 ratios about 1~2.[59] Thus, the manganese-intercalated graphitic, and graphene particles may be better suited as T_1 contrast agents.

Graphene in Biomedical Applications

Graphene has shown excellent potential for *in vitro* and *in vivo* for drug/gene delivery and biological sensing/ imaging applications due to their nanoscopic size, large specific surface area, and physiochemical properties.[60-62] GNPs could be loaded with aromatic drugs (e.g., SN38 and doxorubicin) via Vander Wall (π-πstacking) interactions yielding very high drug loading efficiency, or forming non-covalent bond with cationic polymers such polyethyleneimine by electrostatic interactions to form positively charged complexes that facilitate plasmid DNA (pDNA) and small interfering RNA (siRNA) delivery.[63] Several studies have reported on light absorption properties of graphene from UV to near-infrared (NIR) region[64] and size dependent visible and NIR fluorescence by graphene oxide (GO).[65,66] Largely dislocated π-electrons in graphene allows energy transfer from neighbor molecules resulting in efficient fluorescent quenching.[67] Due to these optical properties, graphene has been used in optical based detection of biomolecules such as oligonucleotides,[68] proteins,[69] pathogens[70] and heavy metal[71] sensing. The strong optical absorbance properties of nanographene oxide functionalized with PEG in NIR region was used for successful photothermal ablation of tumor in the presence of low-power NIR laser irradiation.[72] The intrinsic electromagnetic properties of GNPs could also be harnessed towards the development of probes for fluorescence, photoacoustic and thermocoustic imaging.[73] Despite promising applications of graphene, compared to CNTs and fullerenes, fewer studies have assessed the *in vitro*, and *in vivo* biological effects of graphene nanoparticles. Moreover, no study till date has reported systematic formulation development of graphene for biomedical application.

Research Question

Current clinical CAs are suboptimal, especially at higher magnetic fields (>1.5 Tesla) for advanced MRI applications such as blood pool, cellular and molecular imaging. Theoretically, it is to develop new CAs with relaxivities up to 100X greater (depending on the magnetic field) than current clinical CAs. Additionally, the recent discovery of GCBCAs being associated to NSF has led to FDA restriction on their use in patients with renal insufficiency. Thus, there is a need for a T_1 MRI CA that is safer and more efficacious than clinical Gd^{3+} chelate-based agents. In this regard, the CAs employing Mn^{2+} ions have again received attention and have been proposed as a possible alternative of Gd^{3+} chelate-based agents. Over the past decade, synthesis strategies of covalently or non-covalently functionalizing Gd^{3+} chelate into various carbon nanostructures such as carbon nanotubes, fullerenes and nanodiamonds have shown between two-fold to two-order increase in relaxivity compared to GCBCAs. These studies have laid the foundation for providing nano-confinement of paramagnetic ion in carbon nanostructure as a general strategy to amplify the relaxivity of CA. However, the potential of Mn^{2+}-ion carbon nanostructure complexes as an MRI CA is yet to be investigated. The overall objective of this research is to develop Mn^{2+}- ion-graphene based nanoparticles as a next generation safer and high efficiency MRI CA. The high relaxivity may allow the development of MRI CAs that show the same clinical MRI performance at substantially lower dosages, and could also allow advanced applications such as MRI CAs for blood pool imaging, cellular, and molecular imaging.

Specific Aims

To achieve the research goal, the specific aims proposed are:

<u>Specific Aim 1</u>: To develop dextran functionalized graphene nanoplatelets (Mangradex) formulation for *in vivo* application.

Mangradex nanoparticles were synthesized and their physicochemical characteristics size, morphology and composition were studied. The Mangradex dispersion was prepared in distilled deionized water and essential formulation characteristics for intravenous injection - stability, osmolality, viscosity, partition co-efficient, protein binding and allergic response (by measuring histamine release) were tested.

<u>Specific Aim 2</u>: To investigate acute and sub-acute toxicity, toxicokinetics and pharmacokinetics of Mangradex *in vivo* following intravenous injection.

Mangradex acute toxicity was investigated following intravenous injection at graded dosages 1-500 mg/kg in Wistar rats. Sub-acute toxic effects were studied following intravenous injection at dosages 1, 50 and 100 mg/kg 3 times per week for three weeks. The toxic effects were evaluated by histology, cardiac safety pharmacology, blood chemistry, bio-distribution and pharmacokinetics.

<u>Specific Aim 3</u>: **To investigate the *in vitro* and *in vivo* efficacy of Mangradex as MRI Contrast agent**.

The *in vitro* efficacy of Mangradex was investigated by relaxometry and MRI phantom. The *in vivo* efficacy was evaluated at 7 Tesla magnetic field strength in healthy mice and in 5/6 Nephrex rat model of renal failure.

Each aim will correspond to the consecutive chapters.

Innovation and Impact

There are several innovative aspects involved in all the three aims of this research work, which are listed below.

1) Successful completion of this project will provide key insights and the scientific foundation to develop graphene based formulations suitable as the next generation MRI CA.
2) This study will provide better understanding of the biocompatibility of graphene for biomedical application that requires their IV injection. This is the first systematic and comprehensive study on graphene to find the maximum tolerable dose, acute and sub-acute toxicity with safety pharmacology.
3) The results of specific aim 1 and 2 on physicochemical characterization and toxicity can provide understanding for the preclinical development of nanotechnology based products.
4) The chemical composition, structure, size and the *in vivo* pharmacokinetic properties greatly affect the bioavailability of any drug. The results of specific aim 2 and 3 will provide substantial information on the degree and location of the contrast and will largely determine the use of dextran functionalized graphene as an MRI CA in specific diagnostic tests.

CHAPTER 2

SYNTHESIS, CHARACTERIZATION AND FORMULATION DEVELOPMENT

Abstract

The aim of this chapter is to perform important physicochemical characterization to design an intravenous administration regimen for Mangradex. Graphene nanoplatelets were synthesized by oxidizing graphite using modified Hummer's method in the presence of $KMnO_4$ and functionalized with FDA approved polymer dextran to impart water solubility. Further, Mangradex was characterized for size and morphology by TEM, atomic force microscope (AFM) and Nanoparticle tracker and for component analysis using thermogravimetric analysis (TGA) and Inductive coupled plasma mass spectrometry (ICP-MS). We then assessed six key *in vitro* physicochemical properties required for the regulatory approval of MRI CAs: osmolality, viscosity, partition coefficient, protein binding, thermo-stability and allergy response. Our results indicate that Mangradex are disk shaped nanoparticle with average size ~100 nm and a stack of 3-4 layers of graphene sheets. Manganese is intercalated by 0.1 % w/w and graphene:dextran weight ratio is 3:2. Further, at concentrations between 0.1-100 mg/ml, the Mangradex formulations are hydrophilic, highly water dispersible, and stable in deionized water, as well as iso-osmolar (upon addition of mannitol) and iso-viscous to blood. At potential steady state equilibrium concentrations in blood (0.1-10 mg/ml), the thermo-stability, protein binding, and histamine release studies indicate that the Mangradex formulations are thermally stable with no Mn^{2+} ions dissociation, do not allow non-specific protein adsorption, and elicit negligible allergic response.

Introduction

The two dimensional carbon nanostructure, graphene has attracted a great deal of attention for biomedical applications owing to its unique physicochemical properties.[74] Chapter 1 highlights several areas for biomedical application of graphene. Graphene is hydrophobic and hence, for

biomedical application the major challenge is to develop a suitable intravenous formulation for delivering high doses while minimizing the risk of precipitation upon injection into the blood. Hence, to translate into the clinic, the hydrophobic graphene nanoplatelets need to be water-solubilized at much higher concentrations (in the range of tens of mg/ml) with suitable biocompatible moieties, and their stability needs to be ensured at these high concentrations in biological media or blood.

FDA guidelines on pharmaceutical development suggest that the formulation should be optimized such that it does not cause any adverse effects when administered intravenously and throughout the period of its bio-retention.[75] Therefore, *in vitro* and *in vivo* preclinical assessment of the water-soluble graphene oxide nanoplatelet formulation's physicochemical characteristics, toxicity and efficacy is necessary according to the FDA guidelines.[76-78]

As a first step towards formulation development, we have synthesized and characterized Mn^{2+} intercalated graphene nanoplatelets non-covalently functionalized with the natural polymer dextran (hereafter, called Mangradex), and have assessed eight key *in vitro* physicochemical properties (osmolality, viscosity, partition coefficient, protein binding, thermo-stability, histamine release) required by the FDA during an investigational new drug (IND) application of MRI CAs for approval to perform first-in-human trials.[76-78]

Materials and methods

Synthesis of Mangradex

The Mn^{2+} intercalated graphene oxide nanoplatelets (GNPs) were prepared according to the previously described method.[51] The GNPs were non-covalently functionalized with dextran (technical grade, MW 10000 Da) to synthesize Mangradex as follows. GNPs and dextran were mixed in distilled deionized (DDI) water at a 1:10 weight ratio, and bath sonicated for 30 minutes followed by the addition of ammonium hydroxide (NH_4OH). The mixture was then stirred at 95^oC for 3 hours. Next, the particles were centrifuged at 1000 rpm for 15 minutes, and the supernatant was carefully transferred into falcon tubes to obtain water soluble Mangradex. The supernatant was lyophilized and the solid powder was resuspended in DDI water at desired concentrations. The Mn^{2+} ions concentration in Mangradex was measured by inductively coupled plasma mass spectrometry (ICP-MS) and Mn^{2+} weight percent in the Mangradex was measured to be 0.064%. Mannitol (Sigma Aldrich, M8129, St. Louis, MO) was added to the Mangradex solutions to regulate the osmolality within the range of blood (290 – 320 mOsm/kg).

Characterization of Mangradex

Transmission Electron Microscopy (TEM)

TEM was performed using JOEL 2100F high-resolution and JOEL 1400 transmission electron microscope (HR-TEM) at the Center for Functional Nanomaterials, Brookhaven National Laboratory. The Mangradex solutions (1 mg/ml) were sonicated for 1 minute, and centrifuged at 5000 rpm for 5 minutes. A drop (10 µl) of the resulting supernatant was dropped on TEM grids (300 mesh size, holey lacey carbon, Ted Pella), dried, and imaged at 200 kV accelerating voltage.

Atomic Force Microscopy (AFM)

Mangradex solutions after sonication and centrifugation (5000 rpm, 5 minutes) were spin coated at 3000 rpm for 5 minutes on freshly cleaved silicon wafers (Ted Pella). V-shaped cantilever of frequency f_c = 145-230 kHz, L = 225 µm, W = 40 µm, tip radius < 10 nm and spring constant k = 20-95 *N/m* (APP Nano ACL - 10) was used. Samples were imaged using a NanoSurf EasyScan 2 Flex AFM (NanoScience Instruments Inc., Phoenix), operating in tapping mode under ambient conditions (50% relative humidity, 25°C).

Thermogravimetric Analysis (TGA)

TGA was performed on GNPs, dextran (MW 10000 Da) and Mangradex using Perkin Elmer Diamond 500 instrument at Brookhaven National Laboratory, NY. The samples were heated from 50^{o}C to 700^{o}C with the heating rate of 10^{o}C /min under the air flow of 100 ml/min.

Elemental Analysis

The Mangradex samples were analyzed by ICP-MS (Finnigan ELEMENT 2, Thermo Scientific) to determine the concentration of Mn^{2+} ions. For the ICP analysis, liquid Mangradex samples (known concentration) were treated with concentrated nitric acid HNO_3 and carefully heated to obtain a solid residue. This residue was next treated with 30% H_2O_2 and heated again to remove any carbonaceous material. The remaining non-carbonaceous solid residue was dissolved in 2% HNO_3, and analyzed by ICP-MS.

Stability

The stability of the Mangradex solution was assessed at concentrations 100, 50, 20, 10 and 0.4 mg/ml (as indicated by settling of the nanoparticle) with respect to time. A freshly prepared solution of Mangradex of 1 ml in scintillation vial and digital photographs were taken at 10 min, 1, 2, 4 and 24 hours after preparation of solution.

Osmolality

The osmolality of 300 µl Mangradex solutions at concentrations 100, 50, 20, 10 and 0.4 mg/ml were measured using a freezing point depression osmometer (Advanced Instruments, model # 3D3, Norwood, MA). Mannitol, an osmotic diuretic agent was added to adjust their osmolality to obtain values similar to that of blood.

Viscosity

The viscosity of the Mangradex formulations at concentrations 100, 50, 20, 10 and 0.4 mg/ml and sample volume of 700 µl was measured using a Brookfield rotating spindle viscometer (Brookfield DV-I Prime Digital Viscometer, Middleboro, MA) at 37^{o}C.

Partition co-efficient

The partition coefficient was measured using the well-established flask-shaking method.[79] Briefly, 100 µl of 20 mg/ml Mangradex solution was added to a falcon tube that contained 1-octanol/ distilled deionized water (DDI) mixture (1 ml each phase, n = 3). The two phases were thoroughly mixed by vigorously shaking the falcon tube for ~ 30 seconds. The falcon tube was then kept still for 120 minutes at room temperature to allow the two phases to separate. Aliquots of the aqueous

phase were removed after 145, 205, and 255 minutes. The concentration of the nanoparticles in aqueous phase was determined using UV-Vis spectrophotometry (Thermo Scientific, EVOLUTION 300, Madison, WI) at 254 nm wavelength. The partition coefficient (P_{ow}) was calculated as logarithm of the ratio of the Mangradex concentrations in octanol to water phase as follows.

$$\log P_{ow} = \log ([\text{nanoparticles}]\ \text{octanol} / [\text{nanoparticles}]\ \text{DDI water})$$

Protein binding

Protein binding was studied using micro equilibrium dialyzer chamber (MB 74-1610, Harvard Apparatus, MA). The protein human serum albumin (HSA) and Mangradex (500 µl each) at the concentrations of 0.1, 1, 10 mg/ml, (n = 3 per concentration) were pipetted into two separate chambers of the dialyzer. The two chambers were partitioned by a cellulose acetate membrane (100kDa, MWCO). The dialysis chamber was allowed to equilibrate at 37^{o}C in an incubator for 24 hours. The samples from each chamber were removed after 24 hours. The equilibrated concentration of HSA in both the compartments was quantified by colorimetry using bicinchoninic acid assay (BCA Pierce® BCA Protein Assay Kit, Thermo Scientific, Rockford, IL) at 562 nm, using a plate reader (Tecan, Infinite M200, Morrisville, NC).

Thermostability

The thermal stability of the intercalated Mn^{2+} ions in the Mangradex formulations was characterized at physiological temperature (37^{o}C), and compared with the concentration of free Mn^{2+} ions in the formulation at room temperature (25^{o}C). 1 ml Mangradex solutions at 20, 50 and 100 mg/ml concentrations were incubated at 25^{o}C and 37^{o}C for 24 hours, followed by

centrifugation at 7000 rpm for 10 minutes. The supernatants were analyzed for the presence of free Mn^{2+} ions using sodium bismuthate ($NaBiO_3$) assay.[51] A standard optical absorbance vs. concentration curve was prepared with known concentrations of potassium permanganate ($KMnO_4$), which has distinctive pink color, using UV-Vis spectrophotometry at 578 nm. This standard curve was used to obtain the unknown concentration of permanganate (MnO^{4-}) ions produced by the sodium bismuthate reaction by measuring the absorbance values at 578 nm. This value allowed the determination of the concentration of free Mn^{2+} ions in the supernatant of Mangradex formulations.

Histamine release

Histamine release was measured using Histamine ELISA kit (Immunobiological Laboratories # IB89128, Minneapolis, MN) on heparinized whole human blood (BioChemed, 10761WB-SH-FI, Winchester, VA). The assay was performed according to the protocol provided by the supplier. Mangradex solutions at concentrations of 0.1, 1 and 10 mg/ml (200µl) and control (200µl) (provided with the kit) were first incubated with blood (200 µl) at 37ºC for 60 min. The samples were centrifuged at 700 x g for 10 min and 50 µl of supernatant from each sample was transferred into a reaction plate (provided with kit) for acylation. In the reaction plate, the samples were incubated with 25 µl of acylation reagent (converts any released histamine into N-acylhistamine) for 45 min at room temperature. Acylated controls and test solutions (Mangradex) (25 µl each) were incubated with histamine antiserum (100µl) in histamine microtiter strips (provided with the kit, with solid phase histamine bound to the wells) overnight at 4ºC. The following day, after discarding the content of the well, and rinsing the well with wash buffer (provided with the kit), the wells treated with 100 µl of enzyme conjugate at room temperature for 30 min. Next, the

content of the wells were again discarded, and each well was rinsed with wash buffer. 100µl of stop solution (provided with the kit) was added in the wells, and the absorbance readings were taken at 450 nm with reference wavelength of 630 nm, using an ELISA reader (Tecan, Infinite M200, Morrisville, NC).

Results

Size and morphology

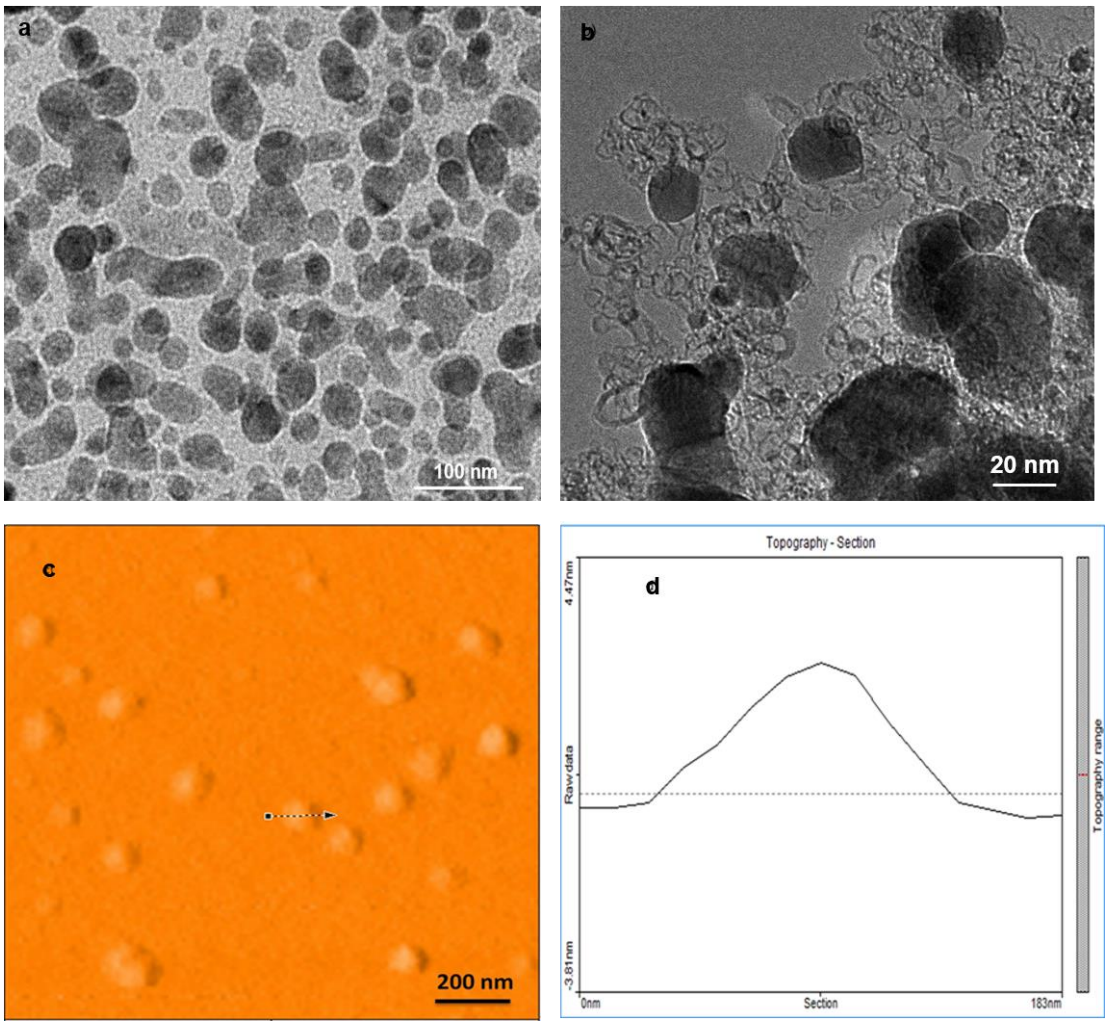

Figure 7. *Representative* ***a)*** *low magnification and* ***b)*** *higher magnification TEM images,* ***c)*** *AFM image of Mangradex,* ***d)*** *AFM thickness profile of Mangradex.*

Figure 7 shows the TEM and AFM images of Mangradex, and provides its structural and morphological information. The low and high resolution TEM images (**Figures 7a and b**) show that Mangradex are disc shaped nanoparticles and a coil-like structure surrounding the GNPs indicate that the dextran uniformly coats the GNPs. The size of the GNPs in Mangradex as seen in **Figure 7a** are in the size range 20-40 nm, while the size of GNPs with dextran coating is ~100-120 nm (**Figure 7b**). Further, the thickness of the Mangradex complex determined by AFM (**Figures 7c and d**) was ~ 3-4 nm.

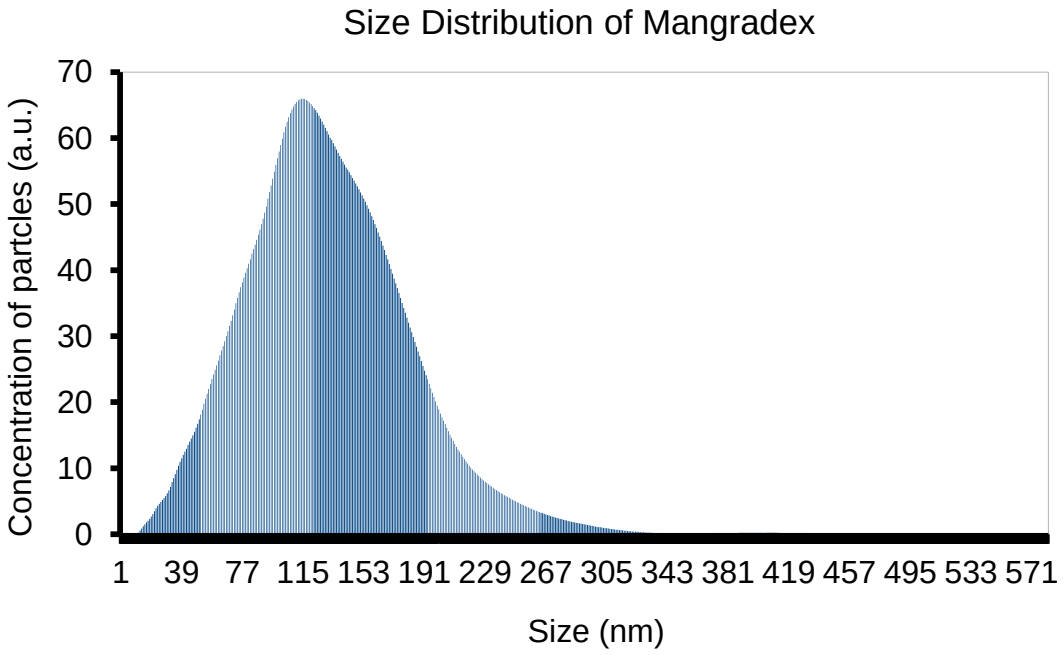

Figure 8*. Nanoparticle tracking analysis of Mangradex.*

The size distribution of the Mangradex was independently verified by nanoparticle tracking analyzer. **Figure 8** demonstrates histogram profile of size (nm) *vs*. particle concentration**.** As seen from the figure, the maxima of the graph is at 115 nm, suggesting maximum number of nanoparticles have size ~115 nm.

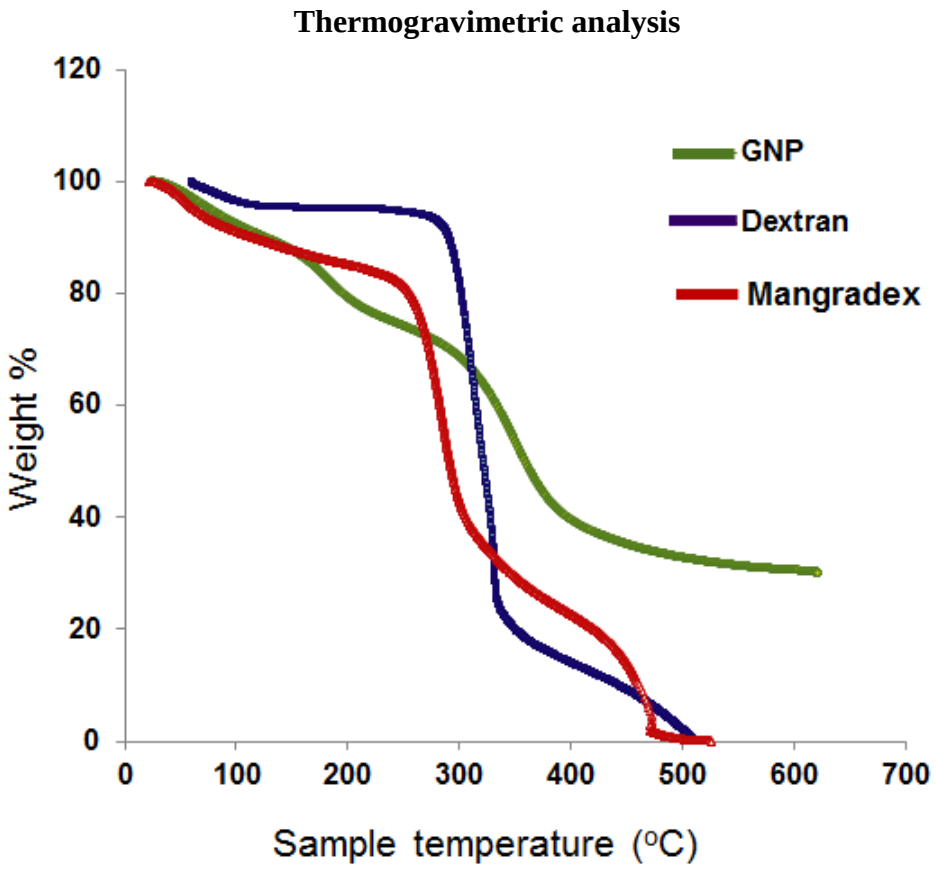

Figure 9. *Representative TGA curve of GNP, dextran and Mangradex.*

Figure 9 shows TGA spectrum of the Mangradex formulation. Also included for comparison are TGA spectra of GNPs, and dextran. The TGA spectra of the GNPs show weight loss of 10% between 10-150°C due to the loss of adsorbed moisture. The weight loss of 20% between 150-200°C can be attributed to the pyrolysis of carboxyl or hydroxyl groups.[52] The dextran curve exhibits 80-90% weight loss between 300-350°C, which is the characteristic decomposition temperature of the polysaccharides.[80] Comparing the thermogram of Mangradex with that of GNPs, and dextran gives information about its composition and chemical modifications. Mangradex thermogram shows 10% weight loss at 100°C due to loss of moisture. The 10% weight loss of Mangradex in the region between 150-200°C is due to loss of the labile oxygen containing

groups.[52] This value is lower than % weight loss observed for the GNPs in this region, which suggests partial reduction of the GNPs during the functionalization with dextran. The 40% weight loss between 250-350^{o}C indicates the presence of the dextran, and implies that Mangradex contains dextran at 40% by weight.

Solubility and stability of formulation

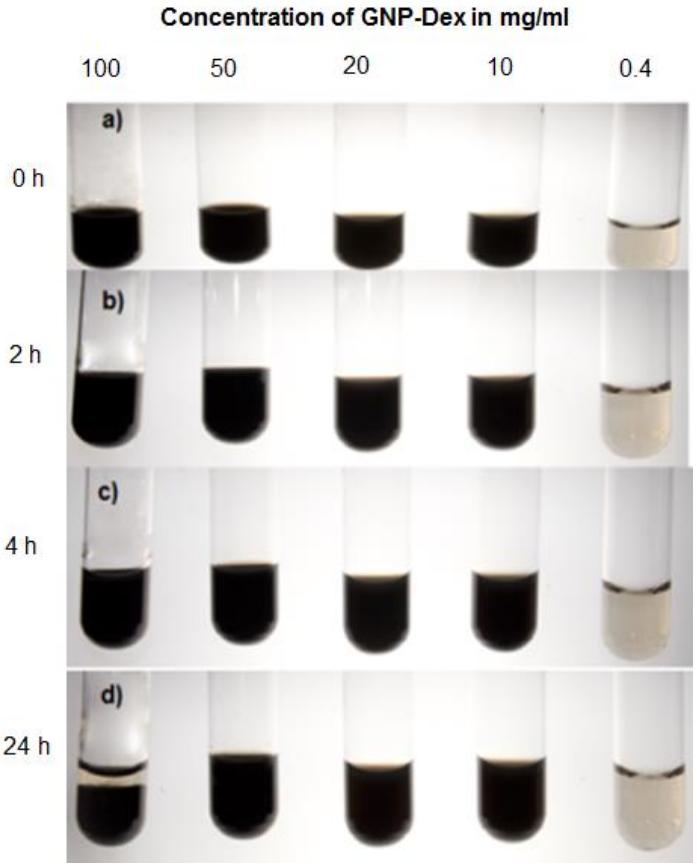

Figure 10. *Digital images of vials containing Mangradex in water (with mannitol) at 100, 50, 20, 10, 0.4 mg/ml concentrations at* ***a)*** *0 hour* ***b)*** *2 hours* ***c)*** *4 hours* ***d)*** *24 hours after preparing the solutions.*

Figure 10 shows digital photographs of Mangradex solutions at 0.4, 10, 20, 50 and 100 mg/ml concentrations (containing mannitol) at 0, 2, 4 and 24 hours after preparation of the solutions. As evident from the images, the solutions at all concentrations are stable up to 4 hours. At 24 hour

time point, the Mangradex solution at 100 mg/ml concentration separated out. However, it could be easily and uniformly redispersed by gentle shaking of the solution.

Osmolality and Viscosity

Concentration (mg/ml)	Osmolality (mOsm/kg) (before addition of mannitol)	Osmolality (mOsm/kg) (after addition of mannitol)
100	33±0.5	306.7±1.5
50	17± 0.3	296±0.0
20	5±0.2	297.7±0.6
10	5±0.1	289.7±1.5
0.4	3±0.0	303±0.0

Table 3*. Osmolality of Mangradex in DDI water before and after the addition of mannitol*

Concentration (mg/ml)	100 rpm (cP)	50 rpm (cP)	20 rpm (cP)
100	ND	2.45	4.46
50	2.37	3.68	2.82
20	1.35	1.39	1.69
10	1.6	2.1	ND
0.4	2.30	3.8	ND

Table 4. Viscosity of Mangradex at different concentrations at 37^{o}C, ND- not determined

Tables 3-8 show the results of key physicochemical properties such as osmolality, viscosity, partition coefficient, protein binding, histamine release, and relaxivity. Osmolality of an MRI CA is an important property that depends on the solute concentration. **Table 3** displays the osmolality values of Mangradex solutions at concentrations between 0.4-100 mg/ml in the absence and presence of mannitol. The results show that the osmolality of the Mangradex increases with increase in concentration. However, the Mangradex formulations are hypo-osmolar at all concentrations (normal blood osmolality = 285 - 295 mOsm/kg of H_2O).[81] Addition of mannitol

increases the osmolality values for all Mangradex concentrations, and these formulations are within the osmolality range observed for normal blood.

Table 4 shows the viscosity of the Mangradex solutions at concentrations between 0.4-100 mg/ml at 37°C. The viscosity values at all concentrations were less than or within the range of blood viscosity (between 3-4 cP at 37°C). The viscosity of the Mangradex solutions were also dependent on shear rate at all concentrations, which suggests that Mangradex solutions at these concentrations behave as a non-newtonian fluid, similar to whole blood.[82]

Partition co-efficient

Parameter	Results	Condition
Partition Coefficient (log P_{ow})	-0.18	20 mg/ml, at 25°C
Protein Binding	< LOD (0.001 mg/ml)	0.1, 1, 10mg/ml at 37°C
Released free Mn^{2+} ions	< LOD (0.01 µM)	20,50,100mg/ml at 37°C
Histamine Release	< Negative control	0.1, 1,10 mg/ml at 25°C

Table 5*. Physicochemical properties of Mangradex*

The partition coefficient of the Mangradex at concentrations 0.1, 1 and 10 mg/ml was calculated to be -0.18 (**Table 5**). This value is comparable to the values reported for clinical MRI CAs developed as extra-vascular agents (**Table 9**). Visual analysis also showed that majority of the Mangradex nanoparticles separated into the aqueous phase, or stayed at the aqueous-octanol interface, and could not be detected in octanol phase. No UV-Vis spectra of the Mangradex nanoparticles in octanol phase could be obtained indicating that the nanoparticles if present were below the detection limit of the instrument.

Protein binding

Concentration of Mangradex (mg/ml)	Concentration of unbound protein in protein compartment (mg/ml)	Concentration of unbound protein in Mangradex compartment (mg/ml)
0.1	0.03	0.03
1	0.55	0.07
10	5.44	0.53

Table 6: *Concentration of unbound protein measured by UV-Vis spectrophotometer at equilibrium.*

Equilibrium dialysis of MRI CA with the protein human serum albumin (HSA) followed by BCA protein assay is one of the most widely-accepted methods to study protein-drug interaction.[83,84] The results (**Table 6**) of the protein binding summarized in **Table 5**, show that HSA protein was not bound to the Mangradex formulations.

In equilibrium dialysis method, at equilibrium, if no protein is bound to the material of interest, the distribution of unbound (free) protein has to be equal (i.e. 0.025 mg/ml, 0.25 mg/ml and 2.5 mg/ml of HSA in each compartment for 0.1, 1 and 10 mg/ml initial concentration of HSA respectively) at the end of equilibrium in both HSA and Mangradex solution compartments. If the protein is binding to the Mangradex, the remaining unbound protein will be distributed equally in both compartments. At equilibrium, 400 µl solutions were retrieved (initial volume 500 µl) from both compartments and were used to measure unbound protein concentration (**Table 6**). The concentration of unbound HSA at the end of 24 hours incubation with nanoparticles, as measured by UV-Vis spectrophotometer at 562 nm did not decrease, which implies that no protein was bound to Mangradex.

Stability with time and temperature

Sample	Concentration Mn^{2+} (µM)
Mangradex (20 mg/ml)	< LOD (0.01µM)
Mangradex (50 mg/ml)	< LOD (0.01µM)
Mangradex (100 mg/ml)	< LOD (0.01µM)

Table 7: *Concentration of released Mn^{2+} ions in Mangradex solutions at 37°C measured by UV-Vis spectrophotometer to determine thermal stability. There was no color change observed by sodium bismuthate ($NaBiO_3$) test in Mangradex solutions at 3 and 24 hours. The Mn^{2+} concentration measured by UV-Vis spectrophotometer was less than limit of detection (LOD).*

The thermal stability experiments (**Table 7** and summarized in **Table 5**) with Mangradex solutions, for 3 or 24 hours, at 20, 50 and 100 mg/ml concentrations, show no presence of free Mn^{2+} ions (limit of detection (LOD) = 0.01µM) at 37°C. The results indicate that Mn^{2+} ions present in the Mangradex formulation are stable at least short-term (24 hours) at simulated physiological temperature.

Histamine Release

Concentration of Mangradex (mg/ml)	Released histamine (ng/ml)
Control	19.8
10	8.80
1	5.59
0.1	5.59

Table 8: Concentration of released histamine in whole human blood in vitro measured after overnight incubation with Mangradex. *The histamine concentration in Mangradex was found to be lower than the control (not treated with Mangradex), which suggests that Mangradex does not trigger histamine release.*

Our results show no significant release of histamine at Mangradex concentrations of 0.1, 1 and 10 mg/ml compared to the control (**Table 8**).

FDA approved MRI CA	Osmolality (mOsm/kg of water)	Viscosity (cP) at 37°C	Partition Coefficient (log P_{ow})	Protein binding
Prohance[41]	630	1.3	-3.6800	None
Multihance[42]	1970	5.3	0.0016	<5%
Magnevist[43]	1960	2.9	-5.4000	None
Omniscan[46]	789	1.4	-2.1000	None
Teslascan[44]	290	0.7	-5.6200	Fodipir chelate (negligible), free Mn^{2+} ions (27%)
Optimark[45]	1110	2.0	-8.2200	None
Mangradex	290	2.4	-0.1800	None

Table 9. *Comparison of Mangradex solution physicochemical properties with clinical MRI CA*

Table 9 compares the values of various physiochemical properties of the Mangradex formulation with other FDA-approved MRI CAs.[6,41,85-88] Most Gd^{3+}-chelate based clinical MRI CAs are hyperosmolar, ranging in values from 630-1970 mOsm/kg,[6,41,85-88] while Mn^{2+}-chelate-based MRI CA Teslascan and iron oxide nanoparticle-based MRI CA Feridex are iso-osmolar.[89] The Mangradex formulations in the presence of mannitol are iso-osmolar over wide range of concentrations (0.1-100 mg/ml). The viscosity values of 1.3–4.4 cP for Mangradex formulations are within the range measured for blood, and are similar to other MRI CAs. Comparison of the partition coefficient value of -0.18 for the Mangradex formulation to clinically approved MRI CAs indicates that, it could be less hydrophilic than Magnevist, Prohance, Omniscan, Teslascan and Optimark, and more hydrophilic than Multihance. Most of the clinical MRI CAs show insignificant protein binding except Multihance and Teslascan. Multihance shows less than 5% of plasma protein binding.[85] In case of Teslascan, the chelate fodipir does not bind to the protein, however,

the Mn^{2+} ions, after dissociating from the chelate show 27% protein binding in whole human blood *in vitro*.[87] The Mangradex did not show significant protein binding.

Discussion

The overall objectives of the studies reported were to: (1) synthesize and characterize water-soluble graphene nanoplatelet formulations that are stable at high concentrations in biological media and blood, (2) Characterize key *in vitro* physicochemical properties of the water-soluble GNPs based on FDA guidelines and investigations performed on other MRI CAs during their translation into clinic.[76-79,90] Concentrations up to 100 mg/ml were used in the studies since, future *in vivo* pre-clinical safety and efficacy studies would require their administration at high dosages (up to possibly 500 mg/kg body weight of the animal) to determine the lethal and therapeutic dosages. Our estimates (see appendix) indicate that to achieve these *in vivo* dosages, stock nanoparticle solutions with concentration as high as 100 mg/ml will be needed. For some physicochemical characterization studies, concentrations between 0.1-10 mg/ml were used, which correspond to their steady state equilibrium concentration in the blood (volume = 12-13 ml) of a rodent (weight ~ 200 g) after the first pass, if the Mangradex formulations are injected intravenously at dosages between 1-500 mg/kg.

The hydrophobic GNPs were non-covalently functionalized with dextran, since previous reports show that it imparts good water solubility to graphene nanoparticles.[62] Additionally, dextran has been used for a number of biomedical applications, including the development of the experimental Gd^{3+}-based,[91] and clinical iron oxide-based MRI CAs.[92] Furthermore, dextran is non-fouling,[93]

could prevent non-specific interactions, as well as, prolong blood circulation half-life *in vivo*;[91] these are essential features for potential advanced MRI applications such as blood pool imaging.

Water being the solvent for the formulation of Mangradex, all physicochemical characterization was carried out in water. An important consideration during *in vivo* administration of Mangradex formulations is that they remain stable long enough for the dose to be poured out and injected.[94] In general, settling is considered a significant issue if the solute cannot be easily and uniformly redispersed.[94] The results indicate that, provided the Mangradex formulations at various concentrations are prepared fresh, and administered immediately, or solutions (especially at very high concentrations) kept for extended period of time are gently shaken, the Mangradex formulations are suitable as stock solutions for *in vivo* administration. The higher stability of the formulations in water can be attributed to the uniform coating of dextran on GNPs, which counteracts the hydrophobic forces exerted by the GNPs that can lead to aggregation.

To the best of our knowledge, this is the highest level of solubility achieved for any water-solubilized graphene nanoparticle. An MRI CA needs to exhibit excellent solubility even at high concentrations to achieve the dose required for bolus injection (the clinical dose of a Gd^{3+} chelate-based MRI CAs can be between 1-100 mg/kg).[95] Additionally, an important consideration is that the water-solubilizing moieties also need to be biocompatible. Different covalent, and non-covalent functionalization approaches have been employed to water-solubilize graphene nanoparticles.[74] Graphene nanoparticles have been covalently functionalized with carboxylic acid, hydroxyl,[96] poly-L-lysine,[97] and non-covalently functionalized with synthetic polymer polyethylene glycol (PEG),[74] or pluronic F127.[51] The maximum solubility reported for these

functionalization approaches has been between 1-2 mg/ml. Recently, graphene nanoparticles have been covalently conjugated with the natural polymer dextran with maximum water solubility of 1 mg/ml.[60,62,98] At the concentration of 1 mg/ml, the volume needed to be injected for *in vivo* small animal safety studies to achieve the above dosages (1-100 mg/kg), would be up to 1.56 to 156.25% of the total blood volume (estimated based on a 200 g rat with total blood volume of ~ 12.8 ml, see appendix), or 1.4 - 140% of the total blood volume (5 liter, of an adult human weighing 70 kg, see appendix for calculation), which is not feasible at higher doses. The Mangradex formulations not only show substantially greater solubility than the other approaches, but are also stable in physiologically-relevant fluids. Additionally, at high concentrations (e.g. 50-100 mg/ml), the Mangradex can be injected at ~4-8% of the rat blood volume to achieve bolus dosages between 50-500 mg/kg, which is practical.

Mannitol is an additive routinely used in osmotherapy as a diuretic agent, and has been employed for the clinical iron oxide based MRI CA Ferridex to maintain its osmolality at 340 mOsm/kg.[82,92] Adverse effects of low or high osmolality (compared to blood osmolality) contrast media include changes in circulatory system such as vasodilation, vasoconstriction, crenation of RBCs, and release of vasopressin.[76,99] Clinically, these changes manifest as sensations of warmth, heat and pain at the site of injection.

Viscosity of the MRI CAs depend on its chemical structure, concentration and temperature.[100] The viscosities of the MRI CA solutions affect its rate of injection and *in vivo* flow characteristics. MRI CAs with viscosity values higher than that of blood typically cannot be injected intravenously as a bolus. They need to be injected at a slower rate. Higher viscosity MRI CAs have been shown

to cause deleterious effects on renal perfusion and renal output.[101] However, these effects can be mitigated by warming up MRI CA prior to its *in vivo* administration to lower its viscosity.[101] Studies show that MRI CAs with high viscosities (greater than that of blood), to a certain extent, affect the intrinsic and extrinsic coagulation cascade pathways, platelet function and vascular endothelial function[82], while low viscosity MRI CAs (lower than that of blood) do not substantially affect these hemodynamic parameters.[82]

The partition coefficient (P_{ow}) of an MRI CA provides a measure of its hydrophilicity and hydrophobicity.[76] These properties in turn, affect their *in vivo* biodistribution profile.[102] The results indicate that most of the Mangradex nanoparticles are hydrophilic, and preferentially accumulate in the aqueous phase, and a small fraction are amphiphilic accumulating at the water-octanol interface.

The propensity of MRI CAs to bind to the protein could affect its targeting capability, pharmacokinetics, and relaxivity.[76,102] The lack of protein binding onto Mangradex can be attributed to the non-fouling property of dextran,[93] and suggests that it could prevent non-specific interactions.

Thermal stability of the intercalated Mn^{2+} ions is a key physiochemical property. It is important to determine if the intercalated Mn^{2+} ions dissociate from the Mangradex nanoparticles and are present as free Mn^{2+} ions under physiological temperatures. Mn^{2+} ion, a natural cellular constituent, functions as a regulatory cofactor for enzymes and receptors.[34] Normal daily dietary requirement for manganese is 2.7-7 mg,[103] and normal serum levels are 0.1 µM.[104] However,

prolonged exposure of high concentrations of Mn^{2+} ions have been reported to be toxic, and result in Parkinson-like neurological disorder 'manganism' and cardiac dysfunction.[34,105] Therefore, it is critical to investigate whether the intercalated Mn^{2+} ions, at the physiological temperature of 37°C, dissociate from Mangradex nanoparticles. Typically, clinical first pass or blood pool CAs have been reported to have average blood half-lives of 1.5 hours, and >95% of the CA is excreted out in 24 hours.[106] Thus, the above results taken together with this information, suggest that provided the *in vivo* blood half-life and the elimination rate of the Mangradex formulations are similar, the intercalated Mn^{2+} ions should be stable within the graphene nanoplatelets *in vivo.* However, the long-term (> 24 hours) *in vitro* and *in vivo* thermal stability of these formulations still needs to be determined before a firm conclusion can be drawn.

It is well documented that MRI CAs can evoke adverse allergic reactions with symptoms that could include urticaria or hives-like inflammation, as well as, swelling and reddening of the tissues, watery eyes, runny nose, migraine headaches, nausea, vomiting, laryngospasm, and bronchospasm.[107-109] Histamine, a naturally occurring biomolecule found *in vivo*, is released as a response to allergic reactions,[109] and is considered to be a good marker to evaluate the propensity of MRI CAs to elicit an allergic response. These results are encouraging since, histamine can also stimulate fibroblast proliferation and collagen production, and can play an important role in skin fibrosis; a major symptom associated with NSF.[109] Studies on Gd^{3+} and Mn^{2+} chelate MRI CAs indicate that, at physiologically relevant plasma concentrations (0.1-10 mM), they do not exhibit propensity to release histamine.[109] At higher dosages (50-150 mM), Gd^{3+}-chelates complexes have been shown to release histamine *in vitro*.[109]

Conclusion

In conclusion, Mangradex formulations show very high solubility (up to 100 mg/ml) and stability in deionized water, and biological buffers. The osmolality of Mangradex is lower than that of blood, and can be adjusted to be similar to blood by the addition of the diuretic mannitol. The viscosities of the Mangradex formulations were within the range of blood viscosity. At physiological temperatures (37ºC), Mangradex was structurally stable and the intercalated Mn^{2+} ions did not dissociate for up to 24 hours. Most of the Mangradex nanoparticles were hydrophilic, and a small fraction was amphiphilic. At potential therapeutic dosages, Mangradex showed very little or no interaction with blood protein HSA, suggesting that they prevent non-specific adsorption of proteins. The formulations also did not trigger histamine release in whole human blood, suggesting that they are unlikely to evoke allergic responses. The *in vitro* results show that the physicochemical properties of Mangradex were comparable or better than clinically approved MRI CAs.

CHAPTER 3

ACUTE AND SUB-ACUTE TOXICITY, SAFETY PHARMACOLOGY AND PHARMACOKIENTICS

Abstract

The aims of this study were to examine toxic effects of Mangradex following acute and sub-acute IV injections and to find the dose that can be injected without any potential adverse effect and to evaluate bio-distribution and pharmacokinetics. For acute toxicity study Wistar rats were injected at 1, 25, 50, 100, 250 or 500 mg/kg dose and monitored short term t = 1 day (n=6 /dose), or long term i.e. t =30 days (n=8 animals) for morbidity, mortality, basic vital and cardiovascular parameters. At the end of the study period, histology and clinical blood chemistry were performed. For the sub-acute toxicity, rats were injected with Mangradex at 1, 50 or 100 mg/kg for 3 days/week for three weeks. The results indicate that for acute toxicity study, the maximum tolerated dose (MTD) for Mangradex formulation was $50 \leq MTD < 125$ mg/kg. Animals did not show any toxic effects in terms of behavior and basic vital parameters such as heart rate, blood pressure, respiration and other important cardiac parameters up to 50 mg/kg. Histology changes were noted at ≥ 250 mg/kg in the heart, liver, lung, spleen, and kidney; we found no changes in the brain and no Mangradex related effects in the cardiovascular parameters or hematological factors (blood, lipid, and metabolic panels) at doses < 125 mg/kg. For sub-acute study, our results indicate that MTD for Mangradex following repeated injection is 50 mg/kg. At 100 mg/kg dose, Mangradex caused mortality in 2/8 animals following 4 or 5 injections. Necropsy performed on these animals showed dark pigment in lungs suggestive of the presence of Mangradex nanoparticles. In the surviving animals at all dosages, Mangradex formulation did not induce any observable toxicity in histology, cardiovascular (blood pressure and heart rate) and clinical blood chemistry parameters (lipid panel, metabolic panel and serum chemistry).

Introduction

Graphene nanoparticles dispersions show immense potential as multifunctional agents for *in vivo* biomedical applications. Carbon nanostructures such as fullerenes, metallofullerenes and carbon nanotubes have been widely investigated as multifunctional materials for applications in tissue engineering, molecular imaging, therapeutics, drug delivery, and biosensing.[110-112] Recently, graphene nanoparticles, (also known as graphene nanoplatelets (GNPs) or simply graphene oxide (GO), (herein referred as GNPs)) show promise *in vitro* and *in vivo* for drug/gene delivery and biological sensing/ imaging applications.[60,63,66,113] There is now a wide body of research documenting the toxicology and pharmacology of fullerenes, metallofullerenes and carbon nanotubes (single-walled and multi-walled carbon nanotubes).[110-112,114] Relatively fewer studies have assessed the *in vitro*,[115-117] and *in vivo* [62,118] biological effects of graphene nanoparticles. These studies on the various carbon nanostructures evaluate their safety for the above healthcare applications, or environmental/ occupational health issues.[114,119,120] Reports to date show that the structure/shape (e.g. spherical, tubular, sheet-like), chemical composition (e.g. pristine, functionalized), synthesis method (e.g. chemical vapor deposition, oxidative exfoliation), and route of administration (e.g. intravenous, nasal) are key factors that influence toxicity and tissue response for carbon nanostructures.[74,111,112,114,121]

Intravenous (IV) administration is a widely employed and preferred mode of systemically introducing pharmaceutical formulations for imaging, drug delivery or therapy. IV injections were employed in a subset of toxicological investigations of carbon nanostructures for such biomedical applications.[62,110-112,122,123] In general, the maximum dosages of a test formulation in toxicity and biodistribution studies depend on concentration of the stock solution of the test formulation, and

the maximum solution volume (typically 2 ml/kg for bolus and 4 ml/kg for slow IV injections) that can be injected without causing adverse side effects to the animals.[124] Hydrophobic carbon nanostructures have typically been covalently or non-covalently functionalized with biocompatible moieties (functional groups, macromolecules) to improve water dispersibility and thus, allow higher doses. For small animal (rodents) toxicology studies that employed IV administration, the reported stock solution concentrations of water-dispersible carbon nanostructures are ≤ 10 mg/ml and maximum permissible doses (MPD) are in the units to low tens mg/kg range.[62,111,112,125,126] Additionally, for a given water-dispersed carbon nanostructure formulation, most investigations have focused on histology, and biodistribution, presenting little information on maximum tolerable doses (MTD), or assessment of other important issues such as respiratory and cardiovascular pharmacology safety. Consequently, the therapeutic indices of these formulations remain unknown. Furthermore, we found no published studies that explicitly followed the preclinical safety pharmacology guidelines of regulatory agencies such as the FDA in USA and the International Conference on Harmonization (ICH) in Europe which suggest assessing toxicity at least 10 to 100 times higher than the projected therapeutic dose.[127-130] Such studies are necessary to receive regulatory approval for first-in-human trials for any carbon nanostructure-based IV formulations for imaging, or therapeutic application.

According to FDA and ICH guidance documents, prerequisites for first-in-human trials of the Mangradex for IV biomedical applications (e.g. drug delivery or imaging contrast agent) include *in vivo* pre-clinical safety pharmacology studies in a rodent and non-rodent model. Thus, as a part of the preclinical *in vivo* safety pharmacology evaluation, here, we report dose response, expanded

acute and sub-acute toxicology, toxicokinetics, biodistribution and respiratory/cardiovascular safety pharmacology assessment of Mangradex in rats.

Materials and method

Animal care, dose ranges for acute and sub-acute toxicity studies

All the experiments were performed according to the guidelines of Institutional Animal Care and Use Committee at Stony Brook University, NY. Acute toxicity (1-day, n=6) and expanded acute toxicity (30-days, n=8) studies were performed at the doses of 1, 25, 50, 125, 250, 500 mg/kg on Wistar male rats weighing 200-250 g. Mannitol (at the concentration of 55 mg/ml added to the Mangradex formulation to control the osmolality) was used as a control. The animals were anesthetized using isoflurane (1-2.5% mixture of O_2/air, via inhalation). Single doses of Mangradex were administered intravenously via the tail vein and the animals were monitored for any adverse effects for 1-day or 30-days. After injection, animals were transferred into metabolic cages to collect urine and feces samples.

Transthoracic echocardiography and blood pressure measurement

Transthoracic echocardiography with Doppler was performed with a high-resolution imaging System (Visual Sonics, Vevo 770, Toronto, Canada) using a 30-MHz linear array transducer (RMV 707B). Mangradex doses of 1, 25, 50, 125, 250 and 500 mg/kg and mannitol were injected into Wistar rats (n=4 at each dose for 30-day expanded acute toxicity group) under anesthesia (1-2.5% mixture of O_2/air with isoflurane, via inhalation). Animals were placed on warming pads to maintain normothermia and their limbs were secured to electrocardiography sensors. Two-dimensional images were captured and recorded before injection as well as at 10 min and 2 hours

post injection in parasternal long- and short-axis projections with 2D guided M-mode recordings at the mid-ventricular level in both views. Left ventricular (LV) dimensions (mass, volume, wall thickness) were measured in the M-mode view and % fractional shortening was calculated. Additionally heart rate, respiration rate, blood velocity, ejection fraction were recorded for both systolic and diastolic phase. An aortic arch or parasternal view (that is as parallel as possible with the sound beam) was used to obtain the pulsed-wave Doppler image to measure the blood flow velocity through the aorta. Visual Sonics software was used to calculate and analyze the data. Blood pressure was measured using a non-invasive occlusion type tail cuff system (Coda 6, Kent Scientific System, PA) 10 min and 2 hour after administration of Mangradex in 1- day group during acute toxicity studies. For sub-acute study, blood pressure and heart rate were measured on days 1, 8 and 15 after administration of Mangradex.

Necropsy

Necropsies were performed on five rats deceased after Mangradex dose of 125, 250 and 500 mg/kg. The procedure was performed by Antech Diagnostics (New Hyde Park, NY). The outcomes and diagnosis from all the necropsies were similar. The pdf copy of one necropsy report titled “necropsy” is uploaded in appendix.

Histology

Tissue samples were initially fixed in 4% paraformaldehyde for 48 hours and were dissected into 3 mm segments. All organs were dissected symmetrically in the same manner to help ensure consistency. The tissues were then dehydrated in graded ethanol and paraffin-embedded. 5 μm sections were cut using a microtome and were stained with Hematoxylin and Eosin (H&E) for

histologic evaluation. Digital photomicroscopy was performed using a bright field microscope at 100X and 400X magnification. Histologic assessment of the tissue sections were performed by an experienced diagnostic and research anatomic pathologist (KRS).

Blood analysis

For acute toxicity, the animals were injected with Mangradex at doses of 25, 50 and 100 mg/kg (n=3 at each dose); dextran at doses 20 and 40 mg/kg (n=3 at each dose) and 55 mg/ml mannitol solution in water were used as controls. Animals were euthanized 1-day after injection and ~8 ml blood was collected from each animal by cardiac puncture for blood analysis. For sub-acute toxicity, animals at 1, 50, or 100 mg/kg dose (n=6, 3 male, 3 female) were sacrificed using 100% CO_2 inhalation on 22nd day (after 3 weeks) and blood was obtained by cardiac puncture technique. Serum chemistry test and complete blood panel analyses were performed in a Clinical Laboratory Improvement Amendments (CLIA) certified facility at Stony Brook University Hospital.

Biodistribution and elimination

One day and 30-day animals for the biodistribution studies received IV injections at 1, 25, 50, 125, 250, 500 mg/kg doses. Urine and feces samples were collected at 8 and 24 hours for the 1-day group, and daily up to a week for the 30-day group. Blood samples (~100 µl from tail vein) were collected at 0.5, 2, 4, 8 and 24 hours after injection for the 1-day group, and every 48 hours after injection up to one week post-injection for the 30-day group. At the end of the respective durations, animals were euthanized using 100% CO_2 and brain, heart, liver, lungs, spleen and kidneys were harvested. Mn^{2+} concentrations in the blood, urine, feces and various tissues were determined using

inductively coupled plasma mass spectrometry (ICP-MS) as described below. The % injected dose values in the blood, urine, feces or various tissues were calculated using the formula [[Mn^{2+} (experimental group)] - [(Mn^{2+} (sham control group)]]/ [Mn^{2+} (injected doses)].

ICP-MS

Blood, urine, feces and organs from different animals at the same dose from the same group (day 1 or day 30) were pooled together, and chemically digested using trace metal grade 70% nitric acid (HNO_3) (catalog # 02650, Sigma Aldrich, St Louis, MO), followed by trace metal grade 30% hydrogen peroxide (H_2O_2) (catalog # 95321, Sigma Aldrich, St Louis, MO) until only inorganic content was left. The digested samples were resuspended in trace metal grade 2% HNO_3 and filtered through a 0.2 µ pore size filter. Samples were analyzed for Mn^{2+} concentration by setting the mass window in the range of 54.8-55.4 atomic mass units using ICP-MS (Thermo, Finnigan ELEMENT 2) with 100 µl sample volume.

Sub-acute toxicity

The 21-day sub-acute toxicity study was conducted at three doses in a total of 44 Wistar rats (male and female) weighing 200-250g. Three groups of 8 rats (4 male and 4 female) had received Mangradex injections intravenously via the tail vein three times per week for three weeks at the doses of 1, 50 and 100 mg/kg of body weight. During injections the animals were anesthetized using isoflurane (1-2.5% mixture of O_2/air, via inhalation). Control groups were given IV injection of mannitol (55 mg/ml), and dextran (at the dose of 40 mg/kg, used for surface functionalization of GNP) according to the same dosing regimen as experimental group. The parameters evaluated included survival, clinical observations, body weight and diet observation. At the end of 3 weeks,

the animals were euthanized with 100% CO_2 and blood was collected using cardiac puncture for blood chemistry analysis. All the major organs (heart, lungs, liver, brain, spleen, and kidneys) from each animal were harvested and prepared for histology analysis. Blood chemistry and histology were performed with the same method mentioned above.

Statistical analysis

Data are expressed as mean ± SD. All data were analyzed for statistical significance by one-way analysis of variance (ANOVA) followed by a Tukey post-hoc test using statistical analysis software GraphPad Prism (GraphPad Software, Inc., La Jolla, CA). The criterion for statistical significance was $p \leq 0.05$.

Results

Acute toxicity

Dose responses

The acute toxicity study for Mangradex was performed in Wistar male rats in two studies. We injected Mangradex via the tail vein at doses between 1-500 mg/kg. One cohort (n=6/dose) was investigated for 1-day, and another one (n=8/dose) for 30-days.

	Mortality in animals (dead/total)							
Dose (mg/kg)	**500 µl/15 sec (dead/total)**				**500 µl/ 5 min (dead/total)**			
	1-day	**30-days**	**Total dead (day 1 and day 30 groups)**	**% of death**	**1-day**	**30-days**	**Total dead (day 1 and day 30 groups)**	**% of death**
Sham	-	0/4	0/4	0	0/6	-	0/6	0
1	-	0/8	0/8	0	0/6	-	0/6	0
25	-	0/4	0/4	0	0/6	0/4	0/10	0
50	-	-	-	-	0/6	0/8	0/14	0
125	3/6	0/4	3/10	30	-	0/4	0/4	0
250	1/1	1/4	2/5	40	0/5	3/4	3/9	33
500	4/6	0/4	4/10	40	-	1/4	1/4	25
Mannitol	1/6	-	1/6	16.67	-	0/4	0/4	0

Table 10. *Mortality observed in animals at injection rates 500 µl/ 15 sec and 500 µl/ 5 min at varying doses of Mangradex.*

As shown in **Table 1,** for the 1-day group, mortality occurred at ≥ 125 mg/kg rapid bolus doses, within ~2 min after Mangradex administration. In the 30-day groups, mortality occurred at ≥ 250 mg/kg rapid bolus doses, again within ~2 min after Mangradex administration. Necropsies suggested that the cause of the death was pulmonary congestion (See necropsy report in appendix). For both the day 1 and day 30 groups, the dosing rate of the Mangradex affected mortality observed at the higher doses (≥ 125 mg/kg). For instance, a rapid bolus (500 µl /15 sec) rate showed higher

mortality than a slower (500 µl/5 min) injection rate. There were no changes in the body weight, breathing, hunching or unusual interactions with cage mates following injection of Mangradex at any dosages in either cohort.

Histology

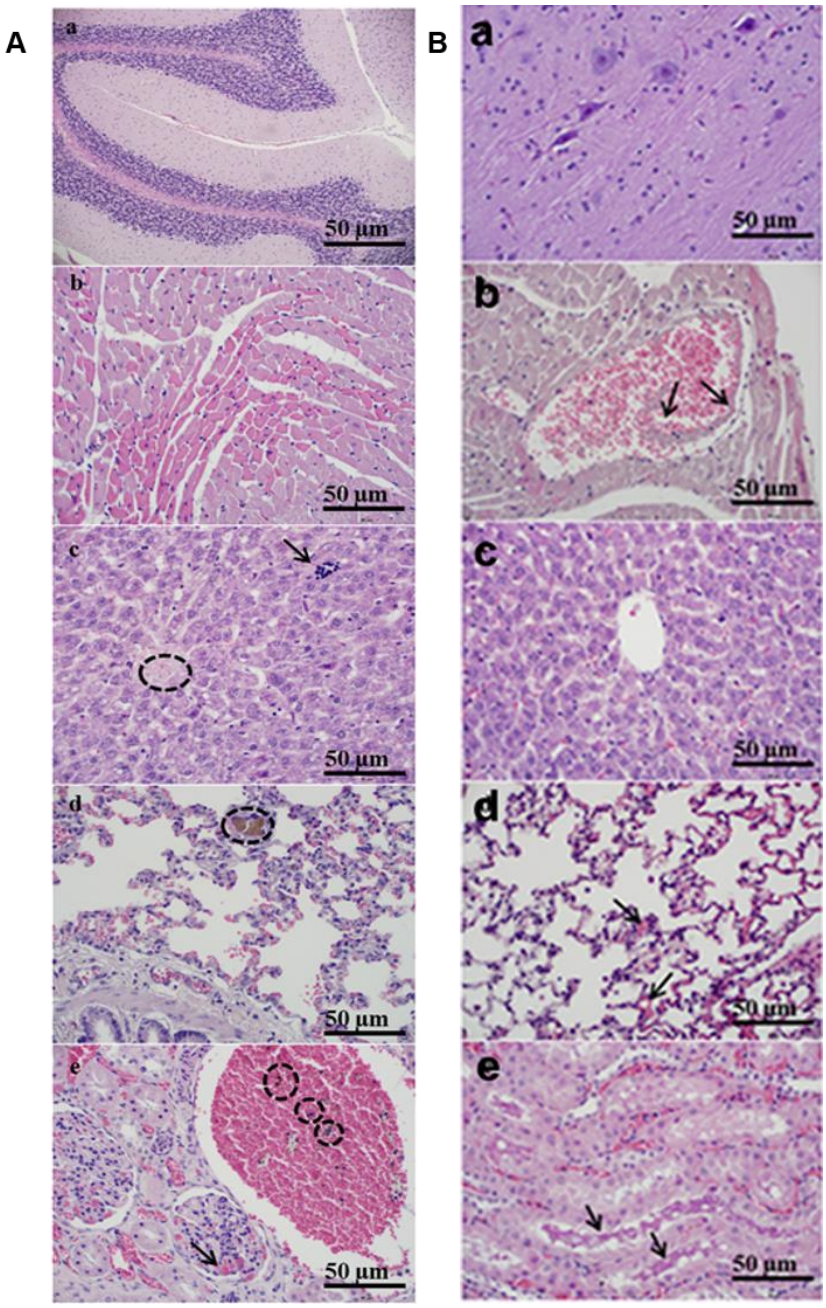

Figure 11. *Representative high (400X) magnification photomicrographs illustrating histology of major organs from A) a day 1 animal at 500 mg/kg of Mangradex dose at 400x magnification a) Cerebellum: without any diagnostic abnormality. b) Heart: without diagnostic abnormalities. c) Liver: hepatic parenchyma with amorphous debris within sinusoids and central vein (circle). A solitary aggregate of neutrophils was noted (arrow), however, there was no evidence of acute or chronic inflammation. d) Lung: pulmonary parenchyma with vascular congestion and intracapillary aggregates of brown pigment (circle). e) Kidney: focal aggregates of brown/black pigment in veins (circle) and glomeruli with mild congestion (arrow). B) a day 1 animal at 250 mg/kg Mangradex dose. a) Cerebral cortex without diagnostic abnormalities. b) Myocardium with vascular congestion. A dilated vein containing red blood cells and amorphous debris (arrows) suggestive of the presence of Mangradex. c) Liver without diagnostic abnormalities. d) Pulmonary parenchyma with mild focal congestion in alveolar capillaries (arrows). e) Renal medulla with vascular congestion and proteinaceous casts in renal tubules (arrows).*

Organs	Mangradex related effects at ≥ 250 mg/kg
Brain	No Mangradex related effects
Heart	Focal congestion with patchy hyper-eosinophilia of cardiomyocytes
Liver	Centrilobular congestion
Lung	Mild focal congestion, focal granular brown pigment, consistent with aggregates of graphene nanoparticles, within capillaries and alveolar spaces
Kidney	Congestion, proteinaceous casts, rare foci of granular brown pigment within vascular spaces

Table 11. *Summary of tissue histology*

Tissue histology of major organs (brain, heart, liver, lung, kidney, spleen) was examined on all experimental and control animals. Histologic sections of experimental animals were compared with controls to identify Mangradex related effects. **Figure 11** shows representative histologic section of a tissue from a rat injected with 250 mg/kg Mangradex and monitored for 1-day. **Table 11** summarizes the general observations in the histologic sections of major organs of 1-day and 30-day rats injected with ≥ 250 mg/kg Mangradex.

Cardiovascular safety

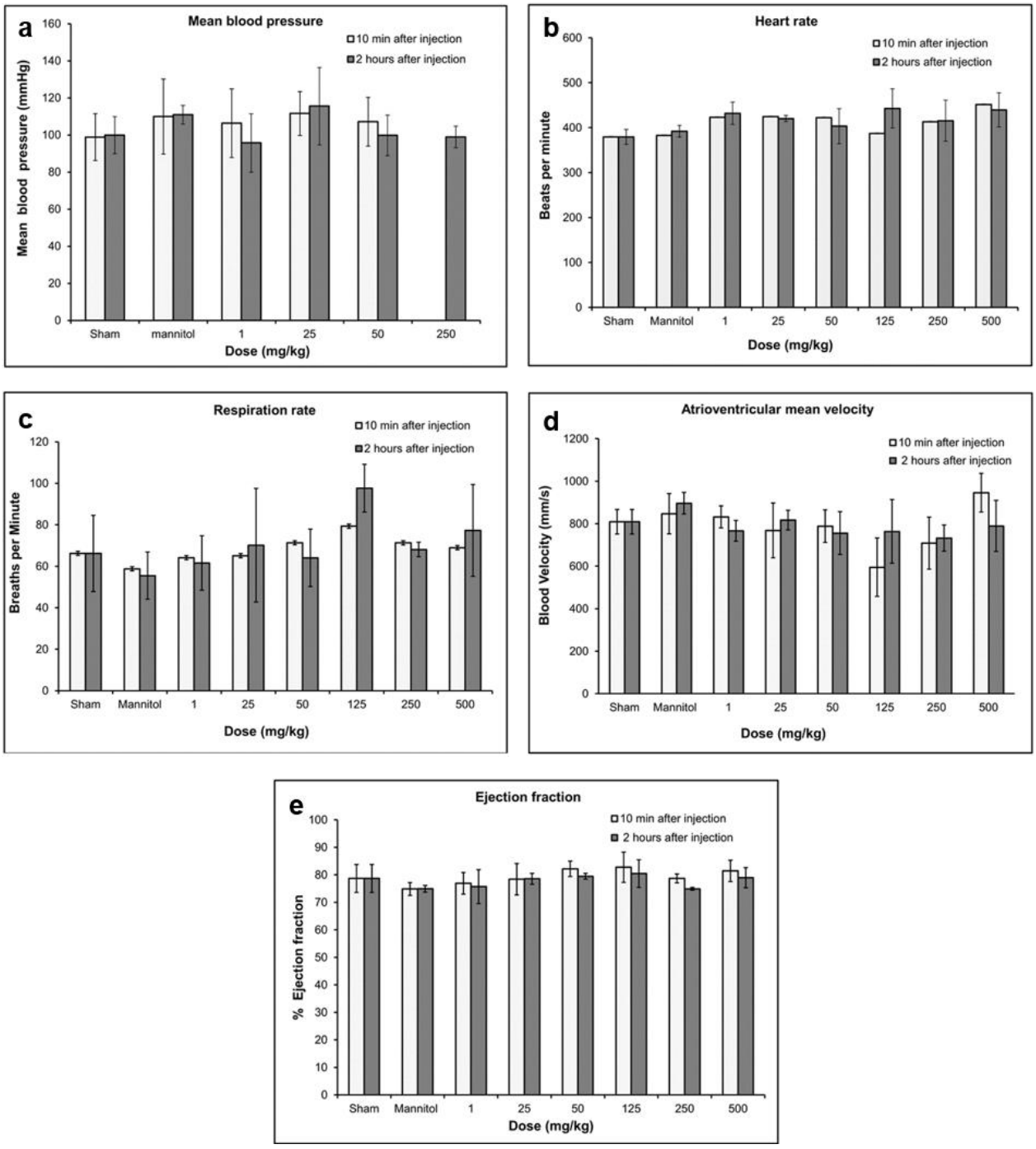

Figure 12. *Hematological results from blood pressure and echocardiography measurements 10 min and 2 hours post injection of Mangradex (doses: 1-500 mg/kg).* ***a****) Blood pressure.* ***b****) Heart rate.* ***c****) Respiration rate.* ***d****) Atrioventricular mean blood velocity.* ***e****) % Ejection fraction.*

For respiratory and cardiovascular safety pharmacology studies, we monitored the blood pressure, respiration rate, heart rate and other important echocardiography parameters - blood velocity and % ejection fraction of the experimental and control rats (**Figures 12 a-e).** Other related parameters such as fractional shortening, systolic and diastolic left ventricular volume, intravascular septum thickness, left ventricular internal septum thickness and left ventricular posterior wall thickness were also in the normal range. There were no statistically significant differences in blood pressure measurements (**Figure 12a**) ($n=6$, $p<0.05$) between the experimental (up to Mangradex doses of 250 mg/kg) and sham (no injection) group. For the rodents receiving 250 mg/kg and 500 mg/kg Mangradex injections, no blood pressure readings could be obtained up to 2 hours after the injection because the tails of all animals in these two high doses groups were taut, which impeded the tail cuff system's ability to give reliable readings. At these high dosages, the animals also exhibited an impaired ability to walk (limping lower limbs) for the first few minutes after injection, a condition similar to intermittent claudication, where the legs are deprived of an oxygenated rich blood supply.[131]

In all surviving rats, there were no statistically significant differences in heart rate (**Figure 12b**), respiration rate (**Figure 12c**), atrioventricular mean blood velocity (**Figure 12d**) and % ejection fraction (**Figure 12e**) at IV doses up to 500 mg/kg following administration of Mangradex compared to controls. Additionally, there were no significant differences between experimental and control animals from 10 min post-dose through 2 hours post-dose at IV Mangradex doses up to 500 mg/kg for the other electrocardiographic parameters, fractional shortening, systolic or diastolic left ventricular volume, intravascular septum thickness, left ventricular internal septum thickness and left ventricular posterior wall thickness.

Blood analysis

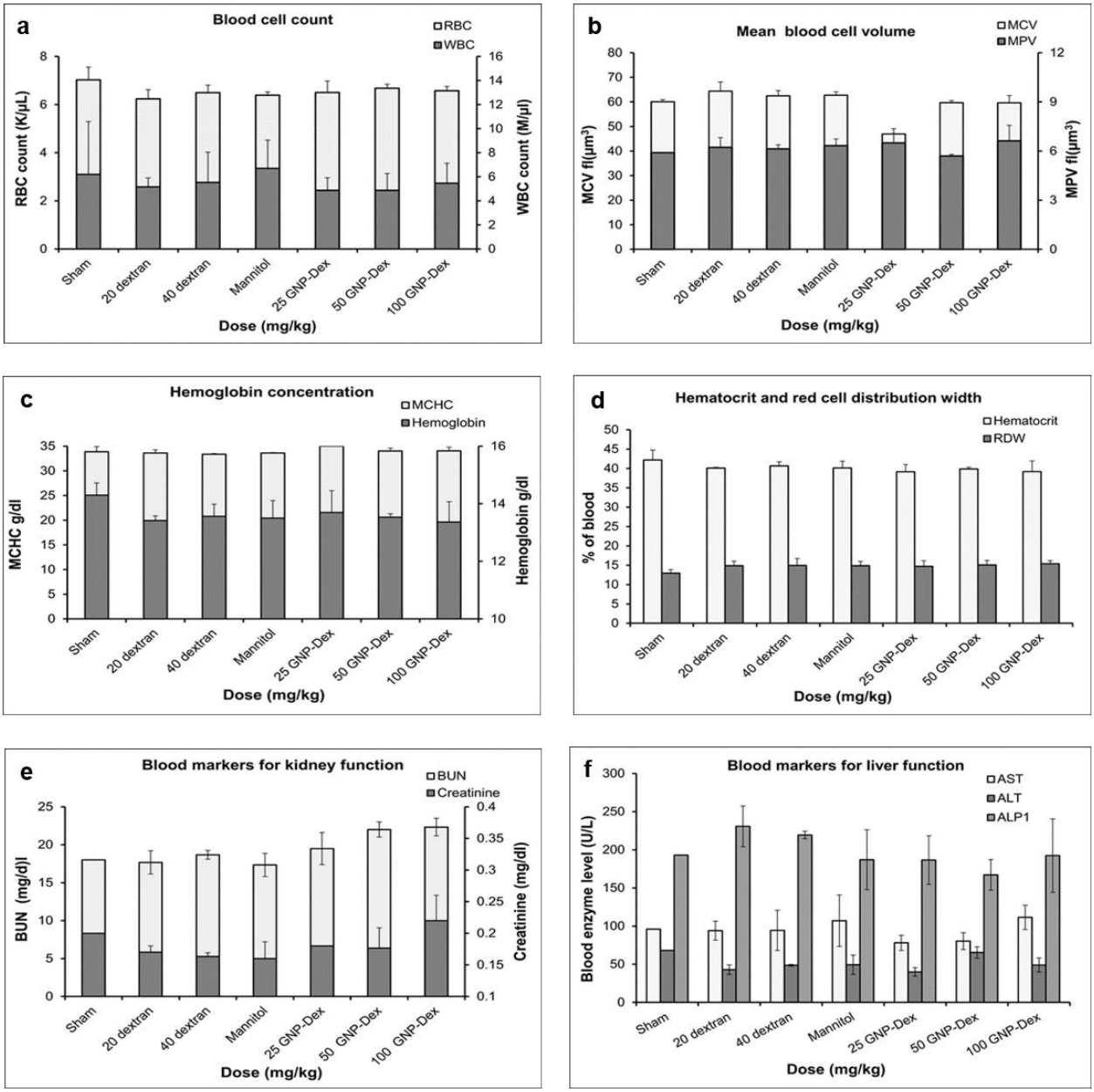

Figure 13. *Blood Chemistry results following injection with Mangradex, dextran or mannitol 1 day after injection (n=3).* ***a****) Red blood cell (RBC) and White blood cell (WBC) count.* ***b****) Mean corpuscular volume (MCV) and mean platelet volume (MPV).* ***c****) Mean corpuscular hemoglobin concentration (MCHC) and total hemoglobin concentration.* ***d****) Hematocrit and red cells distribution width (RDW).* ***e****) Markers for kidney function - blood urea nitrogen (BUN) level and creatinine level.* ***f****) Markers for liver function - alkaline phosphatase (ALP), alanine transaminase (ALT) and aspartate transaminase (AST).*

Hematological factors (blood cell count, lipid panel and metabolic panel) were analyzed at 25, 50 and 100 mg/kg doses. The maximum dose selected for this study was <125 mg/kg in order to assess if the Mangradex, at doses that show no test article related effects in terms of mortality, histopathological findings, or cardiovascular safety pharmacology studies would adversely affect the immune system or induce an inflammatory response. As the ratio of GNP:Dextran in Mangradex is 3:2 by weight, 20 mg/kg and 40 mg/kg doses of dextran that represent the equivalent amount of dextran in 50 and 100 mg/kg of Mangradex were selected as controls. **Figure 13 a-i** displays various hematological parameters for the experimental and control (rats injected with dextran or mannitol (the diuretic solution used to adjust the osmolality of Mangradex formulations)) animal groups, 1-day after administration of Mangradex. The results were also compared to the normal range of blood parameters of Wistar male rats (information provided by the vendor, Charles River Laboratories, Wilmington, MA, USA).[132] **Figure 13 a-d** shows various parameters from the complete blood count analysis. Red blood cells (RBC), white blood cells (WBC) and blood cell volumes (i.e. mean corpuscular volume (MCV), mean platelet volume (MPV), mean corpuscular hemoglobin concentration (MCHC), hemoglobin, hematocrit and red cell distribution width (RDW) level) were within normal limits. Indicators of kidney function such as blood urea nitrogen (BUN) and creatinine (CRE) were also normal (**Figure 13 e**). Similarly, as shown in **figure 13 f and g,** the established serum biochemistry assays for hepatic indicators (alkaline phosphatase (ALP), total protein (TP), albumin (ALB), alanine transaminase (ALT) and aspartate transaminase (AST)) measured 1-days after Mangradex injection showed no sign(s) of liver injury. Blood triglycerides (TG), cholesterol (CHO) and glucose (GLU) levels, blood ion concentrations of Na, K, Cl and CO_2, and blood protein (total protein (TP) and albumin) levels (data not shown) were also in the healthy ranges.

Biodistribution

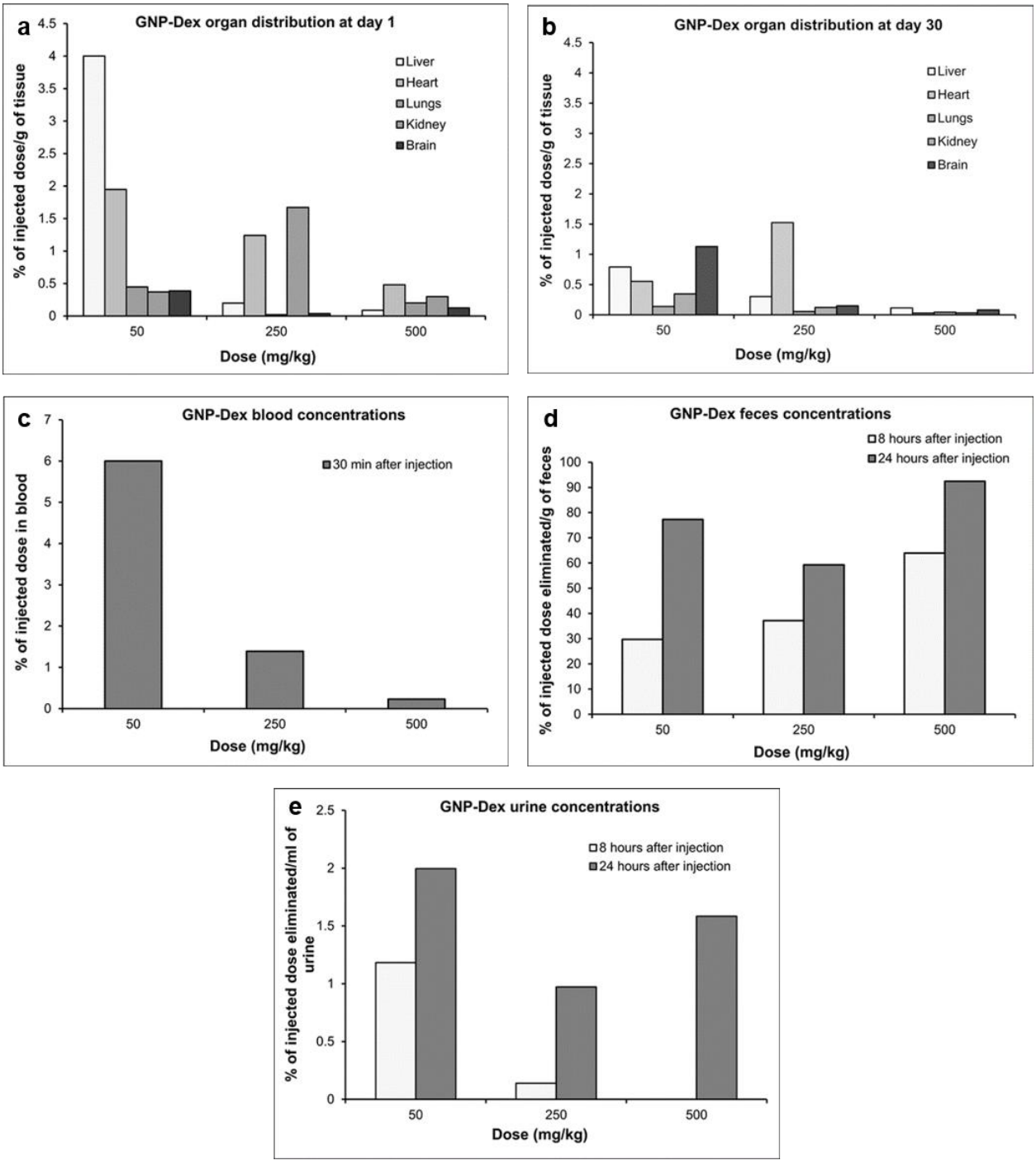

Figure 14*. Biodistribution and elimination of Mangradex in major organs.* ***a****) Biodistribution in organs at 1 day.* ***b****) Biodistribution in organs at 30 days.* ***c****) Blood retention of Mangradex.* ***d)*** *Elimination of Mangradex via feces.* ***e)*** *Elimination of Mangradex via urine.*

Tissue bio-distribution, blood half-life, and elimination at representative low (25 or 50 mg/kg), medium (125 or 250 mg/kg) and high (500 mg/kg) doses of Mangradex are presented in **Figure 14**. Mn^{2+} concentrations in blood, and tissues, urine and feces samples of a number of animals were close to the limits of detection (LOD) of ICP-MS (1 PPB). Thus, data in **Figure 14** are presented as pooled averages as proposed in previous studies;[133] variability and statistically significant differences between the groups could not be determined. Nevertheless, the results still allowed analysis of the trends. **Figure 14 a and b** show bio-distribution of the nanoparticles in major vital organs at day 1 and day 30 respectively. The percent of Mangradex remaining in organs at day 1 was ~0.5-4%, and reduced to close to or the below limits of detection by day 30. In general, a higher percentage of Mangradex was detected in various organ at the low (25 mg/kg) dose, compared to the medium (125 mg/kg) and high (250 mg/kg) dose. Day 1 animals showed more Mangradex in heart and liver than in the kidney, lungs and brain. Day 30 animals showed more Mangradex in heart compared to other organs. The blood concentrations (**Figure 14 c**) of Mangradex at dosages of 50, 250 and 500 at 30 min were 6%, 1.5%, and less than 0.5% respectively. **Figure 14 d and e** show the elimination profile of Mangradex. No urine sample could be obtained at the 8 hour time point for day 1 group in the rats injected with 500 mg/kg. The average amount of Mangradex getting excreted through feces for the various doses was calculated to be ~60-90% over the period of 1-day post injection. A small fraction of Mangradex (0.5 to 2% of injected dose) was excreted by urine. No Mangradex could be detected in urine and feces samples analyzed at day 2 and beyond, in the 30-day group.

Sub-acute toxicity

Group	Dose	Total Animals		No. of Dead animals	
		M	F	M	F
Mangradex	1 mg/kg	4	4	0	0
	50 mg/kg	4	4	0	1
	100 mg/kg	4	4	1*	1 ψ
Control	Mannitol	3	3	0	0
Sham		3	3	0	0
* Mortality on 7th day after 4 injections of 100 mg/kg ψ Mortality on10th day after 5 injections of 100 mg/kg					

Table 12. *Mortality observed in animals at varying doses of Mangradex during the chronic toxicity study. Each animal received IV injections three times per week (Monday, Wednesday and Friday) for three weeks.*

Table 12 summarizes the various groups and any mortality observed for chronic toxicity study. During the 3 weeks multiple-dose (3 times per week) toxicity study in rats, mortality was observed in 2 out of 8 animals (1 M and 1 F) at 100 mg/kg dose during the 2nd week; a male rat deceased after 5 injections and the female rat after 4 injections. Necropsy performed on these animals by in house veterinary technician showed that the lungs were darker than usual suggesting presence of nanoparticles. All other major organs heart, liver, kidneys and brain were normal without any treatment related adverse effects. From the surviving animals, 1 male rat injected with 100 mg/kg dose elicited response at the injection site in the form of local swelling during the 3rd week after 6 injections, this persisted throughout the end of the study. In all other surviving animals, no other treatment related adverse effects were observed. Additionally, in these animals, there were no changes in the animal posture or behavior with cage mates at any of the injected doses of Mangradex. Further, both male and female rats at all dose groups did not show any treatment related changes in terms of body weights, breathing, blood pressure and heart rate.

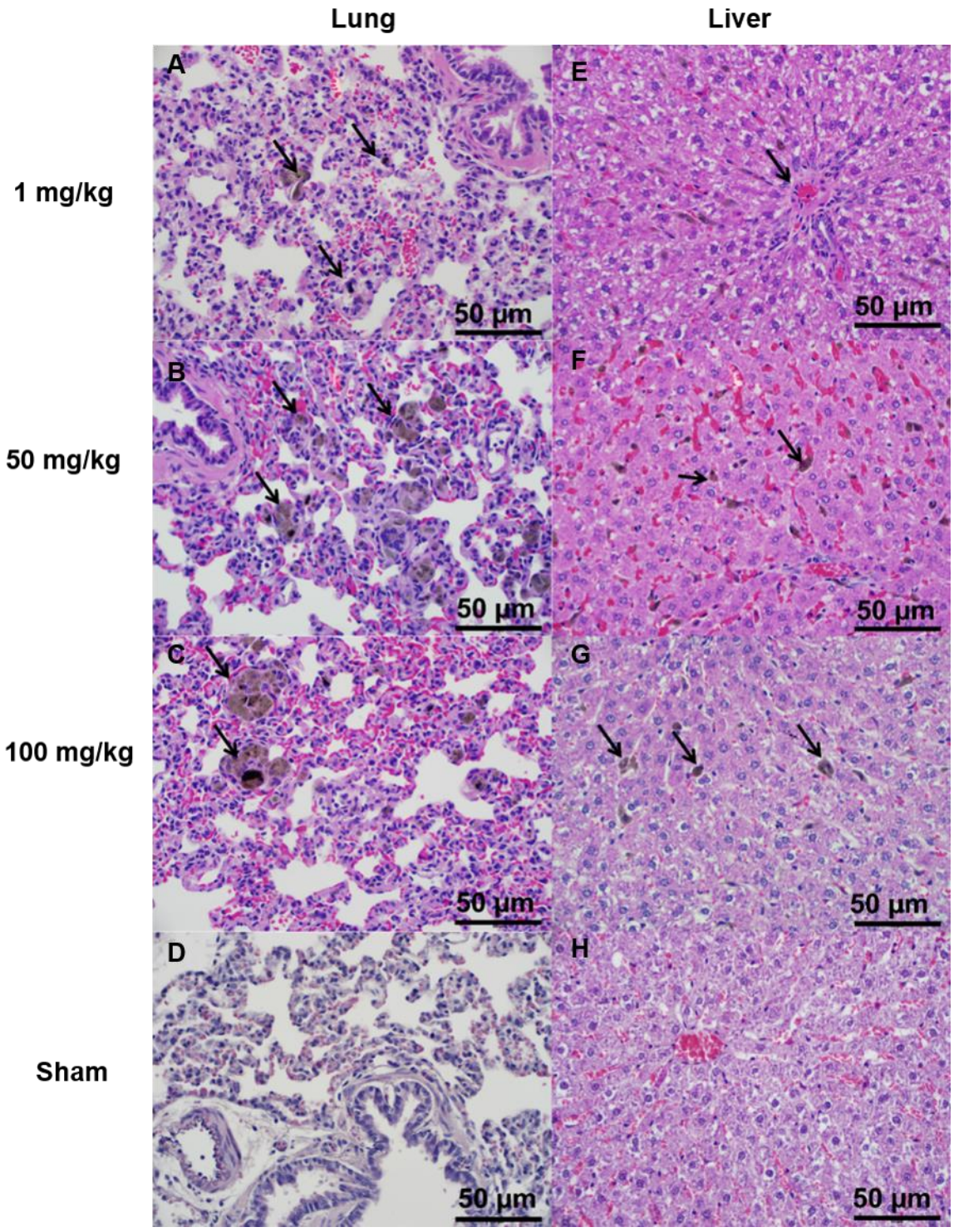

Figure 15*. Representative high (400X) magnification photomicrographs illustrating pulmonary and hepatic histology from chronic study animals at 1 mg/kg, 50 mg/kg, 100 mg/kg Mangradex and sham. Lung A) at 1 mg/kg, B) at 50 mg/kg and C) at 100 mg/kg- with pigment (arrows) within alveolar macrophages suggestive of the presence of graphene nanoparticles, D) sham - without diagnostic abnormality. Liver - E) at 1 mg/kg - showing minimal steatosis, but without diagnostic*

abnormality, F) at 50 mg/kg- showing pigmented macrophage in Kupffer cells suggestive of graphene particles. No sign of inflammation, G) at 100 mg/kg - more pigmented than at lower dose, H) sham - without diagnostic abnormality.

Tissue histology of major organs (brain, heart, liver, lung, kidney, spleen) was performed on sham and experimental animals that survived the entire 3 week duration of the study. **Figure 15** shows representative histologic section at 400 X magnification of tissues from sham and rats injected with 1, 50 or 100 mg/kg Mangradex 9 times over 3 weeks. The most common microscopic findings were the presence of pigment in hepatic Kuppfer cells and in pulmonary alveolar macrophages, consistent with the presence of graphene nanoparticles. Overall, more pigment was observed at higher dosages (50 and 100 mg/kg) in the lungs than at the lower dose. There were no treatment related effects in brain, heart, spleen and kidney. In all dose groups, no histological evidence of inflammation was observed in any tissue.

No.	Test	Sex	Normal	Sham	Mannitol	Dextran	1 mg/kg	50 mg/kg	100 mg/kg
A	ALT (U/L)	**M**	19-48	54.3±7.5*	54.5±2.1*	47.7±7.0	73.3±35.3*	43±6.0	60.3±13.5*
		F	14-64	54.5±19.3	50.0±7.2	53±6.2	38.5±0.7	45.8±11.9	46.0±11.0
B	ALP (U/L)	**M**	36-131	147.3±45.5*	134±32.5*	114.33±8.4	161.3±44.2*	138.8±11.7*	119±13.9
		F	18-62	75.3±15.9*	89.3±21.3*	71.3±13.6*	93.5±2.1*	88.8±25.1*	97.0±12.2*
C	Glucose (mg/dl)	**M**	116-184	220.6±97.2*	207±98.9*	154.11.3	181±32.9	215.7±30.7*	161.7±37.7
		F	89-163	249.3±65.9*	211±81.4*	154±16.7	214±29.7*	183.3±29.6	143.7±7.4
D	TRIG (mg/dL)	**M**	27-160	215.7±76.4*	137.5±0.7	225.3±65.7 *	186.8±55.2*	128.8±48.9	141.8±61.3
		F	16-175	93.3±53.1	65±18.9	69.7±17.5	104±16.9	68.8±17.9	70±40.6
E	WBC (K/µL)	**M**	1.9-11.1	5.5±0.2	6.6±2.5	6.9±1.8	4.9±0.8	7.1±1.9	9.7±1.7
		F	0.9-7.9	4.9±1.8	7.4±1.7	5.2±4.5	4.4±0.6	4.4±1.1	3.0±0.7
F	RBC (M/µL)	**M**	7.6-9.9	7.6±0.2	7.9±0.1	7.7±0.4	6.7±1.9	7.5±0.2	6.7±0.5
		F	7.2-9.2	7.6±0.2	7.7±0.2	7.7±0.5	7.6±0.6	6.8±0.2	6.1±0.5
G	Hemoglobin (g/dL)	**M**	13.6-17.4	15.5±0.6	14.9±0.1	14.7±0.6	14.8±1.3	14.5±0.3	13.3±0.5
		F	13.7-17.2	15.1±0.9	14.4±0.4	14.0±0.5	14.9±0.2	13.8±0.4	12.8±1.4

H	Hematocrit (%)	**M**	38.5-52.0	46.1±0.6	45.9±0.1	44.1±1.1	42.8±6.4	43.2±0.6	40.5±1.4
		F	38.5-49.2	44.5±2.4	43.4±0.1	42.2±1.5	44.6±0.4	40.2±0.8	38.2±2.7
I	Platelet Count (K/µL)	**M**	574-1253	579±60.8	540±181.1	776±181.8	898±113.0	1153.6±389	1194±303.1
		F	599-1144	422.6±127.7	612±87.1	674.7±51.8	930.5±53.0	972.3±197.8	894±213.7
J	MCV (FL)	**M**	46-56	60.4±0.8	58.5±0.9	57.4±1.1	58.8±2.7	57.7±0.6	60.6±4.1
		F	50-57	56.9±2.7	56.5±0.4	54.4±1.7	58.6±4.9	58.8±0.9	62.6±2.6
K	MCH (pg)	**M**	16.3-19.5	20.2±0.3	19.1±0.5	19.2±0.3	23.2±5.5	19.4±0.2	19.9±1.1
		F	17.6-20.3	19.1±0.9	19.2±0.6	18.1±0.6	19.6±1.7	19.9±0.2	20.8±0.8
L	MCHC (g/dL)	**M**	31.9-38.5	33.5±0.9	32.5±0.3	33.4±0.1	39.7±10.9	33.6±0.1	32.9±0.4
		F	33.2-37.8	33.6±0.3	34±0.8	33.2±0.1	33.4±0.3	33.9±0.3	33.3±0.3
M	RDW (%)	**M**	11.6-16.2	13.5±0.1	12.7±0.4	14.3±0.3	12.5±0.4	13.6±0.6	15.3±1.1
		F	10.6-14.6	12.7±1.3	11.9±0.2	9.2±6.9	12.2±1.5	12.8±0.3	15.2±0.9
N	MPV (FL)	**M**	6.1-9.5	5.8±0.1	6.1±0.1	5.9±0.2	6.0±0.3	6.3±0.1	6±0.1
		F	6.4-9.5	6.8±0.1	5.6±0.6	5.6±0.1	5.9±0.2	6.2±0.3	6±0.2
O	BUN (mg/dl)	**M**	10.7-20	22.7±1.5	22±1.4	19.7±1.2	19.5±2.4	22.3±2.8	19.7±2.6
		F	11.7-25	19.8±2.2	20.5±3.1	19±3.6	21±4.3	18.5±0.6	18±3
P	Creatinine (mg/dl)	**M**	0.3-0.5	0.2±0.05	0.2±0.01	0.2±0.03	0.2±0.05	0.2±0.1	0.2±0.1
		F	0.3-0.6	0.3±0.03	0.2±0.1	0.3±0.03	0.25±0.02	0.3±0.1	0.3±0.1
Q	AST (U/L)	**M**	63-175	130.3±33.5	83±16.9	104.3±21.7	103.3±45.7	136.5±95.0	80.7±5.0
		F	64-222	142±54.9	117.3±35.9	121±23.1	96±5.7	85±18.9	122.3±21.4
R	Albumin (g/dL)	**M**	3.6-4.7	4.5±0.1	4.5±0.1	4±0.2	4.3±0.2	4.2±0.3	3.9±0.4
		F	3.7-5.8	4.8±0.3	4.5±0.2	4.9±0.1	4.6±0.1	4.9±0.2	4.6±0.3
S	CHOL (mg/dl)	**M**	37-95	89±11.5	82.5±7.8	74.7±10.7	82.8±8.1	97.5±21.3	93.5±14.4
		F	23-97	78.3±11.5	81±11.6	79.3±19.4	78±1.4	98±9.9	81.7±5.0
T	TP (g/dL)	**M**	5.6-7.6	6.8±0.29	6.7±1.2	6.3±0.4	6.5±0.3	6.7±0.2	6.6±0.4
		F	5.7-8.3	6.9±0.4	6.9±0.4	7.0±0.1	6.8±0.0	7.1±0.6	6.7±0.1
U	Na (mmol/L)	**M**	137-147	146.3±2.1	145±1.4	139.7±1.2	144±4.6	146±0.8	148.3±4.9
		F	135-146	145.8±1.5	150.5±6.1	143.7±1.5	149.5±2.1	146.5±3.4	146.3±1.5
V	K (mmol/L)	**M**	3.9-6.1	6.6±1.5	6.4±0.9	5.5±0.5	6.3±1.3	5.5±1.9	7.6±2.1
		F	3.4-5.1	6.5±0.8	6.8±1.9	5±0.9	5.1±0.2	5.1±0.7	5.9±0.2
W	Cl (mmol/L)	**M**	98-116	97±0.0	96.5±0.7	93.7±0.6	97.3±2.2	98.0±0.6	99.5±.1.9
		F	97-106	99.5±2.9	99.5±4.2	97.7±2.3	103.5±3.5	99.5±1.3	100±1.0
X	CO_2 (mmol/L)	**M**	-	34.7±8.4	39±9.9	34.3±1.5	31.5±3.1	30.5±5.5	24.3±9.9

		F	-	29.5±4.8	30.5±6.81	37.7±1.53	24±14.14	32.8±3.77	33.7±4.9
Y	Ca (g/dl)	**M**	9.1-11.9	13.5±0.5	13.4±1.9	12.1±0.2	12.9±0.8	13.8±0.9	12.4±0.7
		F	9.5-12.1	13.2±0.9	12.3±0.8	11.8±0.5	12.1±0.4	12.6±0.6	12.7±0.4
Abbreviation; ALP: Alkaline Phosphatase; ALT: Alanine amino transferase; TRIG: Triglyceride (E-N) Part of complete blood count tests, and (O-Y) part of comprehensive lipid and metabolic panel tests. Abbreviation - WBC: White blood cell, RBC: Red blood cell, MCV: Mean corpuscular volume; MCH: Mean corpuscular hemoglobin, MCHC: Mean corpuscular hemoglobin concentration, RDW: Red cell distribution width, MPV: Mean platelet volume, BUN: Blood urea nitrogen AST: Aspartate amino transferase, TP: Total protein, CHOL: Cholesterol.									

Table 13*: Blood chemistry results for rats injected with Mangradex, dextran, or mannitol. Also included are sham controls. The data are shown as mean values ± standard deviation, and compared with the normal range published by Charles River Laboratories (n=3). All the values that do not fall in normal range are marked with the symbol *.*

A complete blood count (CBC) and established serum biochemistry assays (comprehensive lipid and metabolic panel) were performed and analyzed for the 1, 50 and 100 mg/kg doses of Mangradex, dextran, mannitol and sham. The results of the experimental groups were compared with sham, mannitol and dextran group, and also with the normal range of blood parameters of Wistar rats (information provided by the vendor, Charles River Laboratories, Wilmington, MA, USA).[134] **Table 13** displays various hematological parameters with values outside the normal range. All other parameters with values either within the normal range are displayed in rows E-N. Indicators of kidney function- blood urea nitrogen (BUN) and creatinine (CRE) were normal. Out of the five important hepatic indicators - alkaline phosphatase (ALP), total protein (TP), albumin (ALB), alanine transaminase (ALT), and aspartate transaminase (AST); ALT and ALP levels were elevated in the experimental groups as well as in sham and control groups. Blood glucose (GLU) levels were above the normal range in sham, mannitol, 1 mg/kg (F) and 50 mg/kg (M) treatment group and Triglycerides (TRIG) levels were above the normal range in sham, dextran and 1 mg/kg (M) treatment group (**Table 13**).

Discussion

Acute toxicity

Six escalating doses (low - 1, 25, 50 mg/kg, medium - 125, 250 mg/kg, and high - 500 mg/kg) were used. We assumed that, similar to other clinically approved pharmaceutical formulations for imaging or therapy (see appendix for rationale); Mangradex could be intravenously administered at units to tens of mg/kg potential therapeutic dosages. Thus, the upper limit of Mangradex dose range in this study was 500 mg/kg, one to two orders of magnitude greater than the anticipated therapeutic dose. This dose is also the maximum permissible dose (MPD) that can be achieved using the highest Mangradex stock concentration of 100 mg/ml.[5]

Necropsies of animals that died (**Table 10)** within ~2 min after Mangradex rapid bolus administration at ≥ 125 mg/kg (1 day group) or at ≥ 250 mg/kg (30 day group) suggested that the cause of the death was pulmonary congestion (See appendix necropsy report). The dosing rates also affected the mortality and the results suggest that slower dose rates are more preferable at these high dosages. For the rodents receiving 250 mg/kg and 500 mg/kg Mangradex injections, the absence of blood pressure readings up to 2 hours injections could be due to the injection of large numbers of Mangradex nanoparticles in a small dispersion volume (~500 µl) into the small diameter of the tail vein (~3.5 mm).[135] The small size of the tail vein combined with the injection of large number of nanoparticles in a short time period could create temporary obstruction at the site of injection, due to accumulation of the nanoparticles; thus, restricting the blood supply. Subsequently, as the Mangradex is absorbed into the circulation, the vasoconstriction is cleared, allowing blood pressure measurement.

Surviving animals showed no clinical signs of obvious toxicity (**Figure 11** and **Table 11**). Essentially, histology changes were noted at ≥ 250 mg/kg in the heart, liver, lung, and kidney; congestion and the presence of brown granular debris/pigment were the most consistent findings across tissues. There were no apparent Mangradex-related effects on the brain. Mangradex dosages <125 mg/kg neither showed any test article related effects in terms of mortality, histopathological findings, respiratory, or cardiovascular safety parameters, nor adversely affect the immune system or induce an inflammatory response.

Multiple reports now demonstrate GNPs synthesized using the Hummer's method or variation thereof leads to robust confinement (intercalation) of trace amounts (ppm levels) Mn^{2+} ions between the graphene sheets.[54,55,136] We had previously validated *in vitro* that the intercalated Mn^{2+} ions are thermally stable at physiological temperatures (37°C) in blood or biological buffers up to 30-days.[5] Thus, the intercalated Mn^{2+} ions do not separate from the Mangradex during the timespan of this study and served as stable endogenous elemental tags to perform ICP-MS elemental analysis and quantify Mangradex concentrations in blood, urine, feces and bio-distribution studies (calculation for extrapolation of the values are given in appendix). ICP-MS elemental analysis is widely-used and an accepted technique for *in vivo* bio-distribution studies as an alternative to relatively more expensive and hazardous radiolabelling methods.[137,138] Additionally, even though radiolabeling is a widely used method for bio-distribution and pharmacokinetics (PK) studies, the type and method of radiolabeling used can affect the PK profile.[139] As molecular weight of the test articles affects PK,[140] introducing a radiolabeling agent in the test article can change its molecular weight and may alter PK profile. Due to these issues of the alternate method, we decided to exploit the presence of the endogenous Mn^{2+} tag in the test article for the bio-distribution and PK studies,

and employed the ICP-MS method. The % weight of manganese in the Mangradex samples was the average of 6 different samples of Mangradex was determined to be 0.064 %. The Mangradex showed a dose-dependent accumulation (~0.5-4%) in the major organs at day 1, with maximum organ accumulation at 50 mg/kg and the least accumulation with 500 mg/kg (**Figure 14 a)**. Further, majority of the Mangradex accumulation were noted in liver, followed by heart, lungs, kidney and brain. However, they were present close to or below LOD levels by day 30, indicating removal from these organs (**Figure 14 and b)**. As the blood concentration (**Figure 14 c**) values of Mangradex at the various dosages were between 0.5 - 6 %; significantly less than 50%, we inferred the blood half-life of Mangradex to be within 30 min. However, we were unable to determine the precise blood half-life since the first time point of blood sampling was 30 minutes after injection. Further studies are currently underway to obtain the complete PK profile and determine the exact blood half-life value. The elimination results (**Figure 14 d and e)** indicate that Mangradex nanoparticles are eliminated through feces within 48 hours. The larger amounts of Mangradex in the feces than in urine suggest that these nanoparticles are excreted more through the bile than through the kidney.

Taken together, the results of this study indicate that the maximum tolerable dose (MTD) of Mangradex is between 50 mg/kg $\leq$ MTD $<$ 125 mg/kg. The classic measure of toxicity, lethal dose (LD_{50}- the dose at which mortality occurs in 50% of the study population) was not achieved even at the highest dose tested (500 mg/kg). However, it should be noted even though LD_{50} considers only mortality as an end point; valuable in forensic science, accidental exposure and environment safety investigations.[141,142] For biomedical/ healthcare applications, LD_{50} results are marginally informative and toxicologically inadequate as they do not take into account the factors affecting

mortality, time frame of death from injection of test article, site and mode of action morbidity, and liver or kidney damage. Hence, reports related to toxicity of test article for biomedical applications have focused on assessment of factors affecting morbidity.[141,142] Additionally, although there were no mortalities at doses ≤ 50 mg/kg even with bolus IV injections, slower injection is preferable. Our previous *in vivo* small animal (hamster cheek pouch model) vasoactivity studies indicate that at potentially high first pass concentrations (50 mg/ml) typically associated with bolus injections show transient arteriolar dilation without any endothelial dysfunction.[143]

Other small animal (mouse) studies, have reported the toxicology of as-prepared GNP suspensions, [125] and GNPs covalently functionalized with PEG[126] or dextran,[62] intravenously injected at relatively low concentrations. As-prepared GNP suspensions at single IV doses between 0.1-0.25 mg/kg showed no adverse effects in mice; while repeated dosing in mice (up to 0.4 mg/animal (mouse) for 30-days) resulted in chronic toxicity with mortality in 4 out of 9 mice.[125] In another study, the blood half-life of as-prepared graphene oxide IV injected into mice at 10 mg/kg dosages was 5.3 hours. That formulation excreted through urine and showed pathological changes including pulmonary edema and granuloma formation over 14 days.[122] Mouse studies with GNPs water-dispersed via covalent functionalization with PEG or dextran, at one or two low doses (relative to the ones used in this study), neither showed any mortality nor significant adverse effects to the animals.[62,126] The pharmacokinetics of PEG functionalized GNPs followed a two-compartment model, and had first and second phase half-lives 0.39 and 6.97 hours, respectively. Those nanoparticles excreted through both urine and feces over 7 days. Moreover, it did not show toxicity in blood chemistry, hematology and histologic studies at 20 mg/kg single dose in mice observed for 3 months.[126] Similarly, graphene covalently functionalized with dextran, also

followed a two-compartment PK profile with first and second phase blood half-lives of 0.19 and 1.81 hours. The formulation excreted by both renal and fecal pathways, and did not elicit noticeable toxicity at 20 mg/kg single dose in mice monitored for 7 days.[62]

The solubility and stability of the Mangradex formulation up to 100 mg/ml allowed us to perform acute toxicity studies at significantly higher dosages (25X greater) than with any other reported graphene IV toxicity studies (maximum 20 mg/kg).[126] The results suggest that the safety profile of Mangradex is better (50 mg/kg ≤ MTD < 125 mg/kg), and the blood half-life is shorter (< 30 min) than the previous GNP formulations. The major route of elimination for Mangradex is fecal (90% of injected dose), while the other GNP formulations eliminate through both urine and feces. Similar to other GNP formulations,[62,122,126] Mangradex shows more accumulation in liver, suggesting possible uptake by RES and eventual clearance by the bile system.

Our results open avenues for pivotal preclinical single and repeat dose safety studies following good laboratory practices (GLP) as required by regulatory agencies;[130] critical for the preclinical development of graphene nanoparticles-based formulations as multifunctional agents for imaging and4 therapy. Traditionally, pharmaceutical formulations possess single functionality (e.g. as imaging or therapeutic agent). For multifunctional IV pharmaceutical products, such as Mangradex, a significant portion of required safety studies are the same regardless of whether the ultimate focus is on development for systemic imaging or as a therapeutic agent. Thus, with burgeoning costs and developmental times for new healthcare technologies, the development of highly efficacious multifunctional graphene nanoparticle biomedical technologies could control costs and developmental times.

Sub-acute toxicity

FDA and ICH guidelines on preclinical safety studies of MRI CAs have also emphasized that repeat dose chronic toxicity studies be conducted to identify potential therapeutic dosages for first-in-human trials.[100,144] These studies are considered important since they reliably provide information not easily predictable by single dose acute toxicology studies; information such as histopathological changes upon repeated or chronic exposure of MRI CA and other cumulative effects. According to FDA guidelines, the recommended duration of chronic toxicity for new pharmaceutical development depends on its duration, therapeutic indication (MRI CA in this case), and scope of the clinical trial and could range from 2 weeks to 9 months.[2,144,145] For FDA approved MRI CAs Gadodiamide (Omniscan),[146] Mn-DPDP (Teslascan),[147] and Gadoversatamide (Optimark)[148] chronic toxicity studies were performed for 3 week duration with the CA administration frequency 3 times/week. Hence, for Mangradex the time points selected were 3 per week for three weeks at three escalating doses (low - 1 mg/kg, medium - 50 mg/kg, and high - 100 mg/kg). The maximum dose (100 mg/kg) selected was based on the outcomes of previous dose ranging, and expanded acute toxicity studies for Mangradex formulation.[87] In those studies, we found the maximum tolerated dose (MTD) for Mangradex was $50 \leq MTD < 125$ mg/kg. Further, neither any test article related adverse effects on the immune system nor any inflammatory response were noted after single IV injections at doses ≤ 100 mg/kg.[87] Hence, in this study, we have assessed chronic toxicity effects at doses ≤ 100 mg/kg. As the ratio of GNP: dextran in Mangradex is 3:2 by weight,[89] 40 mg/kg dose of dextran (equivalent of dextran by weight in 100 mg/kg of Mangradex) was selected as one of the controls. Mannitol (which was used to control osmolality of the Mangradex formulation) was selected as the second control.

The necropsy findings were consistent with acute toxicity results where rats with mortality at higher dosages (>125 mg/kg) showed presence of Mangradex in pulmonary capillaries with symptoms similar to pulmonary congestion.[87] Additionally, the absence of distinguishable toxicity related changes in all major organs (heart, kidney, liver, spleen, and brain) suggest that there may be no secondary cause of death. Our previous biodistribution study showed that ~ 1-2 % of the injected dose of Mangradex remained in lungs one day after single injection.[87] This result taken together with necropsy results suggests that after multiple injections, the nanoparticles that cannot be removed from the lungs may have accumulated in pulmonary capillaries impeding blood flow in microcirculation.

In all surviving animals, at ≥ 50 mg/kg, the absence of Mangradex related histological changes in the brain, heart and spleen and minor histological changes (presence of brown granular pigment) noted in the liver and lung indicate that the cumulative accumulation of Mangradex do not adversely affect the major organs.

Mangradex related unfavorable reaction in the circulatory system can affect the immune system and/or hematological factors. Accordingly, standard serum chemistry test and complete blood panel analyses were performed. The results of blood chemistry parameters for Mangradex dosages and controls were compared with sham and published data by Charles River Laboratories.[134] Blood counts did not differ significantly in any dose groups. Elevated levels of hepatic function markers ALT and ALP are typically attributed to liver injury; however, since above normal values were observed in sham and controls as well, Mangradex treatment alone could not be the attributed as the main reason for the measured elevated values. Similarly, increased levels of glucose and

TRIG found in sham, mannitol or dextran and were not dose dependent with elevation noted in one of the experimental group, and thus, these increases cannot be extrapolated as solely Mangradex associated effects, and could be animal specific outcomes. Other blood chemistry parameters were within the normal healthy ranges and did not differ significantly between groups.

Conclusions

The maximum tolerable dose (MTD) of Mangradex is between 50 mg/kg ≤ MTD < 125 mg/kg. Slower injection is preferable than bolus IV injections. 1 day or 30 days post injection, Mangradex does not significantly affect the respiratory, cardiovascular or hematological factors (blood, lipid, and metabolic panels) at doses < 125 mg/kg. The formulations elicit minor changes in the heart, liver, lung, spleen, or kidney, and no changes in the brain. Mangradex shows a dose-dependent small accumulation (~0.5-4%) in the major organs at day 1 and negligible or no presence in these organs by day 30. However, they were present close to or below LOD levels by day 30, indicating removal from these organs by day 30. The nanoparticles have a blood half-life < 30 minutes, and are mainly excreted within 24 hours through feces. In sub-acute toxicity studies, Mangradex formulation up to 50 mg/kg dosage, did not cause any noticeable adverse effects in cardiovascular (blood pressure and heart beats) and hematological (lipid panel, metabolic panel and serum chemistry) parameters. The formulation elicited dose-dependent presence of pigment in lungs and liver and no changes in heart, brain and kidney without any major adverse effect.

CHAPTER 4

EFFICACY AS AN MRI CONTRAST AGENT

Abstract

The goal of this study was to evaluate the efficacy of Mangradex as MRI CA. The relaxivity r_1 of the Mangradex formulations was 92 $mM^{-1}s^{-1}$ (22 MHz magnetic field) which is ~32 and 21 times greater than clinical Manganese-based (Mn^{2+}-DPDP or Teslascan, r_1 =2.8 $mM^{-1}s^{-1}$) and gadolinium-based ($[Gd^{3+}$-DTPA$]^{2-}$ or Magnevist, r_1 = 4.2 $mM^{-1}s^{-1}$) MRI CA, respectively. T_1 weighted phantom MRI of Mangradex solutions at clinical 1.5 T magnetic field showed significant contrast enhancement even at extremely low Mn^{2+} concentrations (down to 220 nM). Whole body 7 Tesla MRI performed on mice following intravenous injections of Mangradex at a potential therapeutic dose (25 mg/kg or 455 nanomoles Mn^{2+}/kg; ~2 orders of magnitude lower than the paramagnetic ion concentration in a typical clinical dose) showed persistent (up to at least 2 hours) contrast enhancement in the vascular branches (Mn^{2+} concentration in blood at steady state = 300 ppb, per voxel of blood = 45 femtomoles). MRI at 7 tesla magnetic field was performed in renal compromised rat model 5/6 nephrex at the same therapeutic dose (25 mg/kg, [Mn^{2+}] = 455 nmoles/kg) for 90 minutes. Qualitative and quantitative results indicated significant (>100%) and sustained contrast enhancement in the kidney and renal artery at these low paramagnetic ion (Mn^{2+}) concentration; 2 orders of magnitude lower than the paramagnetic ion concentration in a typical clinical dose of long circulating Gd^{3+}-based MRI CA Ablavar (Gadofosveset Trisodium).

Introduction

Gadolinium (Gd^{3+})-based small molecule complexes dominate the MRI-CA market (> 95% market share, >$1 Billion market in 2012),[149] and are considered the "gold standard." The majority of current clinical Gd^{3+}-based MRI CAs are considered as "first pass" agents as they are detectable by MRI the first few minutes within the circulatory system after injection and rapidly extravasate

and are eliminated via the kidneys.[102] However, these MRI CAs, due to their narrow imaging window are not optimal for Magnetic Resonance Angiography (MRA);[150] widely employed to detect vascular abnormalities associated with aneurysm, hemorrhage, embolism, and stroke. Due to heart and respiratory movements, contrast enhanced MRA requires a significant decrease in blood T_1.[151] This decrease is typically achieved by rapid injection of a large dose of clinical first pass agent MRI CAs such as Magnevist.[151] However, the higher dose injection protocols results in a very sharp bolus with marked T_1 variations in image acquisition of the k-space sampling, causing image artifacts.[152,153] Moreover, previous MRI studies indicate that contrast between the arteries and surrounding tissue can significantly decrease due to extravasation of the CA.[150] To overcome these challenges, Gd^{3+}-macromolecule complexes have been designed as advanced intravascular or blood pool agents with longer blood half-life and slower extravasation into the interstitial space compared to first-pass agents with one agent (Ablavar® (Gadofosveset Trisodium),[154,155] previously marketed under the trade names of MS-325 and Vasovist) clinically approved to evaluate aortoiliac occlusive disease in adults with known or suspected peripheral vascular disease.[156] However, studies indicate that r_1 relaxivities (an important measure of imaging efficacy defined as change in the relaxation rate ($r_1=1/T_1$ s^{-1}) of the water protons per unit concentration of CA (mM)) of current clinical MRI CAs, with minimum detectable concentration of tens of μM to provide satisfactory contrast enhancement, are suboptimal for advanced MRI-based molecular and cellular imaging applications,[157,158] and postulate the possibility to design novel MRI CAs with relaxivities (depending on the magnetic field) one to two orders of magnitude greater than current clinical agents.[159,160] Additionally, more and more MRI operate at higher magnetic fields (> 1.5 Tesla) where Gd^{3+}-based small molecule first pass agent or large molecule blood pool MRI CAs show significant drop in relaxivity.[160] Thus, a safe and more efficacious T_1 MRI CA that allows

significant contrast enhancement at substantially lower dosages than (Gd^{3+})-based clinical CAs for advanced applications such as blood pool or cellular or molecular imaging would constitute a significant advancement.

MRI is routinely used in the clinical diagnosis of renal failure, [25] and has the potential to provide both functional[26,27] and anatomical information about individual kidneys.[28] For patients with kidney transplant or renal failure, the use of MRI is becoming highly attractive over other methods such as CT and nuclear imaging as it does not require use of ionizing radiation or nephrotoxic iodinated contrast media and non-invasively renders anatomical details of soft and hard tissues for improved diagnosis of many pathologies and diseases.[29] In order to improve diagnostic confidence in clinical MRI, CAs are routinely employed for kidney imaging to delineate renal cysts from background parenchyma and to detect vascular abnormalities.[161] However, when administered to patients with severe acute or chronic renal insufficiency (GFR < 30 mL/min/1.73m^2), they lead to the rare but potentially fatal disease NSF.[25,162-164] Hence, a new safe CA could be used for non-invasive imaging and monitoring of malignant or benign lesions in the renal system secondary to carcinoma or nephron-sparing surgery, MR urography, and kidney transplant [28]. Additionally, such a MRI CA could also be used for non-invasively imaging and monitoring of other organs in patients with renal failure.

In this chapter, we have investigated efficacy of Mangradex as MRI CA *in vitro* by relaxometry and MRI phantom and *in vivo* in normal heathy mice and 5/6 Nephrex renal compromised rat model at 7 T magnetic field strength.

Materials and methods

Relaxivity

Longitudinal (T_1) relaxation time of 250 µl Mangradex solutions at different concentrations (0.4, 10, 20, 50 and 100 mg/ml) was measured at room temperature using a relaxometer (SpinCore Technologies, Gainesville, FL) at 0.47 T (21.42 MHz resonance frequency) magnetic field. Samples were placed in a clean 8 mm diameter NMR tube (Norell, Landisville, NJ). The T_1 measurements were made using an inversion recovery sequence, where inversion time was varied in 12 steps between 0.5 ms and 5000 ms. The plot of relaxation rate ($1/T_1$ in s^{-1}, y-axis) vs. concentration (mM of Mn^{2+}, x-axis), was fit to a linear least-square regression line. The slope of this line provided the relaxivity r_1 value of the Mangradex. As described above, the Mn^{2+} ions concentration was measured by ICP-MS.

MR Phantom Imaging

The MRI phantoms were prepared at 7.8, 3.9, 1.9, 0.78, 0.39, 0.015 mg/ml concentration of Mangradex in DDI water. Dextran solution (4.68 mg/ml) and DDI water were used as controls. T_1-weighted MRI using spin-echo sequence was performed using a 1.5 T clinical GE scanner (Stony Brook University Hospital, Stony Brook, NY). The echo time (TE) and repetition time (TR) were set at 10 ms and 800 ms respectively. The field of view was set at 100 x100 mm and flip angle was 90^o.

Elemental Analysis

The Mangradex samples were analyzed by ICP-MS (Finnigan ELEMENT 2, Thermo Scientific) to determine the concentration of Mn^{2+} ions. For the ICP analysis, liquid Mangradex samples

(known concentration) were treated with concentrated nitric acid HNO_3 and carefully heated to obtain a solid residue. This residue was next treated with 30% H_2O_2 and heated again to remove any carbonaceous material. The remaining non-carbonaceous solid residue was dissolved in 2% HNO3, and analyzed by ICP-MS.

In Vivo MRI

Contrast agent preparation

For contrast enhanced-MRI studies, 10 mg/ml solution of Mangradex was prepared by dissolving 10 mg of lyophilized Mangradex powder in distilled deionized water. D-Mannitol (Sigma Aldrich, St Louis, MO) was added to make Mangradex solution iso-osmol to blood. The formulation was UV sterilized for 30 min. The dose for Mangradex per kg of mouse weight was 25 mg/kg or 455 nanomoles/Kg Mn^{2+} ion. The injection volume of Mangradex and clinically approved Ablavar (Lantheus Medical Imaging, Inc., N. Billerica, MA) was similar (50 µl). Ablavar diluted in saline dose per kg of mouse weight was 455 nanomoles Gd^{3+} ion.

In vivo imaging

For imaging, C57BL/6 wild type female mice (Taconic farms Inc., Hudson, NY) with weight ranging from 25g to 30g were used. All mice were maintained in agreement with procedures approved by the Institutional Animal Care and Use Committee at New York University School of Medicine. Mice were anesthetized with isoflurane gas delivered via a vaporizer/anesthesia setup (VetEquip, Inc., Pleasanton, CA, USA): 5% isoflurane in air for induction followed by 0.5–1.5% isoflurane in air via nosecone for maintenance. Following anesthetic induction, each animal was catheterized via femoral artery to infuse the contrast agent using a polyethylene tubing PE-10 line

(Intramedic, Becton Dickinson, Parsippany, NJ). Each subject was then placed supine and restrained on a custom made body holder bed with the cannula tubing extended long enough to enable remote infusion using a PHD-2000 computer-controlled syringe pump (Harvard Apparatus, Hollison, MA) while the animal is centered within the magnet bore. Body temperature was maintained between 35-37°C with a warm air thermostat system while all basic physiologic signals (temperature and breathing rate) of the freely-breathing animals were monitored continuously (SA Instruments Inc., Stony Brook, NY). Respiratory motion was monitored using a pneumatic pillow fixed to the abdomen and the body temperature was measured via a rectal probe. The whole mouse bed was then subsequently inserted within a home-built RF coil. This circularly polarized MRI probe was developed in-house to resonate at a proton frequency of 300-MHz in both transmit and receive modes with dimensions (ID=38-mm, L=76-mm, AD=36-mm) insuring a homogenous RF coverage of the adult whole mouse body.

MRI experiment were conducted using a 7-Tesla (7T) micro-MRI system consisting of a 7T 200-mm horizontal bore magnet (Magnex Scientific Ltd., Yarnton, UK) interfaced to a Bruker Biospec Avance-2 console (Bruker, Billerica, MA). The system is equipped with an actively shielded gradient coil (Resonance Research, Billerica, MA: BGA-9S; ID 90-mm, 770-mT/m gradient strength, 100-ms rise time). For *in vivo* micro-MRI (μ-MRI), a modified three-dimensional (3D) spoiled gradient echo (GE) sequence was used to acquire an additional self-gated signal on the readout dephasing gradient within each TR.[165] The gating signal was used retrospectively to generate artifact free image reconstruction sets with the following parameters: 200-μm isotropic spatial resolution; repetition time (TR) = 15ms; bandwidth (BW) = 50 kHz, matrix = 128x128x128; echo time (TE) = 6.2 ms, number of averages (N_{AV}) =3 and imaging time ~ 12 min.

Flip angle (FA) = 34º was chosen to provide the greatest T_1-enhancement contrast[166]. The advantage of the 3D-imaging approach with isotropic resolution is that the image set can be reprocessed in any desired slice orientation using NIH image J software (imagej.nih.gov/ij), facilitating image comparison during co-registration between animals acquired in separate sessions.

T_1-weighted 3D-GE MRI scans of 12 min. duration each were performed serially during every imaging session in mice to compare qualitatively the bio-distribution and pharmacokinetics of Mangradex (Dose = 25 mg/kg, equivalent to 60 nanomoles Mn^{2+} ions/kg body weight) with FDA-approved clinical intravascular agent Ablavar® (Gadofosveset trisodium). The protocol consisted of acquiring an initial image set serving as the contrast-free baseline followed by the infusion of the blood-pool contrast agent and serial scanning of nine image datasets at 12, 24, 36, 48, 60, 72, 84, 96, 108 and 120 minutes post-injection in all subjects.

In vivo imaging in 5/6 Nephrex rats

In vivo T_1-weighted MRI was performed using a 7 T Bruker Biospec 7.0T/20-cm USR horizontal magnet (Bruker, Billerica, Massachusetts). 5/6 Nephrex WKY rats (Charles River Laboratories, MA) were positioned in a coil and maintained in anesthesia at 1.5–2.5% isoflurane. Mangradex formulation at 25 mg/kg (455 nmoles/kg) was injected intravenously via tail vein infusion catheter. Ablavar (Lantheus Medical Imaging, Inc., Billerica, MA) at the same molar concentration (455 nmoles/kg) was used as control. T_1 relaxation time was measured using RAREvtr (variable TR) pulse sequence with 5 TR values 293, 635, 1114, 1926, 6000 mSec. 5 axial slices of 1 mm thickness with 256×256 in plane resolution were collected. T_1 measurements were computed using

Paravision 5.1 software by fitting absolute signal at particular TR. The T_1 value scans were then segmented using ITK snap (www.itksnap.org). T_1 value for each region was computed by calculating average T_1 value for all the voxels in that region of interest (ROI).

Using T_1 weighted scan with TE =12.5 mSec TR = 635 mSec, and by taking the signal (S) to be the mean pixel intensity value in a region of interest (kidney), and the noise to be the standard deviation (σ) in pixel intensity one or multiple ROIs in background air (free of ghosting artifacts). Signal to noise ratio (SNR) was calculated using the following equation.

$$SNR = \frac{S}{\sigma}$$

By taking outside tissue signal (S_t), contrast to noise ratio (CNR) was calculated as

$$CNR = \frac{S}{S_t}$$

Results

Concentration (mg/ml)	T_1 Time (ms)	Mn^{2+} Concentration (mM)
100	10.51±0.27	1.038
50	24.28±1.34	0.273
20	67.64±0.42	0.271
10	108.27±1.94	0.138
0.4	1993.86±227.38	0.006
DI water	5672.92±282.45	0.000

Table 14*. T_1 values of Mangradex solutions and DI water at different concentration and corresponding Mn^{2+} ion concentration*

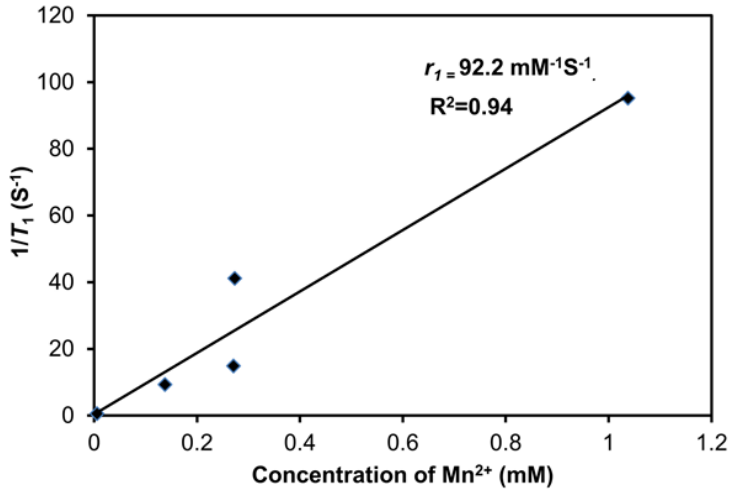

***Figure 16**. Plot of relaxation rate ($1/T_1$) vs. Mn^{2+} ions concentration fit to a linear regression line.*

Table 14 shows T_1 relaxation time at 0.47 T (21.42 MHz proton Larmor frequency) at different doses of Mangradex. Also included are the Mn^{2+} ions concentrations (in µM) for each Mangradex dose. The relaxivity value calculated from the plot (**Figure 16**) of $1/T_1$ vs. Mn^{2+} ion concentration is 92.2 $mM^{-1}S^{-1}$. MR phantom imaging further corroborates this evaluation.

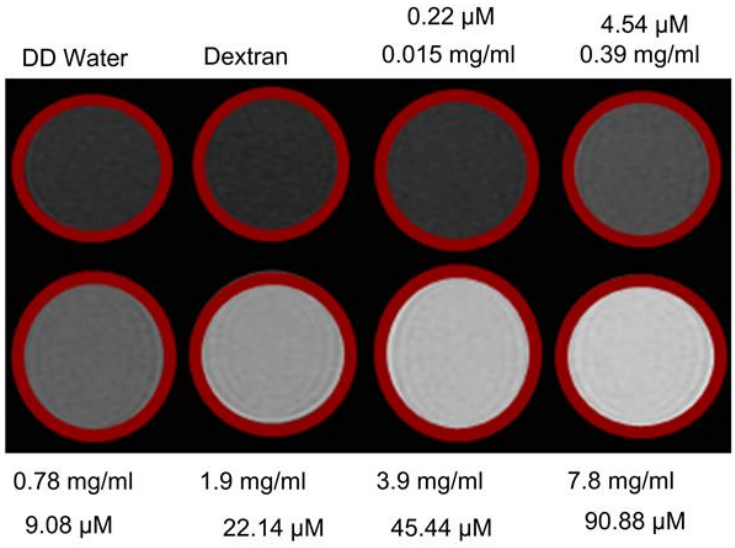

***Figure 17.** T_1 weighted MRI phantom images of Mangradex, DDI water and dextran solution obtained using a 1.5 T clinical scanner. Row 1 (left to right): DDI water and dextran solution in*

water at 4.68 mg/ml, Mangradex at concentrations 0.015, 0.39 mg/ml. Row 2 (left to right): Mangradex at 0.78, 1.9, 3.9 and 7.8 mg/ml. For each Mangradex concentration, the concentration of Mn^{2+} ions in μM is also shown.

Figure 17 displays representative T_1-weighted MR images of Mangradex solutions at different concentrations (0.78-7.8 mg/ml), and the corresponding Mn^{2+} ion concentration (0.22-90.88 μM) for each dose. These concentrations correspond to the equilibrium plasma concentration in rodents (average weight = 200 g), if the Mangradex is injected at doses between 1-500 mg/kg. Also included as baseline controls are T_1-weighted images of distilled deionized (DDI) water, and dextran solution. The images clearly show a substantial dose-dependent contrast enhancement compared to the baseline controls. The plasma concentration of the Gd^{3+}- chelate based CA at a clinical dose of 0.1 mmol/kg in a 200 g rat will be 1.5 mM, which is 17 times higher than the highest concentrations of Mn^{2+} (90.88 μM) in Mangradex solution (See appendix for calculation). This suggests that Mangradex can provide the similar MR contrast at lower dosages.

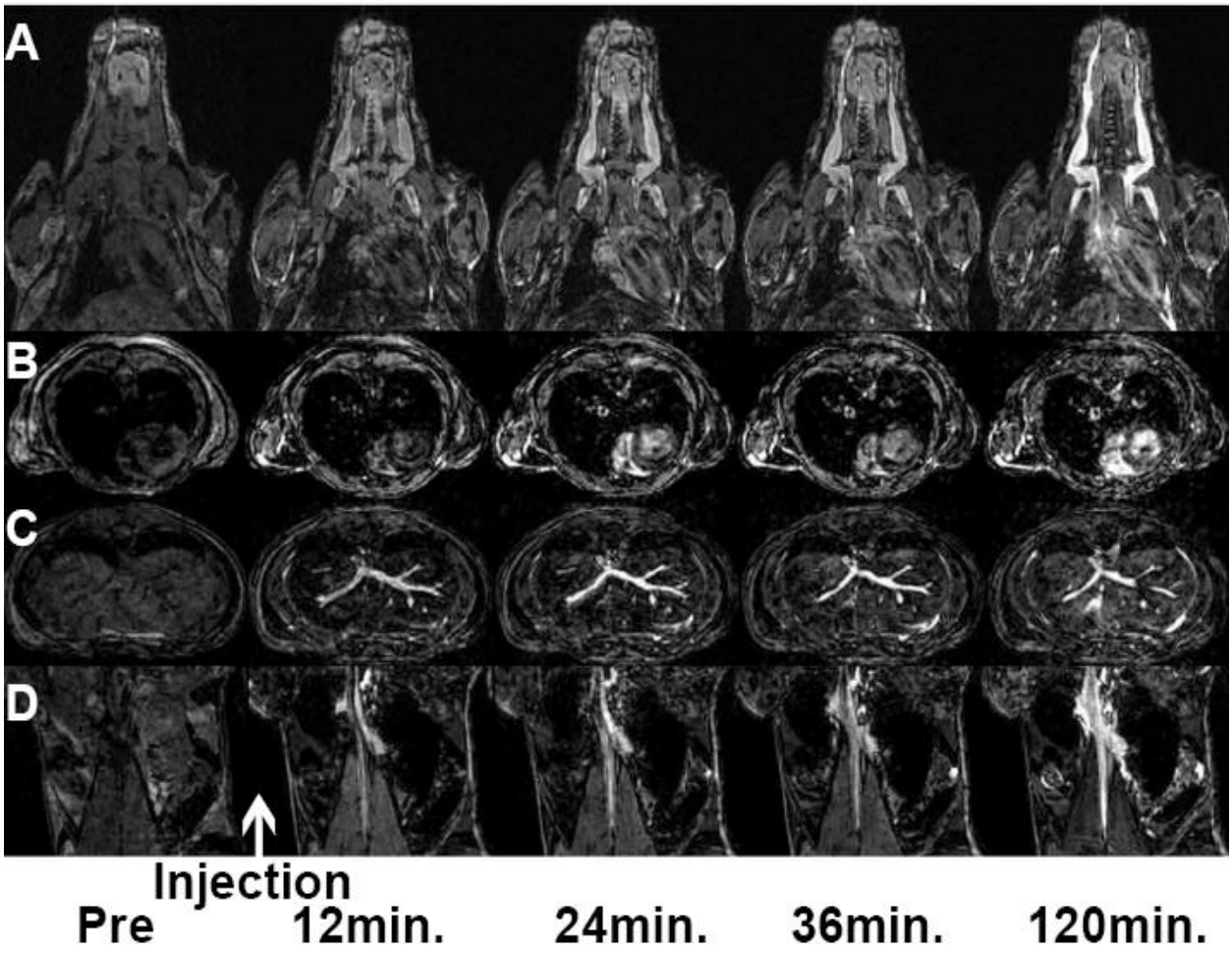

Figure 18. *Three-dimensional (3D) imaging of the whole mouse body in less than 12-minutes using a 7-T mouse MRI scanner equipped with a homemade RF coil enabling serial imaging with 200-µm isotropic spatial resolution. The example of image dataset shown compares different organ and body regions prior and following single injection of Mangradex at 25 mg/kg.* ***A)*** *coronal view covering the upper body including the head, neck, heart and lungs;* ***B)*** *axial slice re-orientation obtained from the same lung and heart area described in* ***A)****;* ***C)*** *the section covering the lung and liver region;* ***D)*** *a coronal view from the lower abdominal region that includes the kidneys and the spleen.*

Figure 20 show the whole body coverage achieved using 7 T mouse MRI after single injection of Mangradex (Dose = 25 mg/kg Mangradex or 455 nanomoles Mn^{2+} ions/kg). With the level of anatomical details achievable by our MR imaging protocol (200-µm isotropic resolution) in combination with our homemade MRI probe enabling full mouse body coverage, we were able to examine most of the main organs and the major vascular branches. The results from the serial MR

imaging performed in contrast agent-free subjects followed by serial acquisitions at 12, 24, 36, 48, 60, 72, 84, 96, 108 and 120 minutes post-injection in all mice clearly demonstrated the blood-pool nature of our compound Mangradex. As illustrated by the example shown in **Figure 18a**, the intravascular space is difficult to discern prior to the injection of the contrast agent (depicted by the column "Pre") throughout the different parts of the mouse body. Each row ranging from A to D corresponds to either coronal (A&D) or axial (B&C) sections at various levels of the mouse body as follow: A) covers the upper body including the head, neck, heart and lungs; B) is an axial slice re-orientation obtained from the same lung and heart area described in A) while in C) the section covers the lung and liver region; D) is a coronal view from the lower abdominal region that includes the kidneys and the spleen. As evidenced by the example shown, there is an obvious signal enhancement starting from the first image set acquired 12-min. post-injection. The greatest tissue contrast emanated from the vascular space in the various regions of the body as well as from the cardiac chambers seen in row A) with a long axis view of the heart & B) through its short axis section. This tissue contrast was most notable within the large vascular branching: head & neck in row A), liver in row C) as well as highlighting the abdominal aorta and inferior vena cava in row D). This enhancement was maintained throughout the two-hour period in which all the subjects were examined every 12-min. and where only a subset of the imaging time points corresponding to 12-, 36- and 120-min. post-injection are shown in **figure 19)**. Surprisingly, the kidneys experienced a dark enhancement that was immediate following the injection and was maintained throughout the imaging session as seen on row D).

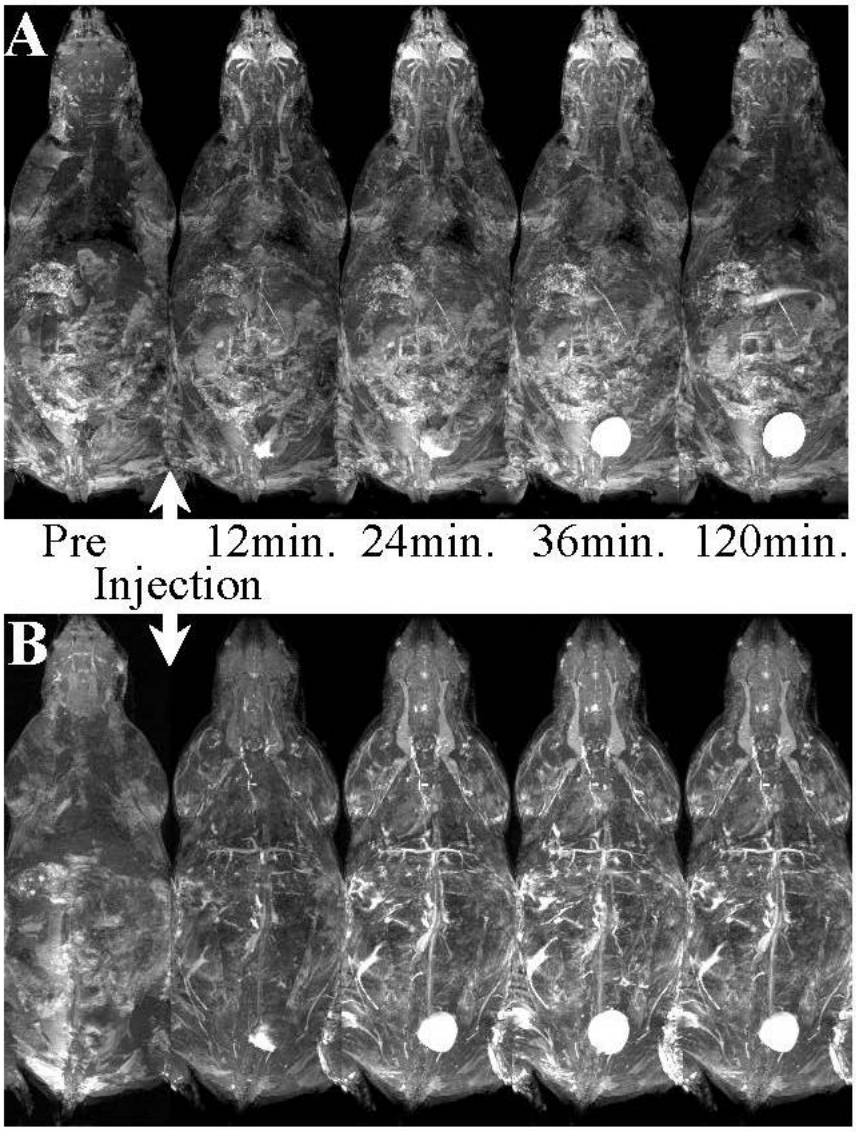

Figure 19. *3D visual rendering of the whole mouse body throughout the time course of this study via maximum-intensity-projections to facilitate the qualitative comparison of the bio-distribution and pharmacokinetics between CA injected in two groups. The effects of the contrast are illustrated as follow:* ***A)*** *Pre- & post- injection of Ablavar® (455 nmoles/kg of* Gd^{3+}*) as well as* ***B)*** *pre- & post Mangradex injection at 25 mg/kg (equivalent to 455 nmoles/kg of* Mn^{2+}*).*

In order to compare qualitatively the image contrast efficacy and enhancement kinetics of Mangradex with the clinical blood pool agent Ablavar® at potential diagnostic dosage (Gd^{3+} ion concentration = 455 nanomoles /kg), 3D image datasets from both mouse groups were analyzed by generating Maximum-Intensity-Projection (MIP) throughout the time course study. In this

approach, the MIP algorithm enables pixels with the highest value crossed via a chosen angle throughout the 3D image set to be projected for display on a 2D plane. This method permitted the visual rendering of the tissues where the contrast agent was distributed due to the signal enhancement it induced by its presence. **Figure 19** illustrates an example from each mouse group corresponding to the same imaging time window displayed in **Figure 18** (12-, 36- and 120-min post-injection). While subtle tissue contrast changes can be seen gradually enhancing in the major vessel branches immediately following the injection of Ablavar (**Figure 19, row A**), these signal enhancement gradually decayed (data not shown) and vanished by the last imaging time point corresponding to 120-min. Expectedly, the kidneys demonstrated immediate and subtle bright enhancement consistent with the renal excretion known to Ablavar following injection. The subtle increase in signal from kidneys can be partially distinguished in **Figure 19, row A** which could be likely overshadowed when using the MIP algorithm by superficial tissue and vessel enhancement. On the other hand, the injection of Mangradex at equivalent concentrations demonstrated an immediate and more pronounced contrast enhancement of the vasculature that persisted throughout the 2-hour imaging examination (**Figure 19, row B**). Importantly, the injection of either Mangradex or Ablavar resulted in gradual and consistent enhancement of the bladder as shown in **Figure 19**.

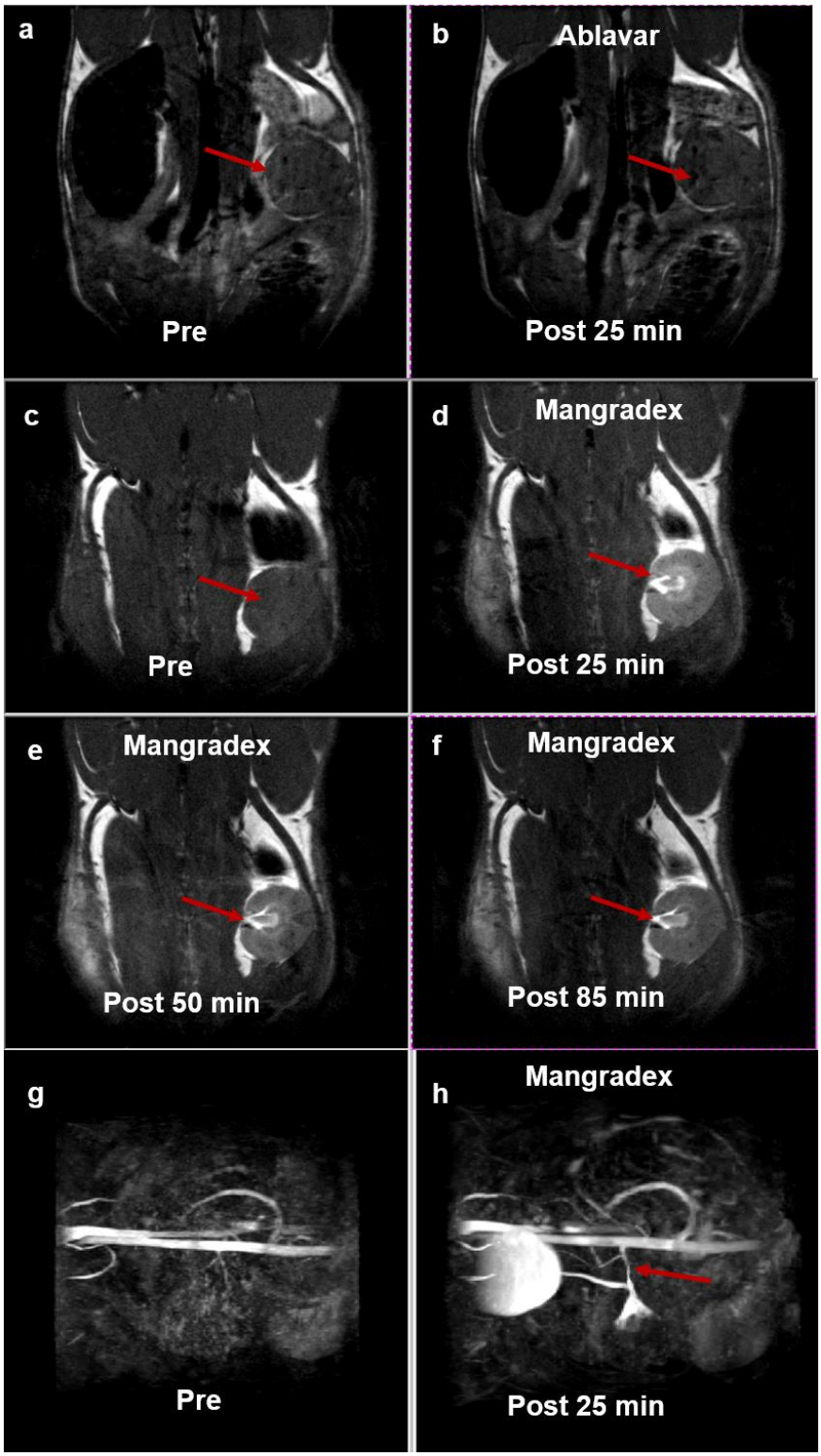

Figure 20. *In vivo MRI (a-f) Representative T_1 weighted MR images of pelvic region (coronal view) that show the subtotally nephroctomized (SNx) rat kidney (red arrow) before (a) and 25 minutes after (b) injection of Ablavar (control); before (c) and 25 (d), 50 (e) and 85 (f) minutes after injection of Mangradex. (g,h) Representative MR angiograms (head of the rat is on the right*

side) of pelvic region that show the renal artery (red arrows) before (g) and 25 minutes after (h) injection of Mangradex.

Figure 20 (a-f)) shows T_1-weighted MRI scans of kidney and renal artery using a 7 Tesla in 5/6 Nephrex rats pre and 25 minutes post injection of Ablavar at 60 nmoles/kg of Gd^{3+} ions, and pre and 25, 50 and 85 minutes post injection of Mangradex at 25 mg/kg (60 nmoles/kg Mn^{2+}). The images show significant and persistent contrast enhancement in kidney with Mangradex injection up to 85 minutes compared to Ablavar (**Figure 20 (a-d))**. **Figure 20 (d)** shows signal intensity increase 25 minutes post Mangradex injection, that falls gradually at 50 and 85 minutes **(Figure 20 (e,f))**. **Figure 20 (h)** shows clear demarcation of renal blood vessels from surrounding structure 25 minutes post Mangradex injection.

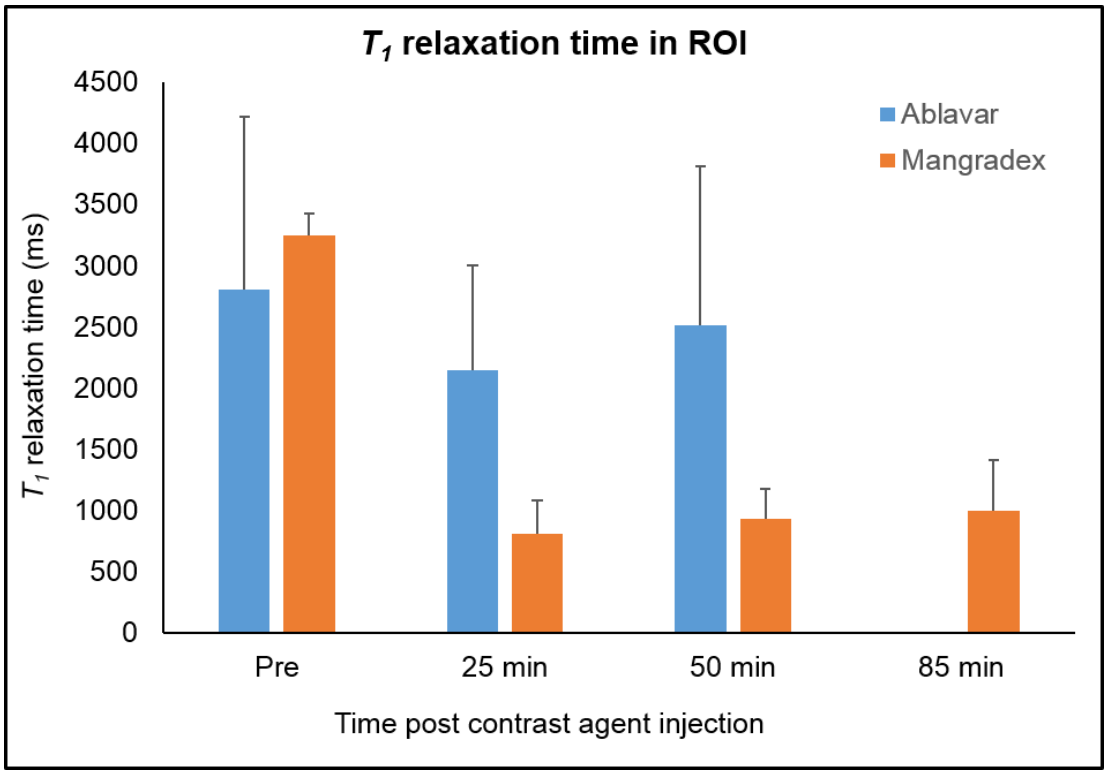

***Figure 21**. Graph showing in vivo T_1 relaxation time in region of interest before and 25, 50 and 85 minutes after injection of Mangradex at 25 mg/kg (455 nmoles/kg of manganese) and Ablavar (455 nmoles/kg of gadolinium.*

MR images parameters calculated from the Figure 3B images.				
MRI Parameter	Pre	Post Ablavar increase	Pre	Post Mangradex increase
SNR (kidney)	8.0	10.9 (25 min.); 36% 8.0 (50 min.); 24%	7.8	86.1 (25 min.); 198.28% 57.8 (50 min.) , 127.55% 55.6 (85 min); 98.98%
CNR (kidney)	0.9	1.1 (25 min.); 22% 0.9 (50 min.) 15%	1.3	15.1 (25 min.); 216% 9.7 (50 min.); 29% 11.1 (85 min.); 69%
SNR (Angio-renal artery)	6.4	7.1 (25 min.); 6.2%	6.3	64.5 (25 min.); 49.87%

Table 15*. A table showing % increase in T_1 relaxation time post injection of Ablavar and Mangradex.*

Figure 21 shows graph of T_1 relaxation time from the region of interest at 25, 50 ad 85 minutes after injection of Mangradex and Ablavar. T_1 relaxation time after Mangradex injection was less or compared to T_1 relaxation time after Ablavar injection. **Table 15** lists the changes in MR images parameters calculated from region of interest (ROI) pre - and post-injection of Mangradex or Ablavar. The Mangradex showed significant increases (~up to 200 times greater) in single to noise (SNR) and contrast to noise (CNR), compared to pre-injection or Ablavar in kidney and up to 42% greater in angiography.

These concentrations correspond to the equilibrium plasma concentration in rodents (average weight = 200 g), if the Mangradex is injected at doses between 1-500 mg/kg. The plasma concentration of the Gd^{3+}- chelate based CA at a clinical dose of 0.1 mmol/kg in a 200 g rat will be 1.5 mM, which is 17 times higher than the highest concentrations of Mn^{2+} (90.88 µM) in Mangradex solution (See appendix for calculation). This suggests that Mangradex can provide the similar MR contrast at lower dosages.

Discussion

Relaxivity is an important measure of efficacy for T_1 MRI CAs.[4] Our previous results show that the r_2/r_1 ratio for water-solubilized GNP solutions is 2.2 which is in the range reported for Mn^{2+} or Gd^{3+}-chelate complexes ($r_2/r_1 \sim$ 1-2.5) T_1 MRI CAs.[51,167] The ratio is also lower than the iron-oxide functionalized graphene nanoparticles ($r_2/r_1 \sim 10$) T_2 MRI CAs.[51] Thus, the Mangradex formulations are more suitable as a T_1 MRI CA.

For the *in vivo* MRI studies, the choice of 25 mg/kg dose was based on the outcomes of all the *in vitro* and *in vivo* (including the repeat dose) safety studies.[86,87,89] Our previous studies indicate that, at concentrations equivalent to first pass of a bolus injection (1-50 mg/ml), the formulation neither elicits any significant allergic response of the immune system, nor induces pro-inflammatory endothelial dysfunction effects.[86,87] Similarly at potentially steady state equilibrium concentrations in blood (0.1-10 mg/ml), we found no protein binding or complement activation.[86,89] The maximum tolerated dose found from acute *in vivo* toxicity studies were 50 mg/kg ≤ MTD < 125 mg/kg[87] and based on the results of this study, the no-observed adverse effect level (NOAEL) was 50 mg/kg. Hence, potential therapeutic dose selected for *in vivo* MRI was less than half of the MTD. The clinical Gd^{3+}-based blood pool agent Ablavar was used as control. The longer blood circulation of Ablavar compared to monomeric imaging agents such as Gd-DTPA or Gd-DOTA is attributed to its strong and high degree of reversible binding to serum albumin, while the longer blood circulation of Mangradex could be because of its hydrophilic properties, which is consistent with our previous *in vitro* studies showing that the partition co-efficient of Mangradex is -0.18 suggesting that majority of the contrast agents remain in liquid phase than in lipid (tissue *in vivo*).[89]

Numerous clinical studies have demonstrated the efficacy of Ablavar® in strongly enhancing blood vessels for MRA examinations.[168] We observed a similar vascular enhancement when injecting Ablavar® in mice and the sensitivity of our imaging setup enabled to trace the recirculation of this blood pool agent for more than 1 hour (data not shown). For Mangradex, our findings from the *in vivo* rodent studies indicated immediate and very strong vascular signal contrast enhancement that was prolonged for more than 2-hours evidenced by the serial imaging depicted by the example shown in **Figure 19, row B**. Other covalently or non-covalently functionalized graphene formulations have shown analogous pharmacokinetics in mice following intravenous administration where sustained recirculation and excretion via the biliary and renal pathways were observed.[169,170] This route of clearance was consistent with our previous study,[87] and corroborated further by the darkening effect seen in the kidney (**Figure 18D**). However, the unexpected signal blackening effect proved particularly puzzling when juxtaposed with the hyper-intense enhancement seen by the same particles in the recirculating blood prior to their renal excretion and subsequent downstream brightening when reaching the bladder. This immediate change in contrast effect when reaching the kidneys and later its positive contrast reversal may likely reflect an important change in the ratio R_2 ($R_2=1/T_2$) to R_1 ($R_1=1/T_1$) relaxivities of Mangradex. This R_2/R_1 alteration is commonly known in iron oxide-based agents [171], and varies with the intrinsic particle size but also reflect the aggregation or dispersion of magnetic particles when they react with surrounding tissue.[172] The degree of Mangradex aggregation and/or compartmentalization combined with the 7-T magnetic field strength may be responsible for the signal "quenching" effect observed in the kidneys. The positive contrast enhancement obtained by Mangradex within the blood stream proved to be far superior to that provided with Ablavar® at equal molar concentration of paramagnetic agent evidenced by the comparative serial imaging

shown in **Figure 19**. From the sub-acute toxicity studies, the safe dose range for Mangradex is 100 mg/kg, which is significantly higher than other MRI CA reported in literature and hence provides a greater margin of safety. Importantly, the enhancement was achieved at a low Mn^{2+}/kg dose of 455 nanomoles/kg; 66X and 220X lower than clinical dose of Ablavar® (Gd^{3+}/kg dose = 0.03 mmol/kg [168]) and Magnevist (Gd^{3+}/kg dose = 0.1 mmol/kg [152]), respectively. This dose is also in the range of average daily dietary intake of manganese (1.8-2.3 mg per day = 33-42 micromoles) [39]. At the Mn^{2+}/kg dose used in this study, the estimated Mn^{2+} steady state blood concentration in mice (weight = 40 grams; total blood volume = 3.2 ml) after the first pass would be ~ 5.7 nmoles/ml or 45 femtomoles /voxel.

The paramagnetic ion (Gd^{3+} ions) concentration in a typical clinical dose of Ablavar is 0.03 mmoles/kg. Thus, paramagnetic ion concentration (Mn^{2+} ions) of the injected Mangradex dose was 60 times lower than the paramagnetic ion concentration in a typical clinical dose. Even at low paramagnetic ion dosages ($[Mn^{2+}] = [Gd^{3+}]$ = 455 nmoles/kg) Mangradex shows significant SNR and CNR up to 85 minutes. Signal intensity drop and contrast to noise ratio drop could be because of the peak blood concentration and half-life of Mangradex is less than 50 minutes. The prolonged contrast in blood vessels suggests that Mangradex has potential to be used for renal artery imaging. Our previous study suggest that blood half-life of Mangradex significantly longer and can provide longer imaging window.

Innovatively, in this novel high-performance MRI CA, graphene acts as an active rather than passive scaffold. Our experimental and theoretical studies show that the graphene sheet does not passively intercalate, and coordinate the Mn^{2+} ion, but actively modulates the interaction of water

molecules with Mn^{2+} ions, and amplifies relaxivity (r_1 at clinical 1.5 Tesla magnetic field = 92 $mM^{-1}s^{-1}$).[51,173] Conversely, the multidentate ligands (chelates) used in clinical Gd^{3+}- or Mn^{2+}-based clinical MRI CAs sequester the toxicity of the naked metal ion. They play a ("passive") minor role or no role in modulating relaxivity (relaxivity r_1 at 1.5 Tesla magnetic field for Gd^{3+}-chelated = 1.9-4.5 $mM^{-1}s^{-1}$ [6], and Mn^{2+}-chelated = 2.8 $mM^{-1}s^{-1}$).[85] Additionally, intercalation and coordination of the Mn^{2+} ions within the graphene sheet improves sequestering of the Mn^{2+} ions and prevents dissociation from the graphene sheet. This intercalation prevents proteins or other biomacromolecules from competitively interacting with and dissociating Mn^{2+} ions. Conversely, Gd^{3+} and Mn^{2+} ions are only coordinated to chelates and are prone to competitive dissociation *in vivo* in the presence of biomacromolecules. Further, Mn^{2+} ion interaction and coordination "affinity" for graphene sheets is not altered by chemical derivatization to graphene's exterior, whereas metal ion coordination affinity of chelate molecules can be significantly decreased upon derivatization of the chelates by other functional groups for targeting purposes.

Our previous relaxometric studies indicate that dynamics of water within nanostructures with multiple layers of graphene, and the interaction between water and Mn^{2+} ions in these confined spaces affect the T_1 relaxation mechanism, and could be responsible for the observed increased contrast enhancement.[136] The molecular dynamics parameters that are modulated include the coordination number of inner-sphere water molecules (q) and water molecule residence lifetime (τ_M) coordinated with the Mn^{2+} ions, and the rotational correlation time (τ_R) of Mangradex. The combination of significant contrast enhancement at low detectable concentrations achieved at a high field strength combined with the longer residence times in the blood introduces Mangradex not only as a great addition to the existing blood pool agent, but also suggests its suitability to be

incorporated in the design of preclinical cellular/molecular imaging probes to monitor the progression of vascular pathologies.

Conclusion

The high r_1 relaxivity (92 $mM^{-1}s^{-1}$) of Mangradex allowed significant contrast enhancement of T_1-weighted MRI phantoms even at modest (nM) concentrations of Mn^{2+} ions. With one potential diagnostic dose, preliminary whole body murine examination at 7-Tesla show significant contrast enhancement in blood vessels for up to 2 hours compared to clinical dose of Ablavar and hence, shows great potential as a blood pool MRI CA. At the same diagnostic dose, *in vivo* MRI on 5/6 Nephrex rats at 7 Tesla magnetic field show significant (>100%) and sustained (for 90 minutes) contrast enhancement of the kidney and renal arteries at a low dosage (~66 to 200 times lower than clinical dosages). These distinctive properties indicate the exciting possibility of the development of Mangradex for diagnosis of renal failure. Taken together, these results should establish the basis for further consideration in studying vascular disease models and subsequently into higher species to make its clinical translation closer.

CHAPTER 5

CONCLUSION AND FUTURE STUDIES

Summary

The aim of this research project was to develop graphene nanoparticle-manganese based safe and a high-efficiency next generation MRI contrast agent that can overcome the limitations faced by current clinical CAs, and has potential to be used for advanced MRI applications. To achieve this goal, we first synthesized graphene nanoplatelets intercalated with paramagnetic Mn^{2+} ions by oxidizing graphite in the presence of potassium permanganate and then mechanically exfoliating the resulting graphene oxide to get GNPs. To impart water solubility and prepare formulation for *in vivo* application we functionalized GNPs using FDA approved polymer dextran. The Mangradex formulations are dispersible in deionized water up to 100 mg/ml concentration and are stable up to at least 4 hours and could be re-dispersed by gentle shaking of the solution. This is the highest water dipersibility for any carbon nanostructure reported so far. The viscosity values of the Mangradex formulations at all concentrations (0.4-100 mg/ml) were within the range of blood viscosity (between 3-4 cP at 37°C). The Mangradex formulation is hypo-osmolar at these concentrations. However, addition of mannitol increases the osmolality values to the range observed for normal blood (285 - 295 mOsm/kg of H_2O). The Mangradex formulation has a partition coefficient of -0.18 which indicates that they are retained mainly in aqueous phase, and thus, hydrophilic. The Mangradex at potential steady state equilibrium concentrations in blood (0.1-10 mg/ml) does not release histamine, suggesting negligible allergic response of the immune system to these nanoparticles. At these dosages, no human serum albumin (HSA) binding was observed, indicating absence of non-specific protein adsorption. Additionally, the nanoparticles were thermally stable, and Mn^{2+} ions did not dissociate from the nanoparticle at 37^{o}C up to 30 days.

The dispersibility and stability of the Mangradex formulation up to 100 mg/ml allowed us to perform acute toxicity studies at significantly higher dosages (25X greater) than with any other reported graphene IV toxicity studies (maximum 20 mg/kg). Our toxicity results suggest that the safety profile of Mangradex is better (50 mg/kg ≤ MTD < 125 mg/kg) than the previous GNP formulations reported in literature. In acute toxicity study, at the dosages < 125 mg/kg, no adverse effects were observed in animals in histology, blood chemistry or cardiovascular parameters. The major route of elimination for Mangradex is fecal (90% of injected dose). Similar to other GNP formulations, Mangradex shows more accumulation in liver, suggesting possible uptake by RES and eventual clearance by bile system. Our sub-acute toxicity study demonstrate that there were no adverse effects in animals as seen by histology and blood chemistry analysis at dosages ≤ 50 mg/kg. Taken together, these data suggest that Mangradex dose ≤ 50 mg/kg can serve as potential diagnostic dose.

The *in vitro* r_1 relaxivity of Mangradex is 92 $mM^{-1}s^{-1}$ (22 MHz proton Larmor frequency); ~20-30 fold greater than clinical gadolinium (Gd^{3+})-and Mn^{2+}-based MRI CAs. MR phantom images of Mangradex solutions at the concentration range 0.78-7.8 mg/ml (corresponding to the equilibrium plasma concentration in rodents if the Mangradex is injected at doses between 1-500 mg/kg), provides significant contrast enhancement at the Mn^{2+} ion concentrations down to 0.22-90.88 μM. Whole body 7 Tesla MRI performed on mice following intravenous injections of Mangradex at a potential diagnostic dose (25 mg/kg or 455 nanomoles Mn^{2+}/kg) showed persistent contrast enhancement up to at least 2 hours in the vascular branches. At this dose of Mangradex, Mn^{2+} concentration in blood at steady state is 300 ppb and per voxel of blood 45 femtomoles. Using the same dose (25 mg/kg) of Mangradex, *in vivo* MRI performed on 5/6 Nephrex rats at 7 Tesla

indicated significant (>100%) and sustained contrast enhancement in the kidney and renal artery up to 90 minutes at these low paramagnetic ion (Mn^{2+}) concentration. Importantly, the enhancement was achieved at a low Mn^{2+}/kg dose of 455 nanomoles/kg; 66X and 220X lower than clinical dose of Ablavar® (Gd^{3+}/kg dose = 0.03 mmol/kg) and Magnevist (Gd^{3+}/kg dose = 0.1 mmol/kg) respectively. Also, the concentration of manganese 455 nanomoles/kg is within the range of average daily dietary intake of manganese (1.8-2.3 mg per day = 33-42 micromoles). These results confirm that graphene sheets in Mangradex are not just the 'passive' carrier for Mn^{2+} ions; rather actively modulate the interaction of water molecules with Mn^{2+} ions, and amplifies relaxivity. Our previous relaxometric studies indicate that dynamics of water within nanostructures with multiple layers of graphene, and the interaction between water and Mn^{2+} ions in these confined spaces affect the T_1 relaxation mechanism, and could be responsible for the observed increased contrast enhancement. The molecular dynamics parameters that are modulated include the coordination number of inner-sphere water molecules (q) and water molecule residence lifetime (τ_M) coordinated with the Mn^{2+} ions, and the rotational correlation time (τ_R) of Mangradex. The combination of significant contrast enhancement at low detectable concentrations achieved at a high field strength combined with the longer residence times in the blood introduces Mangradex not only as a great addition to the existing blood pool agent, but also suggests exciting possibilities of its suitability in the design of preclinical cellular/molecular imaging probes to identify disease specific biomarkers and to monitor the progression of vascular pathologies. Taken together, the results of this research project lay the foundation for pivotal preclinical single and repeat dose safety studies following good laboratory practices (GLP) as required by the regulatory agencies; critical for the investigational new drug (IND) applications for first-in-human trails.

Future work

To realize successful application of Mangradex as an MRI CA some of the hypotheses need to be tested and several future studies should be performed.

Our *in vivo* toxicity study suggests pulmonary congestion as the possible cause of mortality in animals at doses ≥125 mg/kg. Based on the necropsy results and other literature reports,[174-177] we hypothesize that as Mangradex gets into pulmonary micro-circulation during the first pass, a large number of nanoparticles in the very small diameter of the micro vessels (<100 μm)[178] could occlude blood vessel, hamper blood flow in the systemic circulation, and ultimately induce cardiac arrest. Alternatively, the local interaction of Mangradex with endothelium and smooth muscle cells could significantly increase the hydraulic conductivity of the blood vessels, lead to fluid accumulation in alveoli and pulmonary congestion, and eventually death of animals. To test this hypothesis, additional studies that thoroughly examine the biomarkers for lung inflammation and pulmonary edema such as interleukin (IL)-1b, macrophage inflammatory protein (MIP)-1a, macrophage chemoattractant protein (MCP)-1, MIP-2, and keratinocyte chemoattractant (KC) following IV administration of Mangradex should be performed as mentioned in a previous study with nanoparticles elsewhere.[174] Additionally, electron microscopy of the microvasculature of the lungs excised immediately after the animal deceases can provide independent visual confirmation of the accumulation status of Mangradex. The effect of Mangradex accumulation in pulmonary microcirculation can also be studied further in detail with the *ex vivo* isolated lung model as described in a study by Glenny *et al* [179] to determine changes in pulmonary vascular resistance due to blockage by Mangradex nanoparticles. It should be noted that the pulmonary circulation of small animals and higher species can be different and the results obtained in small animals may not

remain valid in larger species. Subsequently, this kind of study should be followed in both small and large animals to determine the safety margin of Mangradex.

Acute and sub-acute toxicity studies did not suggest any histological sign of inflammation. It should be further verified with the serum concentration of inflammation specific markers pro-inflammatory cytokine Human TNF-Alpha (Tumor necrosis factor–Alpha) and anti-inflammatory cytokine IL-10 (Interleukin 10). In the acute and sub-acute toxicity studies reported in chapter 3, the follow up time was up to 4 weeks. It is necessary to study the long term ($\geq$ 6 months) toxic effects Mangradex and also required by regulatory agencies to design FIH clinical trials. Future small and large animal acute and chronic toxicity studies should be performed following longer recovery period. Multiple studies have demonstrated that size of the nanoparticle is a critical attribute affecting its cellular interaction, *in vivo* toxicity and bio-distribution. Hence, it is critical to precisely control the size of the Mangradex. This may be achieved by filtration, size exclusion chromatography and /or density gradient ultracentrifugation. Future toxicity studies should be performed with precisely controlled size of Mangradex.

The biodistribution study reported in chapter 3 is performed using Mn^{2+} as elemental tag to qualitative distribution trend *in vivo*. Mn^{2+} ions generated during the synthesis of GNPs from the oxidizing agent KMnO4 get intercalated between graphene sheets. Hence, manganese served as a stable endogenous elemental tag to quantify Mangradex concentrations in blood, urine, feces and bio-distribution studies. Since the values reported in this study, are based on the pooled samples, it is not possible to estimate the uncertainties introduced by extrapolation calculation. In order to obtain that information, follow up pharmacokinetics studies with the larger animal number should

be performed. The results obtained from ICP should also be corroborated independently with other methods to quantify Mn^{2+} such as X-ray fluorescence as reported in several previous studies.[180-182] Also, method validation using a standard reference material of tissues, urine, feces and blood from National Institute of Standard and Technology (NIST) and recovery after sample spiking with Mn^{2+} would be helpful to determine effects of biological matrix in manganese quantification.

As lower thermal stability of the linear Gd^{3+}- chelate (e.g. Omniscan, Optimark) and dissociation following longer retention *in vivo* is one of the major cause to trigger NSF; we focused on assessing manganese stability with respect to temperature at 37^{o}C. Further stability studies should be performed as a function of pH. Additionally, we studied the stability of the Mangradex formulation in DDI water as a function time and concentration by observing settling of the nanoparticles. Nanoparticle aggregation behavior is affected by pH, temperature and presence of protein in physiologic conditions. This aggregation not only affects the biological interaction of nanoparticles, but in case of MRI CA, can affect its relaxivity.[45,183] Future stability studies for Mangradex should be performed at biologically relevant pH, temperature and physiological buffers (serum, plasma or blood) to address the aggregation behavior and its effects on formulation stability and relaxivity.

In vivo imaging studies should be carried out at widely used 1.5 and 3T scanners to evaluate the performance of Mangradex at those magnetic field strengths. Graphene possesses larger surface area and the sp^2 bonded carbon sheets of graphene can be directly functionalized with targeting moieties for targeted imaging. In addition to that, graphene can also be loaded with aromatic drugs (e.g., SN38 and doxorubicin) via Vander Wall (π-πstacking) interactions yielding very high drug

loading efficiency. By taking advantage of these properties of graphene, the potential of Mangradex for image guided therapy should be explored experimentally.

To understand the mechanism of disease at molecular level, it is important to be able to visually distinguish between biomarkers such as enzymes, proteins, hormones, small molecules at the concentration they are present biologically (nano to picomolar range). For cellular (imaging of targeted cells and cellular processes in living organisms) or molecular imaging (imaging of targeted macromolecules and biological processes in living organisms), delivery of sufficient quantity of CA to obtain enough sensitivity at the target area is essential. Theory predicts that contrast enhancement of 10 to 100-fold beyond current agents are required to achieve this goal.[4,13,14,157] The high relaxivity of Mangradex (20-40X greater than current clinical agents) and the ability of graphene and dextran to provide functional groups for chemical linkage with antibody, proteins and ligands, can offer exciting opportunities to introduce Mangradex as cellular/molecular imaging agent. These type of applications would require labeling cells with Mangradex. In a recent study, Talukdar *et al.* has shown that GNPs are uptaken by mesenchymal stem cells (MSCs).[184] In a clinical setting, for the future success of cell transplantation therapy, MR tracking can play significant role by providing the capability to monitor cell migration from the transplantation site to relevant disease site, speed of cell migration and cell survival in the target organ necessary for exhibiting their regenerative properties. The ability to label stem cells by Mangradex in culture condition, may allow *in vivo* tracking of stem cells (including cell migration and cell trafficking) after transplantation and transfusion. Further exploitation of this possibility would require some proof of principle studies followed by deeper insight into the *in vivo* dynamics of cell biology.

Finally, the field of carbon nanostructure based MRI CAs will continue to improve and realize clinical translation when the challenges in scale-up production such as high level purity and uniformity will be addressed. The use of graphene nanoplaletelets as MRI CA (or for any intravenous biomedical application) requires unambiguous characterization of its physicochemical properties such as chemical, geometric, and magnetic characteristics attributing to their properties as MRI contrast agents. Further, the *in vivo* safety studies performed with graphene nanoplatelets (or referred as graphene oxide in some studies) so far across different groups, have used different size, concentration and surface coating and hence, do not provide platform for direct comparison. In this scenario, future development of a standard graphene reference material from NIST for biomedical application will be significant advancement towards its clinical translation.

REFERENCE LIST

1 Strijkers, G. J., Mulder, W. J., van Tilborg, G. A. & Nicolay, K. MRI contrast agents: current status and future perspectives. *Anti-cancer agents in medicinal chemistry* **7**, 291-305 (2007).

2 Barrett, T., Kobayashi, H., Brechbiel, M. & Choyke, P. L. Macromolecular MRI contrast agents for imaging tumor angiogenesis. *European journal of radiology* **60**, 353-366, doi:10.1016/j.ejrad.2006.06.025 (2006).

3 Lee, N. & Hyeon, T. Designed synthesis of uniformly sized iron oxide nanoparticles for efficient magnetic resonance imaging contrast agents. *Chemical Society reviews* **41**, 2575-2589, doi:10.1039/c1cs15248c (2012).

4 Sitharaman, B. & Wilson, L. J. Gadofullerenes and gadonanotubes: A new paradigm for high-performance magnetic resonance imaging contrast agent probes. *J Biomed Nanotechnol* **3**, 342-352, doi:Doi 10.1166/Jbn2007.043 (2007).

5 Kanakia S, T. J., Chowdhury SM, Lalwani G, Tembulkar T, Button T, Shroyer K, Moore W, Sitharaman B. Physicochemical characterization of a novel graphene based magnetic resonance imaging contrast agent. *International Journal of Nanomedicine* **8**, 2821-2833 (2013).

6 Rohrer, M., Bauer, H., Mintorovitch, J., Requardt, M. & Weinmann, H.-J. Comparison of magnetic properties of MRI contrast media solutions at different magnetic field strengths. *Investigative radiology* **40**, 715-724 (2005).

7 Laurent, S. *et al.* Magnetic iron oxide nanoparticles: synthesis, stabilization, vectorization, physicochemical characterizations, and biological applications. *Chemical reviews* **108**, 2064-2110, doi:10.1021/cr068445e (2008).

8 Que, E. L. & Chang, C. J. Responsive magnetic resonance imaging contrast agents as chemical sensors for metals in biology and medicine. *Chemical Society reviews* **39**, 51-60, doi:10.1039/b914348n (2010).

9 Solomon, I. Relaxation Processes in a System of Two Spins. *Physical Review* **99**, 559-565, doi:10.1103/PhysRev.99.559 (1955).

10 Bloembergen, N. Proton Relaxation Times in Paramagnetic Solutions. *The Journal of Chemical Physics* **27**, 572, doi:10.1063/1.1743771 (1957).

11 Bloembergen, N. & Morgan, L. O. Proton Relaxation Times in Paramagnetic Solutions. Effects of Electron Spin Relaxation. *The Journal of Chemical Physics* **34**, 842, doi:10.1063/1.1731684 (1961).

12 Caravan, P., Ellison, J. J., McMurry, T. J. & Lauffer, R. B. Gadolinium(III) Chelates as MRI Contrast Agents: Structure, Dynamics, and Applications. *Chemical reviews* **99**, 2293-2352 (1999).

13 Datta, A. & Raymond, K. N. Gd-hydroxypyridinone (HOPO)-based high-relaxivity magnetic resonance imaging (MRI) contrast agents. *Accounts of chemical research* **42**, 938-947, doi:10.1021/ar800250h (2009).

14 Aime, S., Castelli, D. D., Crich, S. G., Gianolio, E. & Terreno, E. Pushing the sensitivity envelope of lanthanide-based magnetic resonance imaging (MRI) contrast agents for molecular imaging applications. *Accounts of chemical research* **42**, 822-831, doi:10.1021/ar800192p (2009).

15 Stratta, P., Canavese, C., Quaglia, M. & Fenoglio, R. Gadolinium-associated nephrogenic systemic fibrosis in patients with renal failure: the need for an interdisciplinary helping network. *Rheumatology* **49**, 821-823, doi:10.1093/rheumatology/kep403 (2010).
16 Braverman, I. M. & Cowper, S. Nephrogenic systemic fibrosis. *F1000 medicine reports* **2**, 84, doi:10.3410/M2-84 (2010).
17 Gauden, A. J., Phal, P. M. & Drummond, K. J. MRI safety: nephrogenic systemic fibrosis and other risks. *Journal of clinical neuroscience : official journal of the Neurosurgical Society of Australasia* **17**, 1097-1104, doi:10.1016/j.jocn.2010.01.016 (2010).
18 Partain, C. L. On the potential causal relationship between gadolinium-containing MRI agents and nephrogenic systemic fibrosis. *Journal of magnetic resonance imaging : JMRI* **25**, 879-880, doi:10.1002/jmri.20982 (2007).
19 Issa, N. *et al.* Nephrogenic systemic fibrosis and its association with gadolinium exposure during MRI. *Cleveland Clinic journal of medicine* **75**, 95-97, 103-104, 106 passim (2008).
20 Gibson, S. E., Farver, C. F. & Prayson, R. A. Multiorgan involvement in nephrogenic fibrosing dermopathy: an autopsy case and review of the literature. *Archives of pathology & laboratory medicine* **130**, 209-212, doi:10.1043/1543-2165(2006)130[209:MIINFD]2.0.CO;2 (2006).
21 Ting, W. W., Stone, M. S., Madison, K. C. & Kurtz, K. Nephrogenic fibrosing dermopathy with systemic involvement. *Archives of dermatology* **139**, 903-906, doi:10.1001/archderm.139.7.903 (2003).
22 Chopra, T., Kandukurti, K., Shah, S., Ahmed, R. & Panesar, M. Understanding nephrogenic systemic fibrosis. *International journal of nephrology* **2012**, 912189, doi:10.1155/2012/912189 (2012).
23 Hoste, E. A. J. & Schurgers, M. Epidemiology of acute kidney injury: How big is the problem? *Critical Care Medicine* **36**, S146-S151 110.1097/CCM.1090b1013e318168c318590 (2008).
24 Robinson, B. E. Epidemiology of Chronic Kidney Disease and Anemia. *Journal of the American Medical Directors Association* **7**, S3-S6, doi:10.1016/j.jamda.2006.09.004 (2006).
25 Runge, V. M. Safety of Magnetic Resonance Contrast Media. *Topics in Magnetic Resonance Imaging* **12**, 309-314 (2001).
26 Grenier, N. *et al.* Functional MRI of the kidney. *Abdominal imaging* **28**, 164-175, doi:10.1007/s00261-001-0183-8 (2003).
27 Grenier, N., Pedersen, M. & Hauger, O. Contrast agents for functional and cellular MRI of the kidney. *European journal of radiology* **60**, 341-352, doi:10.1016/j.ejrad.2006.06.024 (2006).
28 Nikken, J. J. & Krestin, G. P. MRI of the kidney—state of the art. *Eur Radiol* **17**, 2780-2793, doi:10.1007/s00330-007-0701-3 (2007).
29 Pooley, R. A. Fundamental Physics of MR Imaging. *Radiographics* **25**, 1087-1099, doi:10.1148/rg.254055027 (2005).
30 US FDA (2007) Information on gadolinium- containing contrast agents., http://www.fda.gov/cder/drug/infopage/gcca/ (2008).
31 Shellock, F. G. & Spinazzi, A. MRI safety update 2008: part 1, MRI contrast agents and nephrogenic systemic fibrosis. *AJR. American journal of roentgenology* **191**, 1129-1139, doi:10.2214/AJR.08.1038.1 (2008).

32 Marckmann, P. *et al.* Nephrogenic systemic fibrosis: suspected causative role of gadodiamide used for contrast-enhanced magnetic resonance imaging. *Journal of the American Society of Nephrology : JASN* **17**, 2359-2362, doi:10.1681/ASN.2006060601 (2006).
33 Rydahl, C., Thomsen, H. S. & Marckmann, P. High prevalence of nephrogenic systemic fibrosis in chronic renal failure patients exposed to gadodiamide, a gadolinium-containing magnetic resonance contrast agent. *Investigative radiology* **43**, 141-144, doi:10.1097/RLI.0b013e31815a3407 (2008).
34 Pan, D. *et al.* Revisiting an old friend: manganese-based MRI contrast agents. *Wiley Interdisciplinary Reviews: Nanomedicine and Nanobiotechnology* **3**, 162-173, doi:10.1002/wnan.116 (2011).
35 Drahoš, B., Lukeš, I. & Tóth, É. Manganese(II) Complexes as Potential Contrast Agents for MRI. *European Journal of Inorganic Chemistry* **2012**, 1975-1986, doi:10.1002/ejic.201101336 (2012).
36 Lauterbur, P. C. Image formation by induced local interactions. Examples employing nuclear magnetic resonance. 1973. *Clinical orthopaedics and related research*, 3-6 (1989).
37 Mendonça-Dias, M. H., Gaggelli, E. & Lauterbur, P. C. Paramagnetic contrast agents in nuclear magnetic resonance medical imaging. *Seminars in Nuclear Medicine* **13**, 364-376, doi:http://dx.doi.org/10.1016/S0001-2998(83)80048-8 (1983).
38 Federle, M. P. *et al.* Safety and Efficacy of Mangafodipir Trisodium (MnDPDP) Injection for Hepatic MRI in Adults: Results of the U.S. Multicenter Phase III Clinical Trials (Safety). *Journal of Magnetic Resonance Imaging* **12**, 186-197, doi:10.1002/1522-2586(200007)12:1<186::aid-jmri21>3.0.co;2-2 (2000).
39 Food and Nutrition Board, Institute of Medicine. Manganese. Dietary reference intakes for vitamin A, vitamin K, boron, chromium, copper, iodine, iron, manganese, molybdenum, nickel, silicon, vanadium, and zinc. 394-419 (National Academy Press, Washington, D.C., 2001).
40 Kobayashi, H. & Brechbiel, M. W. Nano-sized MRI contrast agents with dendrimer cores. *Adv Drug Deliv Rev* **57**, 2271-2286, doi:10.1016/j.addr.2005.09.016 (2005).
41 Na, H. B. & Hyeon, T. Nanostructured T1 MRI contrast agents. *Journal of Materials Chemistry* **19**, 6267-6273, doi:10.1039/B902685A (2009).
42 Sitharaman, B. *et al.* Gadofullerenes as nanoscale magnetic labels for cellular MRI. *Contrast media & molecular imaging* **2**, 139-146, doi:10.1002/cmmi.140 (2007).
43 Sitharaman, B. *et al.* Superparamagnetic gadonanotubes are high-performance MRI contrast agents. *Chem Commun (Camb)*, 3915-3917, doi:10.1039/b504435a (2005).
44 Sitharaman, B. & Wilson, L. J. Gadonanotubes as new high-performance MRI contrast agents. *Int J Nanomedicine* **1**, 291-295 (2006).
45 Toth, E. *et al.* Water-soluble gadofullerenes: toward high-relaxivity, pH-responsive MRI contrast agents. *Journal of the American Chemical Society* **127**, 799-805, doi:10.1021/ja044688h (2005).
46 Vittorio, O., Duce, S. L., Pietrabissa, A. & Cuschieri, A. Multiwall carbon nanotubes as MRI contrast agents for tracking stem cells. *Nanotechnology* **22**, 095706, doi:10.1088/0957-4484/22/9/095706 (2011).
47 Manus, L. M. *et al.* Gd(III)-nanodiamond conjugates for MRI contrast enhancement. *Nano letters* **10**, 484-489, doi:10.1021/nl903264h (2010).

48 Ananta, J. S. *et al.* Geometrical confinement of gadolinium-based contrast agents in nanoporous particles enhances T_1 contrast. *Nature Nanotechnology* **5**, 815-821 (2010).
49 Bresinska, I. & Balkus, K. J. J. Studies of Gd(III)-exchanged Y-type zeolites relevant to magnetic resonance imaging. *J. Phys. Chem.* **98**, 12989–12994 (1994).
50 Sitharaman, B. *et al.* Superparamagnetic gadonanotubes are high-performance MRI contrast agents. *Chem. Commun.*, 3915-3917 (**2005**).
51 Paratala BS, J. B., Kanakia S, Francis LD, Sitharaman B. Physicochemical Characterization, and Relaxometry Studies of Micro-Graphite Oxide, Graphene Nanoplatelets, and Nanoribbons. *PLoS ONE* **7**, e38185. , doi:10.1371/journal.pone.0038185 (2012).
52 Stankovich, S. *et al.* Synthesis of graphene-based nanosheets via chemical reduction of exfoliated graphite oxide. *Carbon* **45**, 1558-1565, doi:http://dx.doi.org/10.1016/j.carbon.2007.02.034 (2007).
53 Kosynkin, D. *et al.* Longitudinal unzipping of carbon nanotubes to form graphene nanoribbons. *Nature* **458**, 872-876 (2009).
54 Panich, A. M., Shames, A. I. & Sergeev, N. A. Paramagnetic Impurities in Graphene Oxide. *Appl Magn Reson* **44**, 107-116, doi:10.1007/s00723-012-0392-z (2013).
55 Panich, A. M., Shames, A. I., Aleksenskii, A. E. & Dideikin, A. Magnetic resonance evidence of manganese–graphene complexes in reduced graphene oxide. *Solid State Communications* **152**, 466-468, doi:http://dx.doi.org/10.1016/j.ssc.2012.01.005 (2012).
56 Wong, C. H. *et al.* Synthetic routes contaminate graphene materials with a whole spectrum of unanticipated metallic elements. *Proceedings of the National Academy of Sciences of the United States of America* **111**, 13774-13779, doi:10.1073/pnas.1413389111 (2014).
57 Makarova, T. Magnetic properties of carbon structures. *Semiconductors* **38**, 615-638 (2004).
58 Wang, Y. *et al.* Room-temperature ferromagnetism of graphene. *Nano Letters* **9**, 220-224 (2008).
59 Laurent, S. *et al.* Magnetic iron oxide nanoparticles: synthesis, stabilization, vectorization, physicochemical characterizations, and biological applications. *Chemical Reviews* **108**, 2064-2110, doi:10.1021/cr068445e (2008).
60 Liu, Z., Robinson, J. T., Sun, X. & Dai, H. PEGylated nanographene oxide for delivery of water-insoluble cancer drugs. *Journal of the American Chemical Society* **130**, 10876-10877, doi:10.1021/ja803688x (2008).
61 Yang, K. *et al.* Multimodal imaging guided photothermal therapy using functionalized graphene nanosheets anchored with magnetic nanoparticles. *Adv Mater* **24**, 1868-1872, doi:10.1002/adma.201104964 (2012).
62 Zhang, S., Yang, K., Feng, L. & Liu, Z. In vitro and in vivo behaviors of dextran functionalized graphene. *Carbon* **49**, 4040-4049 (2011).
63 Feng, L., Zhang, S. & Liu, Z. Graphene based gene transfection. *Nanoscale* **3**, 1252-1257 (2011).
64 Loh, K. P., Bao, Q., Eda, G. & Chhowalla, M. Graphene oxide as a chemically tunable platform for optical applications. *Nature chemistry* **2**, 1015-1024, doi:10.1038/nchem.907 (2010).

65 Pan, D., Zhang, J., Li, Z. & Wu, M. Hydrothermal route for cutting graphene sheets into blue-luminescent graphene quantum dots. *Adv Mater* **22**, 734-738, doi:10.1002/adma.200902825 (2010).
66 Sun, X. *et al.* Nano-Graphene Oxide for Cellular Imaging and Drug Delivery. *Nano Res* **1**, 203-212 (2008).
67 Lu, C. H. *et al.* Increasing the sensitivity and single-base mismatch selectivity of the molecular beacon using graphene oxide as the "nanoquencher". *Chemistry* **16**, 4889-4894, doi:10.1002/chem.200903071 (2010).
68 Wang, Y. *et al.* Aptamer/graphene oxide nanocomplex for in situ molecular probing in living cells. *Journal of the American Chemical Society* **132**, 9274-9276, doi:10.1021/ja103169v (2010).
69 Chang, H., Tang, L., Wang, Y., Jiang, J. & Li, J. Graphene fluorescence resonance energy transfer aptasensor for the thrombin detection. *Analytical chemistry* **82**, 2341-2346, doi:10.1021/ac9025384 (2010).
70 Jung, J. H., Cheon, D. S., Liu, F., Lee, K. B. & Seo, T. S. A graphene oxide based immuno-biosensor for pathogen detection. *Angewandte Chemie* **49**, 5708-5711, doi:10.1002/anie.201001428 (2010).
71 Wen, Y. *et al.* A graphene-based fluorescent nanoprobe for silver(I) ions detection by using graphene oxide and a silver-specific oligonucleotide. *Chem Commun (Camb)* **46**, 2596-2598, doi:10.1039/b924832c (2010).
72 Markovic, Z. M. *et al.* In vitro comparison of the photothermal anticancer activity of graphene nanoparticles and carbon nanotubes. *Biomaterials* **32**, 1121-1129, doi:10.1016/j.biomaterials.2010.10.030 (2011).
73 Lalwani, G., Cai, X., Nie, L., Wang, L. V. & Sitharaman, B. Graphene-based contrast agents for photoacoustic and thermoacoustic tomography. *Photoacoustics* **1**, 62-67, doi:10.1016/j.pacs.2013.10.001 (2013).
74 Feng, L. & Liu, Z. Graphene in biomedicine: opportunities and challenges. *Nanomedicine (Lond)* **6**, 317-324, doi:10.2217/nnm.10.158 (2011).
75 Guidance for Industry Q8R(2) Pharamceutical Development. (2009).
76 Vogler, H. *et al.* Pre-clinical evaluation of gadobutrol: a new, neutral, extracellular contrast agent for magnetic resonance imaging. *European journal of radiology* **21**, 1-10 (1995).
77 Safety pharmacology studies for human pharmaceuticals. (2000).
78 Developing medical imaging drug and biological products part 1: conducting safety assessments. (2004).
79 (OECD), T. O. f. E. C.-o. a. D. in *Partition Coefficient (n-octanol/water): Shake Flask Method* (1995).
80 Minhua Tang, H. D., Kang Sun. One-step synthesis of dextran-based stable nanoparticles assisted by self-assembly. *Polymer* **47**, 728–734 (2006).
81 Quick guide to contrast media. (American Society of Health-System Pharmacists, 2010).
82 Pugh, N. D. Haemodynamic and rheological effects of contrast media: the role of viscosity and osmolality. *European Radiology* **6 Suppl 2**, S13-S15 (1996).
83 Van Liempd, S., Morrison, D., Sysmans, L., Nelis, P. & Mortishire-Smith, R. Development and validation of a higher-throughput equilibrium dialysis assay for plasma protein binding. *Journal of laboratory automation* **16**, 56-67, doi:10.1016/j.jala.2010.06.002 (2011).

84 Rimkus, G., Bremer-Streck, S., Gruttner, C., Kaiser, W. A. & Hilger, I. Can we accurately quantify nanoparticle associated proteins when constructing high-affinity MRI molecular imaging probes? *Contrast media & molecular imaging* **6**, 119-125, doi:10.1002/cmmi.405 (2011).
85 Pan, D. *et al.* Revisiting an old friend: manganese-based MRI contrast agents. *WIREs Nanomedicine and Nanobiotechnology* **3**, 162-173 (2010).
86 Chowdhury, S. M. *et al.* In vitro and in vivo assessment of hemodynamic properties of dextran functionalized graphene nanoparticles. *Scientific Reports*, (In Preparation) (2012).
87 Kanakia, S. *et al.* Dose ranging, expanded acute toxicity and safety pharmacology studies for intravenously administered functionalized graphene nanoparticle formulations. *Biomaterials* **35**, 7022-7031, doi:10.1016/j.biomaterials.2014.04.066 (2014).
88 Optimark package insert http://www.mallinckrodt.com/webforms/threecolumn.aspx?id=497.
89 Kanakia, S. *et al.* Physicochemical characterization of a novel graphene-based magnetic resonance imaging contrast agent. *Int J Nanomedicine* **8**, 2821-2833, doi:10.2147/IJN.S47062 (2013).
90 Runge, V. M. Safety of approved MR contrast media for intravenous injection. *Journal of magnetic resonance imaging : JMRI* **12**, 205-213 (2000).
91 Sirlin, C. B. *et al.* Gadolinium-DTPA-dextran: a macromolecular MR blood pool contrast agent. *Academic radiology* **11**, 1361-1369, doi:10.1016/j.acra.2004.11.016 (2004).
92 Gizzatov, A. *et al.* Enhanced MRI relaxivity of aquated Gd3+ ions by carboxyphenylated water-dispersed graphene nanoribbons. *Nanoscale* **6**, 3059-3063, doi:10.1039/c3nr06026h (2014).
93 Martwiset, S., Koh, A. E. & Chen, W. Nonfouling characteristics of dextran-containing surfaces. *Langmuir : the ACS journal of surfaces and colloids* **22**, 8192-8196, doi:10.1021/la061064b (2006).
94 Zatz, J. Physical stability of suspensions. *Journal of the Society of Cosmetic Chemists* **36**, 393-411 (1985).
95 Tweedle, M. F. The ProHance story: the making of a novel MRI contrast agent. *Eur Radiol* **7 Suppl 5**, 225-230 (1997).
96 Hummers, W. S. & Offeman, R. E. Preparation of Graphitic Oxide. *Journal of the American Chemical Society* **80**, 1339-1339, doi:10.1021/ja01539a017 (1958).
97 Shan, C. *et al.* Water-soluble graphene covalently functionalized by biocompatible poly-L-lysine. *Langmuir : the ACS journal of surfaces and colloids* **25**, 12030-12033, doi:10.1021/la903265p (2009).
98 Kim, Y. K., Kim, M. H. & Min, D. H. Biocompatible reduced graphene oxide prepared by using dextran as a multifunctional reducing agent. *Chem Commun (Camb)* **47**, 3195-3197, doi:10.1039/c0cc05005a (2011).
99 Deray, G. & Jacobs, C. Are low osmolality contrast media less nephrotoxic? *Nephrology, dialysis, transplantation : official publication of the European Dialysis and Transplant Association - European Renal Association* **11**, 930-931 (1996).
100 Voeltz, M. D., Nelson, M. A., McDaniel, M. C. & Manoukian, S. V. The important properties of contrast media: focus on viscosity. *The Journal of invasive cardiology* **19**, 1A-9A (2007).

101 Lancelot, E., Idee, J. M., Lacledere, C., Santus, R. & Corot, C. Effects of two dimeric iodinated contrast media on renal medullary blood perfusion and oxygenation in dogs. *Investigative radiology* **37**, 368-375 (2002).
102 Aime, S. & Caravan, P. Biodistribution of gadolinium-based contrast agents, including gadolinium deposition. *Journal of magnetic resonance imaging : JMRI* **30**, 1259-1267, doi:10.1002/jmri.21969 (2009).
103 Watts, D. L. The Nutritional Relationships of Manganese. *Journal of Orthomolecular Medicine* **5**, 219-222 (1990).
104 Sullivan, J. F., Blotcky, A. J., Jetton, M. M., Hahn, H. K. & Burch, R. E. Serum levels of selenium, calcium, copper magnesium, manganese and zinc in various human diseases. *The Journal of nutrition* **109**, 1432-1437 (1979).
105 Aschner, M. & Aschner, J. L. Manganese neurotoxicity: cellular effects and blood-brain barrier transport. *Neuroscience and biobehavioral reviews* **15**, 333-340 (1991).
106 Morcos, S. K., Thomsen, H. S. & Webb, J. A. Dialysis and contrast media. *Eur Radiol* **12**, 3026-3030, doi:10.1007/s00330-002-1629-2 (2002).
107 Prince, M. R., Zhang, H., Zou, Z., Staron, R. B. & Brill, P. W. Incidence of immediate gadolinium contrast media reactions. *AJR. American journal of roentgenology* **196**, W138-W143, doi:10.2214/AJR.10.4885 (2011).
108 Dillman, J. R., Ellis, J. H., Cohan, R. H., Strouse, P. J. & Jan, S. C. Allergic-like breakthrough reactions to gadolinium contrast agents after corticosteroid and antihistamine premedication. *AJR. American journal of roentgenology* **190**, 187-190, doi:10.2214/AJR.07.2718 (2008).
109 Kuefner, M. A., Feurle, J., Uder, M., Bautz, W. & Schwelberger, H. G. Influence of magnetic resonance contrast media on the activity of histamine inactivating enzymes. *Academic radiology* **16**, 358-362, doi:10.1016/j.acra.2008.09.005 (2009).
110 Nakamura, E. & Isobe, H. Functionalized fullerenes in water. The first 10 years of their chemistry, biology, and nanoscience. *Accounts of chemical research* **36**, 807-815 (2003).
111 Liu, Z., Tabakman, S., Welsher, K. & Dai, H. J. Carbon Nanotubes in Biology and Medicine: In vitro and in vivo Detection, Imaging and Drug Delivery. *Nano Res* **2**, 85-120 (2009).
112 Lalwani, G. & Sitharaman, B. Multifunctional fullerene- and metallofullerene-based nanobiomaterials. *NanoLIFE* **3**, 1342003 (2013).
113 Yang, X. *et al.* High-Efficiency Loading and Controlled Release of Doxorubicin Hydrochloride on Graphene Oxide. *The Journal of Physical Chemistry C* **112**, 17554-17558 (2008).
114 Lacerda, L., Bianco, A., Prato, M. & Kostarelos, K. Carbon nanotubes as nanomedicines: From toxicology to pharmacology. *Adv Drug Deliver Rev* **58**, 1460-1470 (2006).
115 Singh, S. K. *et al.* Thrombus inducing property of atomically thin graphene oxide sheets. *ACS Nano* **5**, 4987–4996 (2011).
116 Chang, Y. *et al.* In vitro toxicity evaluation of graphene oxide on A549 cells. *Toxicology Letters* **200**, 201–210 (2011).
117 Sasidharan, A. *et al.* Differential nano-bio interactions and toxicity effects of pristine versus functionalized graphene. *Nanoscale* **3**, 2461-2464 (2011).
118 Yang, K. *et al.* In vivo biodistribution and toxicology of functionalized nano-graphene oxide in mice after oral and intraperitoneal administration. *Biomaterials* **34**, 2787-2795, doi:10.1016/j.biomaterials.2013.01.001 (2013).

119 Poland, C. A. *et al.* Carbon nanotubes introduced into the abdominal cavity of mice show asbestos-like pathogenicity in a pilot study. *Nature nanotechnology* **3**, 423-428, doi:10.1038/nnano.2008.111 (2008).
120 Colvin, V. L. The potential environmental impact of engineered nanomaterials. *Nature biotechnology* **21**, 1166-1170, doi:10.1038/nbt875 (2003).
121 Kolosnjaj-Tabi, J. *et al.* In Vivo Behavior of Large Doses of Ultrashort and Full-Length Single-Walled Carbon Nanotubes after Oral and Intraperitoneal Administration to Swiss Mice. *ACS Nano* **4**, 1481-1492 (2010).
122 Zhang, X. *et al.* Distribution and biocompatibility studies of graphene oxide in mice after intravenous administration. *Carbon* **49**, 986-995, doi:http://dx.doi.org/10.1016/j.carbon.2010.11.005 (2011).
123 Liu, Z. *et al.* In vivo biodistribution and highly efficient tumour targeting of carbon nanotubes in mice. *Nature nanotechnology* **2**, 47-52, doi:10.1038/nnano.2006.170 (2007).
124 Diehl, K. H. *et al.* A good practice guide to the administration of substances and removal of blood, including routes and volumes. *Journal of applied toxicology : JAT* **21**, 15-23 (2001).
125 Wang, K. *et al.* Biocompatibility of Graphene Oxide. *Nanoscale Res Lett* **6**, 8 (2011).
126 Yang, K. *et al.* In vivo pharmacokinetics, long-term biodistribution, and toxicology of pEGylated graphene in mice. *ACS Nano* **5**, 516–522 (2011).
127 ICH guidance on toxicokinetics: The assessment of systemic exposure in toxicity studies S3A. *http://www.ich.org/fileadmin/Public_Web_Site/ICH_Products/Guidelines/Safety/S3A/Step4/S3A_Guideline.pdf* (1994).
128 OECD guidelines for the testing of the chemicals-Draft proposal for a revised TG 417: Toxicokinetics. *http://www.oecd.org/env/ehs/testing/41690691.pdf* (2008).
129 M3(R2) Nonclinical Safety Studies for the Conduct of Human Clinical Trials and Marketing Authorization for Pharmaceuticals. *http://www.fda.gov/RegulatoryInformation/Guidances/ucm129520.htm* (2010).
130 Guidance for Industry, Developing Medical Imaging Drug and Biological Products, Part 1: Conducting Safety Assessments. *Center for Drug Evaluation and Research, Food and Drug Administration, http://www.fda.gov/cber/guidelines.htm.* (2004).
131 Murabito, J. M., D'Agostino, R. B., Silbershatz, H. & Wilson, W. F. Intermittent claudication. A risk profile from The Framingham Heart Study. *Circulation* **96**, 44-49 (1997).
132 Baseline hematology and clinical chemistry values for charles river wistar rats. *http://www.criver.com/files/pdfs/rms/wistar-rats/rm_rm_r_hematology_crl_wi_br_sex_age* (1998).
133 Krystek, P. A review on approaches to bio distribution studies about gold and silver engineered nanoparticles by inductively coupled plasma mass spectrometry. *Microchemical Journal* **105**, 39-43 (2012).
134 Mary L.A. Giknis, C. B. C. Clinical laboratory parameters for crl: WI (Han) http://www.criver.com/files/pdfs/rms/wistarhan/rm_rm_r_wistar_han_clin_lab_parameters_08.aspx. (2008).
135 Staszyk, C., Bohnet, W., Gasse, H. & Hackbarth, H. Blood vessels of the rat tail: a histological re-examination with respect to blood vessel puncture methods. *Laboratory animals* **37**, 121-125, doi:10.1258/00236770360563750 (2003).

136 Paratala, B. S., Jacobson, B. D., Kanakia, S., Francis, L. D. & Sitharaman, B. Physicochemical characterization, and relaxometry studies of micro-graphite oxide, graphene nanoplatelets, and nanoribbons. *PLoS One* **7**, e38185, doi:10.1371/journal.pone.0038185 (2012).
137 Lee, L.-W. *et al.* Manganese enhancement in non-CNS organs. *NMR in Biomedicine* **23**, 931-938, doi:10.1002/nbm.1513 (2010).
138 Yicheng Ni, C. P., H. Bosmans, Y. Miao, D. Grant, A. L. Baert, G. Marchal. Comparison of manganese biodistribution and MR contrast enhancement in rats after intravenous injection of MnDPDP and MnCl2. *Acta Radiologica* **38**, 700-707, doi:doi:10.1080/02841859709172402 (1997).
139 Nishikawa, M., Staud, F., Takemura, S., Takakura, Y. & Hashida, M. Pharmacokinetic evaluation of biodistribution data obtained with radiolabeled proteins in mice. *Biological & pharmaceutical bulletin* **22**, 214-218 (1999).
140 Vexler, V. S., Clément, O., Schmitt-Willich, H. & Brasch, R. C. Effect of varying the molecular weight of the MR contrast agent Gd-DTPA-polylysine on blood pharmacokinetics and enhancement patterns. *Journal of Magnetic Resonance Imaging* **4**, 381-388 (1994).
141 Sperling, F. & McLaughlin, J. L. Biological parameters and the acute LD50 test. *Journal - Association of Official Analytical Chemists* **59**, 734-736 (1976).
142 Zbinden, G. & Flury-Roversi, M. Significance of the LD50-test for the toxicological evaluation of chemical substances. *Archives of toxicology* **47**, 77-99 (1981).
143 Sayan Mullick Chowdhury, S. K., Jimmy Toussaint, Mary D. Frame, Anthony M. Dewar,Kenneth R. Shroyer, William Moore, Balaji Sitharaman. In vitro hematological and in vivo vasoactivity assessment of dextran functionalized graphene. *Scientific Reports* **3** (2013).
144 Guidance for Industry: M3(R2) Nonclinical Safety Studies for the Conduct of Human Clinical Trials and Marketing Authorization for Pharmaceuticals (2010).
145 Duration of chronic toxicity testing in animals (rodent and nonrodent toxicity testing) http://www.ich.org/fileadmin/Public_Web_Site/ICH_Products/Guidelines/Safety/S4/Step4/S4_Guideline.pdf. (1998).
146 Harpur, E. S. *et al.* Preclinical safety assessment and pharmacokinetics of gadodiamide injection, a new magnetic resonance imaging contrast agent. *Investigative radiology* **28 Suppl 1**, S28-43 (1993).
147 Larsen, L. E. & Grant, D. General toxicology of MnDPDP. *Acta radiologica* **38**, 770-779 (1997).
148 Wible, J. H., Jr. *et al.* Toxicological assessment of gadoversetamide injection (OptiMARK), a new contrast-enhancement agent for use in magnetic resonance imaging. *Investigative radiology* **36**, 401-412 (2001).
149 Feng, L., Zhang, S. & Liu, Z. Graphene based gene transfection. *Nanoscale* **3**, 1252-1257 (2011).
150 Robert, P., Violas, X., Santus, R., Le Bihan, D. & Corot, C. Optimization of a blood pool contrast agent injection protocol for MR angiography. *Journal of Magnetic Resonance Imaging* **21**, 611-619, doi:10.1002/jmri.20324 (2005).
151 Johansson, L. O., Fischer, S. E. & Lorenz, C. H. Benefit of T1 reduction for magnetic resonance coronary angiography: A numerical simulation and phantom study. *Journal of*

Magnetic Resonance Imaging **9**, 552-556, doi:10.1002/(sici)1522-2586(199904)9:4<552::aid-jmri7>3.0.co;2-5 (1999).
152 Maki, J. H., Prince, M. R., Londy, F. J. & Chenevert, T. L. The effects of time varying intravascular signal intensity and k-space acquisition order on three-dimensional MR angiography image quality. *Journal of Magnetic Resonance Imaging* **6**, 642-651, doi:10.1002/jmri.1880060413 (1996).
153 Svensson, J. *et al.* Image artifacts due to a time-varying contrast medium concentration in 3D contrast-enhanced MRA. *Journal of Magnetic Resonance Imaging* **10**, 919-928, doi:10.1002/(sici)1522-2586(199912)10:6<919::aid-jmri3>3.0.co;2-w (1999).
154 MS-325: albumin-targeted contrast agent for MR angiography. *Radiology* **207**, 529-538, doi:doi:10.1148/radiology.207.2.9577506 (1998).
155 Caravan, P. *et al.* The Interaction of MS-325 with Human Serum Albumin and Its Effect on Proton Relaxation Rates. *Journal of the American Chemical Society* **124**, 3152-3162, doi:10.1021/ja017168k (2002).
156 Geraldes, C. F. G. C. & Laurent, S. Classification and basic properties of contrast agents for magnetic resonance imaging. *Contrast Media & Molecular Imaging* **4**, 1-23, doi:10.1002/cmmi.265 (2009).
157 Nunn, A., D., Linder, K. E. & Tweedle, M. F. Can receptors be imaged with MRI agents? *Q J Nucl Med.* **41**, 155-162 (1997).
158 Ahrens, E. T., Rothbächer, U., Jacobs, R. E. & Fraser, S. E. A model for MRI contrast enhancement using T1 agents *PNAS* **95**, 8443-8448 (1998).
159 Merbach, A. E. & Toth, E. *The Chemistry of Contrast Agents in Medical Magnetic Resonance Imaging*. (John Wiley & Sons, 2001).
160 Caravan, P., Farrar, C. T., Frullano, L. & Uppal, R. Influence of molecular parameters and increasing magnetic field strength on relaxivity of gadolinium- and manganese-based T1 contrast agents. *Contrast Media & Molecular Imaging* **4**, 89-100, doi:10.1002/cmmi.267 (2009).
161 Bae, K. T. *et al.* MRI-based kidney volume measurements in ADPKD: reliability and effect of gadolinium enhancement. *Clinical journal of the American Society of Nephrology : CJASN* **4**, 719-725, doi:10.2215/CJN.03750708 (2009).
162 Broome, D. R. Nephrogenic systemic fibrosis associated with gadolinium based contrast agents: a summary of the medical literature reporting. *European journal of radiology* **66**, 230-234, doi:10.1016/j.ejrad.2008.02.011 (2008).
163 Grobner, T. Gadolinium--a specific trigger for the development of nephrogenic fibrosing dermopathy and nephrogenic systemic fibrosis? *Nephrology, dialysis, transplantation : official publication of the European Dialysis and Transplant Association - European Renal Association* **21**, 1104-1108, doi:10.1093/ndt/gfk062 (2006).
164 Cowper, S. E., Kuo, P. H. & Bucala, R. Nephrogenic systemic fibrosis and gadolinium exposure: association and lessons for idiopathic fibrosing disorders. *Arthritis and rheumatism* **56**, 3173-3175, doi:10.1002/art.22926 (2007).
165 Nieman, B. J., Szulc, K. U. & Turnbull, D. H. Three-dimensional, in vivo MRI with self-gating and image coregistration in the mouse. *Magnetic resonance in medicine : official journal of the Society of Magnetic Resonance in Medicine / Society of Magnetic Resonance in Medicine* **61**, 1148-1157, doi:10.1002/mrm.21945 (2009).

166 Neelavalli, J. & Haacke, E. M. A simplified formula for T1 contrast optimization for short-TR steady-state incoherent (spoiled) gradient echo sequences. *Magnetic resonance imaging* **25**, 1397-1401, doi:10.1016/j.mri.2007.03.026 (2007).
167 Rohrer, M., Bauer, H., Mintorovitch, J., Requardt, M. & Weinmann, H. J. Comparison of magnetic properties of MRI contrast media solutions at different magnetic field strengths. *Investigative radiology* **40**, 715-724 (2005).
168 Lewis, M., Yanny, S. & Malcolm, P. N. Advantages of blood pool contrast agents in MR angiography: A pictorial review. *Journal of Medical Imaging and Radiation Oncology* **56**, 187-191, doi:10.1111/j.1754-9485.2012.02347.x (2012).
169 Yang, K. *et al.* Graphene in Mice: Ultrahigh In Vivo Tumor Uptake and Efficient Photothermal Therapy. *Nano Letters* **10**, 3318-3323, doi:10.1021/nl100996u (2010).
170 Nurunnabi, M. *et al.* In Vivo Biodistribution and Toxicology of Carboxylated Graphene Quantum Dots. *ACS Nano* **7**, 6858-6867, doi:10.1021/nn402043c (2013).
171 Josephson, L., Lewis, J., Jacobs, P., Hahn, P. F. & Stark, D. D. The effects of iron oxides on proton relaxivity. *Magn Reson Imaging* **6**, 647-653, doi:http://dx.doi.org/10.1016/0730-725X(88)90088-4 (1988).
172 Bjørnerud, A. & Johansson, L. The utility of superparamagnetic contrast agents in MRI: theoretical consideration and applications in the cardiovascular system. *NMR in Biomedicine* **17**, 465-477, doi:10.1002/nbm.904 (2004).
173 Kanakia, S. *et al.* Physicochemical characterization of a novel graphene-based magnetic resonance imaging contrast agent. *International Journal of Nanomedicine* **8**, 2821-2833 (2013).
174 Inoue, K. Promoting effects of nanoparticles/materials on sensitive lung inflammatory diseases. *Environmental health and preventive medicine* **16**, 139-143, doi:10.1007/s12199-010-0177-7 (2011).
175 Song, Y., Li, X. & Du, X. Exposure to nanoparticles is related to pleural effusion, pulmonary fibrosis and granuloma. *The European respiratory journal* **34**, 559-567, doi:10.1183/09031936.00178308 (2009).
176 Phillips, J. I., Green, F. Y., Davies, J. C. & Murray, J. Pulmonary and systemic toxicity following exposure to nickel nanoparticles. *American journal of industrial medicine* **53**, 763-767, doi:10.1002/ajim.20855 (2010).
177 Li, N., Xia, T. & Nel, A. E. The role of oxidative stress in ambient particulate matter-induced lung diseases and its implications in the toxicity of engineered nanoparticles. *Free radical biology & medicine* **44**, 1689-1699, doi:10.1016/j.freeradbiomed.2008.01.028 (2008).
178 Tabuchi, A., Mertens, M., Kuppe, H., Pries, A. R. & Kuebler, W. M. Intravital microscopy of the murine pulmonary microcirculation. *Journal of applied physiology* **104**, 338-346, doi:10.1152/japplphysiol.00348.2007 (2008).
179 Glenny, R. W., Bernard, S. L. & Lamm, W. J. Hemodynamic effects of 15-microm-diameter microspheres on the rat pulmonary circulation. *Journal of applied physiology* **89**, 499-504 (2000).
180 Rashkow, J. T., Patel, S. C., Tappero, R. & Sitharaman, B. Quantification of single-cell nanoparticle concentrations and the distribution of these concentrations in cell population. *Journal of the Royal Society, Interface / the Royal Society* **11**, 20131152, doi:10.1098/rsif.2013.1152 (2014).

181 Hummer, A. A. & Rompel, A. The use of X-ray absorption and synchrotron based micro-X-ray fluorescence spectroscopy to investigate anti-cancer metal compounds in vivo and in vitro. *Metallomics : integrated biometal science* **5**, 597-614, doi:10.1039/c3mt20261e (2013).
182 Milne, D. B., Sims, R. L. & Ralston, N. V. Manganese content of the cellular components of blood. *Clinical chemistry* **36**, 450-452 (1990).
183 Sitharaman, B., Bolskar, R. D., Rusakova, I. & Wilson, L. J. Gd@C60[C(COOH)2]10and Gd@C60(OH)x: Nanoscale Aggregation Studies of Two Metallofullerene MRI Contrast Agents in Aqueous Solution. *Nano letters* **4**, 2373-2378, doi:10.1021/nl0485713 (2004).
184 Talukdar, Y., Rashkow, J. T., Lalwani, G., Kanakia, S. & Sitharaman, B. The effects of graphene nanostructures on mesenchymal stem cells. *Biomaterials* **35**, 4863-4877, doi:10.1016/j.biomaterials.2014.02.054 (2014).

APPENDIX

1. Calculation of the dose:

If the concentration of the MRI CA solution is 1 mg/ml, and one requires to intravenously administer it at a dose of 100 mg/kg in a 200 g rat. The CA injection volume (v) is calculated as follows.

v (ml) x 1 mg/ml = 100 mg/kg x 200g

v (ml) x 1 mg/ml = (100 mg/1000 g) x 200 g

v (ml) x 1 mg/ml = 20 mg

v (ml) = 20 mg/ 1 mg/ml

v (ml) = 20 ml

The total circulating blood volume in a 200 g rat has been assumed to be ~12.8 ml.

Therefore, the injected volume percent (% (P) is calculated as follows

P % = (20 ml/12.8 ml) x 100%

P (%) = 156.25 %

Similarly, if the concentration of the MRI CA solution is 1 mg/ml, and one requires to intravenously administer it at a dose of 1 mg/kg in a 200 g rat, the CA injection volume (v) is calculated as follows.

v (ml) x 1 mg/ml = 1 mg/kg x 200g

v (ml) x 1 mg/ml = (1 mg/1000 g) x 200 g

v (ml) x 1 mg/ml = 2 mg

v (ml) = 2 mg/ 1 mg/ml

v (ml) = 2 ml

The injected volume percent (% (P) can be calculated as follows

12.8 ml x P (%) = 2 ml x 100 %

P (%) = (2 ml/12.8 ml) x 100%

P (%) = 1.56 %

In humans, the total circulating blood volume in a 70 kg adult human is 5 liter.

Therefore, if the concentration of the MRI CA solution is 1 mg/ml, and one has to administer a 100 mg/kg dose in a 70 kg human, the injection volume (v) of CA can be calculated as below.

v (ml) x 1 mg/ml = 100 mg/kg x 70000 g

v (ml) x 1 mg/ml = (100 mg/1000 g) x 70000 g

v (ml) x 1 mg/ml = 7000 mg

v (ml) = 7000 mg/ 1 mg/ml

v (ml) = 7000 ml

The injected volume percent (% (P) can be calculated as follows:

5000 ml x P (%) = 7000 ml x 100 %

P (%) = (7000 ml/5000 ml) x 100%

P (%) = 140 %

Similarly, if the concentration of the MRI CA solution is 1 mg/ml, and one requires to intravenously administer it at a dose of 1 mg/kg in a70 kg human, the CA injection volume (v) is calculated as follows.

v (ml) x 1 mg/ml = 1 mg/kg x 70000 g

v (ml) x 1 mg/ml = (1 mg/1000 g) x 70000 g

v (ml) x 1 mg/ml = 7 mg

v (ml) = 7 mg/ 1 mg/ml

v (ml) = 7 ml

The injected volume percent (% (P) can be calculated as follows

5000 ml x P (%) = 7 ml x 100 %

P (%) = (7 ml/5000 ml) x 100%

P (%) = 1.4 %

If the concentration of the MRI CA solution is 100 mg/ml and one requires to intravenously administer it at a dose of 500 mg/kg in a 200 g rat, the CA injection volume (v) is calculated as follows.

v (ml) x 100 mg/ml = 500 mg/kg x 200 g

v (ml) x 100 mg/ml = (500 mg/1000 g) x 200 g

v (ml) x 100 mg/ml = 100 mg

v (ml) = 100 mg/ 100 mg/ml

v (ml) = 1 ml

The total circulating blood volume in a 200 g rat has been assumed to be ~12.8 ml.

There, the injected volume percent (% (P) can be calculated as follows:

12.8 ml x P (%) = 1 ml x 100 %

P (%) = (1 ml/12.8 ml) x 100%

P (%) = 7.8

2. Calculation of the plasma concentration for relaxivity

At 0.1 mmol/kg clinical dose, the total amount of the MRI CA that will be injected in a 200 g rat

will be 0.1 mmol/kg x 0.2 kg = 0.02 mmol.

With a total circulating blood volume of ~12.8 ml, the plasma concentration of Gd^{3+} CA can be calculated as follows.

0.02 mmole/12.8 ml = 0.001562mmol/ml = 1562 µM.

From the inductive coupled plasma mass spectrometry (ICP-MS), the Mn^{2+} in Mangradex by weight is 0.064%. Therefore, the weight z (mg) of Mn^{2+} ions in 1 ml of 7.8 mg/ml solution of Mangradex can be calculated as follows.

100 mg x z (mg) = 7.8 mg x 0.064 mg

z (mg) = (7.8 mg/100 mg) x 0.064 mg

z (mg) = 0. 005 mg

Converting mass of Mn^{2+} into moles (MW of Mn^{2+} 54.93)

0.5 mg = (0.005×10^{-3} g/54.93 g/mole) = 9.08×10^{-8} moles

Thus, 7.8 mg/ml Mangradex solution has 9.08×10^{-8} moles/ml or 90.80 µM of Mn^{2+} ions.

This value is 17 times lower than plasma concentration of Gd^{3+}-chelate based CA (1562 µM) at clinical dose.

3. Rationale for choosing the medium and high Mangradex doses. The potential clinical therapeutic doses of graphene-based formulations for potential imaging or therapeutic applications still need to be determined. Therefore, published values of other clinical imaging and therapeutic agents; shown in the table below, were used as representative examples. We assumed that Mangradex could also be eventually administered, as a therapeutic or imaging agent, at similar doses. Based on this assumption and published regulatory guidelines, we chose medium to high doses 10-100 times the doses of these other clinical approved pharmaceuticals. The upper limit (500 mg/kg) was limited by the maximum permissible dose (MPD) that could be achieved using the highest Mangradex stock concentration of 100 mg/ml.

Clinically approve therapeutic and diagnostic agents	**Recommended clinical dose**	**Equivalent mg/kg dose**
Myocet - Liposomal doxorubicin	60 -75 mg/m^2 [5454]	1.632-2.04 mg/kg*
Abraxane – Albumin bound Paclitaxel nanoparticles	100-250 mg/m^2 [5555]	2.72 -6.8 mg/kg*
Doxorubicin - chemotherapeutic	60 mg/m^2 [138138]	1.632 mg/kg*
Ablavar – Blood pool magnetic resonance imaging contrast agent	0.03 mmol/kg [137137]	29 mg/kg

*Note: The conversion to mg/kg doses were performed based on the body weight and body surface area information provided at following webpage.

http://www.vspn.org/Library/Misc/VSPN_M02372.htm

4. Extrapolation of % of Mangradex

The % of manganese calculated in the Mangradex samples was average of 6 different samples of Mangradex. The ICP MS system used in this study allows detection even at concentrations up to1 ppb.

For the biodistribution studies, with the tested three doses 50, 250 and 500 mg/kg, a total of 12.5, 62.5 and 125 mg of Mangradex injected in a 250 g rat. Considering 0.064 wt% of manganese in the sample, the amount of manganese injected in rats will be 8, 40 and 80 µg for 50, 250 and 500 mg/kg respectively. Hence, 8, 40 and 80 µg of manganese was considered as 100% injected dose in each animal injected with 50, 250 and 500 mg/kg respectively.

If tissue sample is pooled from 6 animals for chemical digestion, then the measured manganese i.e. [Mn^{2+} (experimental group)] = [concentration obtained from ICP]/6.

Similarly, tissue sample pooled from 6 sham animals [(Mn^{2+} (sham control group)] = [concentration obtained from ICP]/6.

The % injected dose values in various tissues were calculated using the formula [Mn^{2+} (experimental group)] - [(Mn^{2+} (sham control group)]/ [Mn^{2+} (injected doses)]]*100.

5. Necropsy report

ANTECH DIAGNOSTICS

800-872-1001

Suny At Stony Brook
ANTECH Acct No. 8952

Doctor ZIMMERMAN

Accession No. **NYBB02121604**
Received 06/18/2012
Reported 06/25/2012 11:45 AM

Owner	Pet Name	Species	Breed	Sex	Pet Age	Chart#
SITHARAMAN	RAT 250-7	Rodent		F	16W	N

Test Requested	Results	Reference Range	Units

HISTOPATHOLOGY, FULL WRITTEN REPORT

Biopsy

NYBB 02121604 Sitharaman Dr. Zimmerman Rat 250-7

CLINICAL HISTORY: The thoracic pluck (heart and lung) is submitted from a 16 week old female rat, one of five animals which died after the injection of nanoparticles. The only gross lesion was red discolored lung.

MICROSCOPIC DESCRIPTION: A longitudinal biventricular section of heart characterizes an histologically unremarkable epicardium, myocardium, and endocardium with normal valvular structure and major vessels of the aorticopulmonary outflow tract. A small hilar lymph node is non-hyperplastic. Lung is markedly and diffusely atelectatic with moderate to marked, diffuse microvascular congestion (arterioles, venules, and the entire interalveolar septal capillary network). Focally disseminated throughout the lung is gold/brown-staining amorphous material of extremely fine granularity, accompanied by a few narrow rectangular to spike-like particles of the same tinctorial qualities. This material appears to exist within the interalveolar capillary septal microvasculature and interstitium as well as within a few alveolar lumina but is devoid of a secondary cellular infiltrate (i.e. neutrophils or macrophages). There is no necrosis/infarction. The same gold/brown amorphous granular or finely particulate matter is identified within blood of the cardiac chambers but is not encountered within the fibromuscular interstitium of the atrioventricular walls or within the myocardial microvasculature.

MICROSCOPIC FINDINGS:

- Heart-
  1. Normal epicardium, myocardium, endocardium, and valves
  2. Atrioventricular intraluminal amorphous to particulate gold/brown pigment
- Lung-
  1. Moderate to marked, diffuse atelectasis
  2. Marked, diffuse microvascular congestion
  3. Intravascular, interstitial, and alveolar intraluminal amorphous to particulate gold/brown pigment

COMMENTS: The histologic lesion which correlates with the gross necropsy observation of red discolored lungs is marked, diffuse pulmonary vascular congestion. In combination with atelectasis, this is a frequent observation in postmortem lung, often a feature of terminal, agonal cardiopulmonary collapse. The pulmonary congestion may be either physiologic or pathologic, depending upon whether or not there is coexisting heart disease i.e.: (pulmonary passive congestion). However, there are no cardiac lesions to suggest the latter, which is also unlikely in an animal of this young age. The finely to coarsely granular, particulate, and amorphous gold/brown material identified within blood of the cardiac chambers and within the lung is somewhat reminiscent of hemosiderin, but this is unlikely since there is no evidence of hemorrhage. It is more likely directly related to the experimental injection (?). There is no evidence of infectious/inflammatory disease.

The lesions described above for this mouse of are virtually identical

Accession No.	Doctor	Owner	Pet Name
NYBB02121604	ZIMMERMAN	SITHARAMAN	RAT 250-7

Test Requested	Results	Reference Range	Units

to those in the remaining 4 mice. In this mouse the stainable pulmonary amorphous to particulate material is present in moderate to large quantity, and similar pigmented material is identified within the blood of the cardiac chambers.

ADDITIONAL COMMENTS (Summary): as indicated by these 5 independent reports, a feature in common shared by the lung of all rats is gold/brown stainable pulmonary intravascular particulate material and moderate to severe diffuse congestion. It is the latter which is responsible for the gross necropsy identification of red discolored lungs. There is no pulmonary hemorrhage. The variably amorphous to granular to particulate material within the pulmonary vasculature of all rats and in a few instances also within the blood of the cardiac chambers (rat 500-16 and rat 250-7) is a noteworthy observation but is of questionable significance with regard to be immediate cause of death of these experiment the rats. This pigmented material does not affect the airways. It is likely that for source of this material was the experimental injection, particularly if the latter was intravascular. The more immediate cause of death may be related to intravascular accumulation of this pigmented material within the microvasculature other organs such as the kidney or brain (?). The thoracic organs of these five rats contain no evidence of infectious/contagious, necrotizing or inflammatory disease.

Ken Mero, DVM, PhD
Pathologist
;tag

REPORT NOTES:
RAT LUNG

ANTECH DIAGNOSTICS

800-872-1001

Suny At Stony Brook
ANTECH Acct No. 8952

Doctor ZIMMERMAN

Accession No. **NYBB02121533**
Received 06/18/2012
Reported 06/25/2012 11:34 AM

Owner	Pet Name	Species	Breed	Sex	Pet Age	Chart#
SITHARAMAN	RAT 500-16	Rodent		F	16W	N

Test Requested	Results	Reference Range	Units

HISTOPATHOLOGY, FULL WRITTEN REPORT

Biopsy

NYBB 02121533 Sitharaman Dr. Zimmerman Rat 500-16

CLINICAL HISTORY: The thoracic pluck (heart and lung) is submitted from a 16 week old female rat, one of five animals which died after the injection of nanoparticles. The only gross lesion was red discolored lung.

MICROSCOPIC DESCRIPTION: A longitudinal biventricular section of heart characterizes an histologically unremarkable epicardium, myocardium, and endocardium with normal valvular structure and major vessels of the aorticopulmonary outflow tract. A small hilar lymph node is non-hyperplastic. Lung is markedly and diffusely atelectatic with moderate to marked, diffuse microvascular congestion (arterioles, venules, and the entire interalveolar septal capillary network). Focally disseminated throughout the lung is gold/brown-staining amorphous material of extremely fine granularity, accompanied by a few narrow rectangular to spike-like particles of the same tinctorial qualities. This material appears to exist within the interalveolar capillary septal microvasculature and interstitium as well as within a few alveolar lumina but is devoid of a secondary cellular infiltrate (i.e. neutrophils or macrophages). There is no necrosis/infarction. The same gold/brown amorphous granular or finely particulate matter is identified within blood of the cardiac chambers but is not encountered within the fibromuscular interstitium of the atrioventricular walls or within the myocardial microvasculature.

MICROSCOPIC FINDINGS:

- Heart-
  1. Normal epicardium, myocardium, endocardium, and valves
  2. Atrioventricular intraluminal amorphous to particulate gold/brown pigment
- Lung-
  1. Moderate to marked, diffuse atelectasis
  2. Marked, diffuse microvascular congestion
  3. Intravascular, interstitial, and alveolar intraluminal amorphous to particulate gold/brown pigment

COMMENTS: The histologic lesion which correlates with the gross necropsy observation of red discolored lungs is marked, diffuse pulmonary vascular congestion. In combination with atelectasis, this is a frequent observation in postmortem lung, often a feature of terminal, agonal cardiopulmonary collapse. The pulmonary congestion may be either physiologic or pathologic, depending upon whether or not there is coexisting heart disease i.e.: (pulmonary passive congestion). However, there are no cardiac lesions to suggest the latter, which is also unlikely in an animal of this young age. The finely to coarsely granular, particulate, and amorphous gold/brown material identified within blood of the cardiac chambers and within the lung is somewhat reminiscent of hemosiderin, but this is unlikely since there is no evidence of hemorrhage. It is more likely directly related to the experimental injection (?). There is no evidence of infectious/inflammatory disease.

The lesions described above for this mouse are virtually identical to

Accession No.	Doctor	Owner	Pet Name
NYBB02121533	ZIMMERMAN	**SITHARAMAN**	RAT 500-16

Test Requested	Results	Reference Range	Units

those in the remaining 4 mice. In this mouse the stainable pulmonary amorphous to particulate material is present in moderate to large quantity and is also encountered in the blood of the cardiac chambers.

Ken Mero, DVM, PhD
Pathologist
;tag

REPORT NOTES:
RAT LUNG

ANTECH DIAGNOSTICS

800-872-1001

Suny At Stony Brook
ANTECH Acct No. 8952

Accession No. **NYBB02121561**
Received 06/18/2012
Reported 06/25/2012 11:37 AM

Doctor ZIMMERMAN

Owner	Pet Name	Species	Breed	Sex	Pet Age	Chart#
SITHARAMAN	RAT 125-19	Rodent		U	16W	N

Test Requested	Results	Reference Range	Units

HISTOPATHOLOGY, FULL WRITTEN REPORT

Biopsy

NYBB 02121561 Sitharaman Dr. Zimmerman Rat 125-19

CLINICAL HISTORY: The thoracic pluck (heart and lung) is submitted from a 16 week old female rat, one of five animals which died after the injection of nanoparticles. The only gross lesion was red discolored lung.

MICROSCOPIC DESCRIPTION: A longitudinal biventricular section of heart characterizes an histologically unremarkable epicardium, myocardium, and endocardium with normal valvular structure and major vessels of the aorticopulmonary outflow tract. A small hilar lymph node is non-hyperplastic. Lung is markedly and diffusely atelectatic with moderate to marked, diffuse microvascular congestion (arterioles, venules, and the entire interalveolar septal capillary network). Focally disseminated throughout the lung is gold/brown-staining amorphous material of extremely fine granularity, accompanied by a few narrow rectangular to spike-like particles of the same tinctorial qualities. This material appears to exist within the interalveolar capillary septal microvasculature and interstitium as well as within a few alveolar lumina but is devoid of a secondary cellular infiltrate (i.e. neutrophils or macrophages). There is no necrosis/infarction.

MICROSCOPIC FINDINGS:
- Heart-
1. Normal epicardium, myocardium, endocardium, and valves
- Lung-
1. Moderate to marked, diffuse atelectasis
2. Marked, diffuse microvascular congestion
3. Intravascular, interstitial, and alveolar intraluminal amorphous to particulate gold/brown pigment

COMMENTS: The histologic lesion which correlates with the gross necropsy observation of red discolored lungs is marked, diffuse pulmonary vascular congestion. In combination with atelectasis, this is a frequent observation in postmortem lung, often a feature of terminal, agonal cardiopulmonary collapse. The pulmonary congestion may be either physiologic or pathologic, depending upon whether or not there is coexisting heart disease i.e.: (pulmonary passive congestion). However, there are no cardiac lesions to suggest the latter, which is also unlikely in an animal of this young age. The finely to coarsely granular, particulate, and amorphous gold/brown material identified within lung is somewhat reminiscent of hemosiderin, but this is unlikely since there is no evidence of hemorrhage. It is more likely directly related to the experimental injection (?). There is no evidence of infectious/inflammatory disease.

The lesions described above for this mouse of are virtually identical to those in the remaining 4 mice. In this mouse the stainable

Accession No.	Doctor	Owner	Pet Name
NYBB02121561	ZIMMERMAN	SITHARAMAN	RAT 125-19

Test Requested	Results	Reference Range	Units

pulmonary amorphous to particulate material is present in moderate quantity, but similar pigmented material is not identified within the blood of the cardiac chambers.

Ken Mero, DVM, PhD
Pathologist
;tag

REPORT NOTES:
RAT LUNG